SISSA **ISAS**

SCUOLA INTERNAZIONALE SUPERIORE DI STUDI AVANZATI
INTERNATIONAL SCHOOL FOR ADVANCED STUDIES

The demography of the youngest radio sources

Thesis submitted for the degree of
Doctor Philosophiæ

CANDIDATE:
Sara Tinti

SUPERVISORS:
Prof. Gianfranco De Zotti
Prof. Annalisa Celotti
Dr. Daniele Dallacasa

October 2005

Table of Contents

Citations to Previously Published Works

Part of the contents of this Thesis has already appeared in the following papers:

Refereed Journals:

- **Constrains on Evolutionary Properties of GHz Peaked Spectrum Galaxies**
  Tinti, S. & De Zotti, G.
  12 pages, 4 figures, accepted for publication in Astronomy & Astrophysics.

- **High Frequency Peakers: young radio sources or flaring blazars?**
  Tinti, S.; Dallacasa, D.; De Zotti, G.; Celotti, A.; Stanghellini, C.
  Astronomy & Astrophysics, v.432, p.31-43 (2005). astro-ph/0410663

- **The B3-VLA CSS sample. V. VLBA images at 6 and 3.6 cm**
  Orienti, M.; Dallacasa, D.; Fanti, C.; Fanti, R.; **Tinti, S.**; Stanghellini, C.
  Astronomy & Astrophysics, v.426, p.463-470 (2004)

- **The B3-VLA CSS sample. II. VLBA images at 18 cm**
  Dallacasa, D.; **Tinti, S.**; Fanti, C.; Fanti, R.; Gregorini, L.; Stanghellini, C.; Vigotti, M.
  Astronomy & Astrophysics, v.389, p.115-125 (2002). astro-ph/0205200

- **VLBA Observations of Bright High Frequency Peakers**
  Tinti, S.; Dallacasa, D. ; Stanghellini, C. ; Celotti, A.
  Refereed Proceeding: Publications of the Astronomical Society of Australia, Volume 20, Issue 1, pp. 110-112.

In Preparation:

- **VLBA Images of High Frequency Peakers**
  Orienti, M.; Dallacasa, D.; **Tinti, S.**; Stanghellini, C.

Non-referred Proceedings:

- **Surveys of extragalactic sources with Planck**
  De Zotti, G.; Burigana, C.; Negrello, M.; **Tinti, S.**; Ricci, R.; Silva, L.; Gonzalez-

Acknowledgments

I am pleased to have this opportunity to acknowledge all the people that have contributed to the successful completion of my period of studentship in SISSA.

First, I wish to express my gratitude to my supervisor, Prof. Gianfranco De Zotti, for his continuous support during my doctoral research. His professional advice during the whole work, his sense of clarity, precision and his patience have been essential factors to the success of my work. I would like to acknowledge Prof. Annalisa Celotti, for useful discussions about all the contents of this thesis. Thanks also to Dr. Daniele Dallacasa who always update me with new data and guided me in the more technical part of this work.

I would also like to thank the whole faculty and staff of the Astrophysics Sector in SISSA, among them a special thanks to Luciano Rezzolla, who supported and encouraged me several times during the last four years.

Many thanks also to all my colleagues, both old and new, for their friendship and support, for creating a good work ambience and for all the special moments we shared during these years. They are for me now very good friends.

Apart from the professional work, my biggest and most important gratitude goes to my family, my parents and my sister, for their constant presence, patient and encouragement. I owe to them this part of my life and of my career and I dedicate to them this dissertation.

Finally, my warmest thank goes to Capitano, I came in Trieste following one of my dreams and I found the most important one.

Chapter 1

Introduction

1.1 Scientific Background

The number of radio sources unresolved on arcsecond scales is rather conspicuous in all modern catalogues. These sources can be either intrinsically small or larger sources shortened by projection effects. Blazars (flat spectrum radio quasars and BL Lacs) are well known examples of sources shortened by projection. Their radio spectrum is flat or inverted up to very high frequencies and they are characterized by flux density and polarisation variability. There is also a significant fraction of radio sources, from 15% to 30% depending on the selection frequency and flux limit, that are found to be intrinsically small objects. At higher angular resolution [especially at that achievable with long baseline interferometry (VLBI)], previously unresolved sources turned out to have morphologies remarkably similar to the already well studied large-scale radio sources. These sources are named Gigahertz Peaked Spectrum (GPS) and Compact Steep Spectrum (CSS) radio sources. Typical GPS, CSS and lobe-dominated FRII sources, in samples of bright sources, have the same appearance, but they have very different size scales. In principle, the small sources could be classified as FRII sources on the basis of morphology but these classes were named on the basis of their radio spectral properties long before the morphology was determined: the overall radio spectrum is convex, with a turnover frequency occurring between 100 MHz (CSS) and a few GHz (GPS). Observational studies have also revealed

an anti-correlation between the turnover frequencies and the projected linear size for GPS and CSS sources. GPS sources are smaller than 1 kpc, CSS sources are between 1 and 20 kpc and FRIIs are larger than 20 kpc. If we compare these sizes to galactic structures, GPS's radio emission is within the extent of the Narrow Line Region (NLR), CSS are subgalactic in size and FRII sources have expanded well beyond the stellar borders of the galaxy. Once the morphological similarity was established and the anticorrelation between turnover frequency in the spectrum and projected linear size confirmed for a significant number of GPS/CSS sources, evolutionary scenarios for radio sources were proposed by a number of people (Fanti et al. 1995; Begelman 1996; Readhead et al. 1996; O'Dea & Baum 1997, Snellen et al. 2000). Radio sources seem to evolve along the GPS-CSS-FRII sequence increasing their radio size and decreasing the frequency at which the turnover in the radio spectrum occurs (see Fig.1.1). Since the GPS/CSS sources are a high fraction among distant (z>0.2) radio sources of high power in the radio catalosgues, it was necessary to explain the relative number densities of the objects observed. A possibility proposed by Fanti et al. (1995) and O'Dea & Baum (1997) is that during the evolution from GPS to CSS and FRII they decline by a factor of ~ 10 in radio luminosity as they increase in size from a few kpc to hundreds of kpc [but see Snellen et al. (2000) and Alexander (2000) for a different view].

1.2 Thesis Project

In the framework of the evolutionary model for radio sources mentioned above and described in detail in Chapter 2, the well defined anti-correlation between the radio turnover frequency, ν_p, and the projected angular size, θ (O'Dea & Baum 1997; Fanti et al. 2002) means that the youngest objects have the highest turnover frequencies and that the peak frequency is expected to move towards lower frequencies as the source expands and the energy density decreases. In principle, the highest the turnover frequency, the youngest the radio source is.

The aim of this thesis is to search and study "extreme" GPS sources, with spectral peaks at frequencies of tens of GHz, that may offer an opportunity to study radio sources

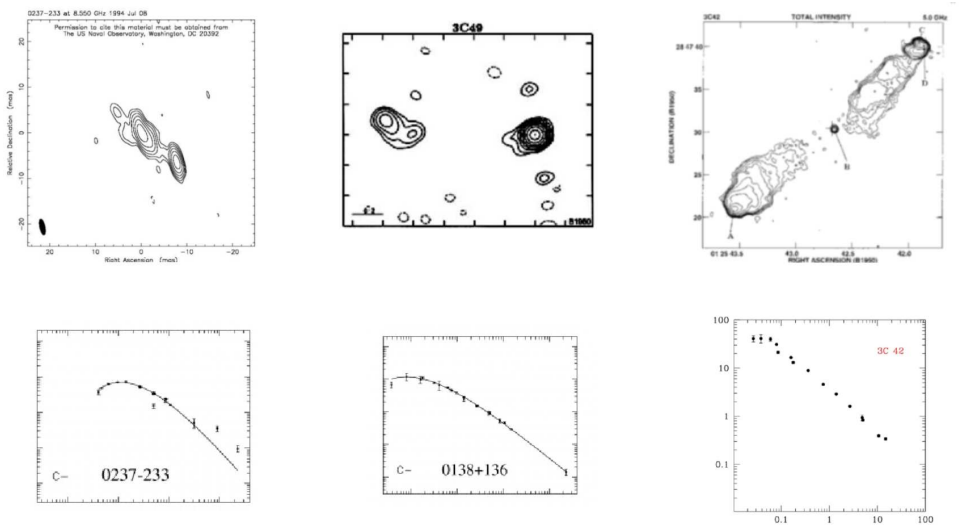

Figure 1.1: Comparison of radio morphology and spectrum of a GPS (linear size LS= 0.158 kpc, $\nu_{\rm max}$ = 1 GHz), a CSS (LS= 5.529 kpc, $\nu_{\rm max}$ = 0.12 GHz) and a FRII radio source (LS= 119 kpc, $\nu_{\rm max} < 0.03$ GHz).

very close to their birth. These objects, however, are likely to be very rare because their expansion rate, and therefore the rate of decrease of their peak frequency, is thought to be very rapid. The shape of the radio spectrum and the turnover frequency have been used as selection tools for this class of objects. A complete sample of bright candidate GPS sources peaking above $\simeq$ 5 GHz has been obtained by Dallacasa et al. (2000), who termed such sources "High Frequency Peakers" (HFPs). Only a fraction of their objects are expected to be truly newborn sources since the sample is contaminated by beamed, flat-spectrum quasars (see also Snellen et al. 1999, Stanghellini et al. 2003) caught during a flaring phase of a strongly self-absorbed component that dominates the radio spectrum. Since the process that characterizes both flaring blazars and young radio sources is the expansion of an emitting blob in the ISM, i.e. the lobes in the case of young sources, a knot of the jet that dominates the radio spectrum for blazars, it is quite difficult to distinguish the two phenomena with a single observation. Howeever, their time evolution has quite different timescales: GPS/CSS sources are thought to expand at mildly relativistic velocities with marginal or no influence on the radio spectrum while large Doppler factors in blazars boost the variability amplitudes in the spectrum and decrease the corrisponding

observed timescales. In order to disentangle the two classes in our sample we have carried out various observational projects (described in Chapter 3) to:

- study the spectral shape evolution and the variability properties of the sample;
- determine the polarisation properties;
- look for extended emission that may indicate that we are really dealing with an evolved-old source but can also be the relic of previous large scale radio activity in a re-born radio source;
- study the milliarcsecond morphology of the candidates.

The information on variability of HFP candidates, on their morphology at different resolutions and the polarimetric study can help us to define criteria to discriminate between the two classes of objects. In Chapter 4 we discuss various criteria and the consistency of their indications on the source nature.

Since it has been proved that the incidence of blazar objects in a spectral selected sample increases with increasing selection frequency and, as a consequence, with increasing turnover frequency (Stanghellini 2003), this kind of analysis is crucial to select truly young radio sources. Clearly, a serious blazar contamination of GPS samples may lead astray analyses of their statistical properties and implies that evolutionary models based on them need to be reconsidered. To effectively explore the luminosity and peak frequency evolution of GPS sources, we need samples that provide a wide coverage of the turnover frequency and flux density (ν_p–S_p) plane. In Chapter 5 we give an account of the data sets we used. We also analyze the effect of the different selection criteria adopted to define the samples. We have finally studied an evolutionary model in the framework of the self-similar evolution scenario by Fanti et al. (1995) and Begelman (1996) comparing the redshift and peak frequency distribution yielded by the model with the observed ones. A summary of the main results are given in Chapter 6.

Chapter 2

The Compact Steep-Spectrum and Gigahertz Peaked-Spectrum Radio Sources

2.1 Abstract

In this chapter the observational advances in the study of the Gigahertz Peaked-Spectrum (GPS) and Compact Steep-Spectrum (CSS) radio sources will be presented along with the current hypotheses for their origin and their location in the evolutionary sequence of powerful radio galaxies.

2.2 Definitions

The CSS and GPS sources are two classes of intrinsically compact objects (linear size $<$ 10–1 kpc) defined on the basis of their spectral properties: the overall radio spectrum is convex, with a turnover frequency occurring between 100 MHz (CSS) and a few GHz (GPS); the spectral index at high frequencies is steep, $\alpha > 0.5, S_\nu \sim \nu^{-\alpha}$ (see O'Dea 1998 for a complete review). GPS sources are powerful ($\log P_{1.4} \gtrsim 25 \mathrm{WHz}^{-1}$) and entirely contained within the narrow line region (NLR) ($\lesssim$ 1 kpc), while CSS sources are just as

powerful but substantially larger ($\lesssim$ 15 kpc), contained entirely within the host galaxy. GPS and CSS sources are a significant fraction of radio sources, from 15% to 30% depending on the selection frequency and the flux limit.

Fanti et al. (1990) have shown that most of the CSS sources ($\geq$ 70%) are likely to be intrinsically small and not foreshortened by projection effects and that there is no significant amplification of radio luminosity by Doppler effects. Two models have been proposed to explain why these sources are **compact**, **very luminous** (as powerful as the large 3CR classical doubles) and a **significant fraction of the radio source populations**; they can be summarized as follows:

- The **frustration model** (van Breugel et al. 1984, O'Dea et al. 1991): the radio emitting plasma is permanently confined within the host galaxy by an external medium which is dense enough to prevent the expansion of the radio source.

- The **youth model** (Fanti et al. 1990, 1995; Begelman 1996; Readhead et al. 1996): based on the idea by Phillips & Mutel (1982), this model suggests that GPS/CSS sources are small because they are young; according to the evolutionary scheme, in the GPS phase the source is confined in the NLR where the radio jet starts to dig a way in the medium, then (during the CSS phase) the jet expands into a more tenuous ISM before plunging into the IGM possibly with FRII morphology (see Figure 2.1). In this sequence the source increases its size, progressively decreases its radio luminosity by about one order of magnitude; the turnover in the radio spectrum moves from frequencies $\sim$ 1 GHz for GPSs to $\sim$ hundreds of MHz for CSSs.

In order to understand the nature of GPS/CSS sources I review their radio properties (radio spectra, radio morphology, radio polarisation and radio variability) in more details and summarize also their main properties in the other observational bands.

2.3 Radio Spectra

The turnover in the radio spectrum of GPS/CSS objects is one of the most important identifying characteristics of these sources since it contains information on the source

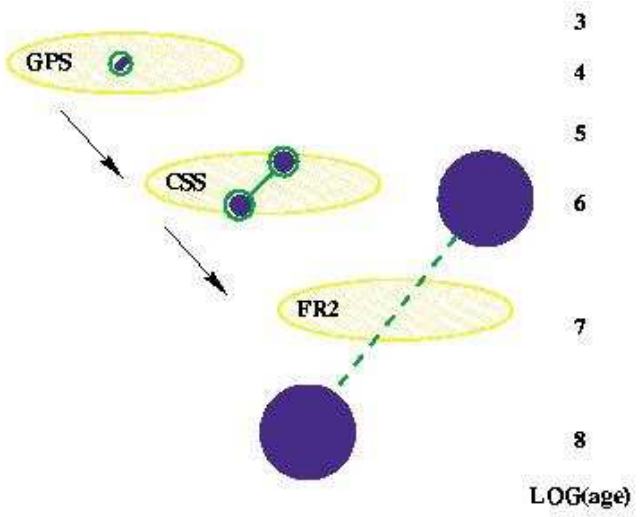

Figure 2.1: Simple schematic of radio source evolution along the GPS-CSS-FR II sequence from de Vries (2003). The yellow ellipse represents the host galaxy, the blue spheres are the radio lobes. The age is expressed in units of years.

size, its physical properties, and its environment. Because of their small angular size, GPS/CSS sources are unresolved for most conventional arrays (like VLA, WSRT, etc.), it is however possible to use these interferometers to study their *integrated* spectra.

These sources have simple peaked spectra with steep spectral indices at high frequencies. O'Dea et al. (1990b, 1991) showed that the spectra of GPS sources can be quite narrow with values for the full width at half the peak flux density of around 1-1.5 decades in frequency. The distributions of spectral indices above the peak is broad, from 0.5 to 1.3, and it is quite similar for GPS and CSS sources. There is a slight indication that the GPS sources have a flatter spectra than the CSSs, but this may be due to the fact that the spectral indices are measured closer to the spectral peak in the GPSs than in the CSSs.

de Vries et al. (1997a) have determined an "average" radio spectrum of 72 GPS radio sources. The average spectral indices, α, below and above the spectral peak are -0.56 and 0.77, respectively ($S \propto \nu^{-\alpha}$). More recently, Snellen et al. (1998c) found for his sample of faint GPS sources optically thick and thin spectral indices of respectively -0.8 and 0.75.

The average value of $\alpha \sim 0.77$ is also typical for the large-scale powerful sources (Kellermann 1966b), suggesting that relativistic electron acceleration and energy loss mech-

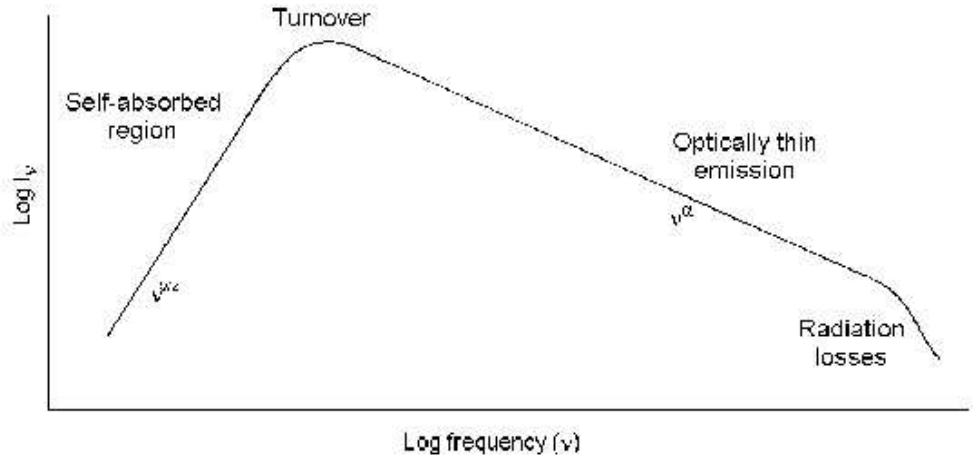

Figure 2.2: Simple schematic of radio source synchrotron spectrum.

anisms preserve the same average spectral index over most of the lifetime of the source. The spectral index remains constant at high frequencies with a few sources showing either steepening from radiation losses, or flattening possibly due to a compact component. This has implications for the inferred **spectral age** of the radiating electrons.

2.3.1 Spectral ageing

In principle, it is possible, under simple assumptions, to relate the higher frequency curvature of the optically thin synchrotron spectrum (see Fig.2.2) to the age of the radiating particles (Kardashev 1962; Kellermann 1964; Pacholczyk 1970; Jaffe & Perola 1974), following a method known as *spectral ageing*. Synchrotron losses are proportional to the electron energy, leading to a depletion of the high-energy electron population and a steepening in the emission spectrum. The *break frequency*, ν_{br}, depends on the radiative age, t_{syn}, and magnetic field, B, as $\nu_{br} \propto B^{-3} t_{syn}^{-2}$. Expressing the radiative age in years, the magnetic field in mG and the break frequency in GHz one finds:

$$t_{syn} = 5.03 \times 10^4 \cdot B_{mG}^{-1.5} [(1+z)\nu_{br}]^{-0.5} (yr) \tag{2.1}$$

where z is the source redshift.

Although synchrotron losses always lead to a high-frequency steepening, the exact shape of the spectral curvature depends on the evolution of the energy input into the relativistic electrons. The "standard" synchrotron loss models consider the evolution of the emission from an electron population with an initial power law energy distribution. Two limiting situations can be considered: (i) a single injection episode of relativistic particles, (ii) a continuous particle injection. For both models the emission spectrum below the break frequency, where radiative losses are not relevant, is a power law. The models differ in the shape of their high-frequency steepening. In the first case there is an exponential cut-off in the emission spectrum (JP model: Jaffe & Perola 1974). In the second case, the continuous energy supply limits the change in spectral index at the break frequency to 0.5 instead of an exponential drop (CI model: Kardashev 1962).

Murgia et al. (1999, 2003) studied two samples of CSS sources: the sample selected from the 3CR and the Peacock & Wall (1981) catalogues (Fanti et al. 1995), and the B3-VLA CSS sample (Fanti et al. 2001). By fitting a numerically computed CI spectrum to the data, they estimated the break frequencies, from which the source ages are obtained if the magnetic field is known. Murgia et al. (1999) assumed equipartition magnetic field of the order of few mG. They found that in **lobe dominated** sources the estimated ages are in the range between $\mathbf{10^2}$ **and** $\mathbf{10^5}$ **yr**, supporting the view that these sources are young. However, the correspondence between electron lifetime and source age is not straightforward. If the source spectrum is dominated by a jet or by hot spots, the radiative age likely represents the lifetime of the electrons in that component and it is expected to be less than the source age. Only when the lobes, which have accumulated the electrons produced over the source lifetime, account for the largest part of the total flux density of the source spectrum, the radiative age likely represents the age of the source.

2.3.2 The spectral turnover and the absorption mechanism

The interpretation of the turnover and of its possible evolution depends on the mechanism producing it. In the GPS/CSS sources the two possibilities that have been discussed so far in the literature are **synchrotron self-absorption** and **free-free absorption**.

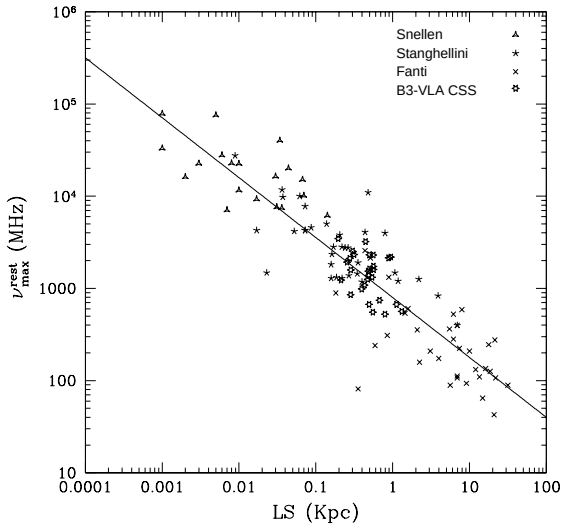

Figure 2.3: Rest frame turnover frequency vs. linear size for the Fanti et al. (1990) CSS sample and Stanghellini et al. (1998), Snellen et al. (1998c) GPS samples. The line is the expected correlation between the linear size, LS, and ν_p in case of synchrotron self-absorption (Fanti et al. private communication).

If the turnover in the spectrum is due to synchrotron self-absorption (SSA), then the turnover frequency in a homogeneous, self-absorbed, incoherent synchrotron radio source with a power-law electron energy distribution is given by:

$$\nu_p \propto B^{1/5} S_p^{2/5} \theta^{-4/5} (1+z)^{1/5} \tag{2.2}$$

where B is the magnetic field, S_p the flux density at the peak, z is the redshift and θ is the angular size. Fanti et al. (1990) and O'Dea & Baum (1997) showed that there is a strong anticorrelation between the linear size and the turnover frequencies of GPS/CSS sources (see next section), as expected for SSA (see Figure 2.3).

However, more recently it was suggested by Bicknell, Dopita & O'Dea (1997) that such correlation can also be explained by a particular model in which these sources undergo free-free absorption by ionized gas surrounding the lobes, where the radiation from shock heated the plasma. In their scenario, the radiation produced by the shock heated plasma is primarely responsable for gas excitation and the consequent emission of the narrow lines in the optical/UV spectrum. Some observations support this theory: de Vries et al. (1997,

1999) have shown radio emission alignment in CSS galaxies; O'Dea et al. (2002) have discovered systematic velocity offsets of the emission lines together with broad profiles and split lines. These features are consistent with motion of the shock excited gas. Moreover, Mutoh et al. (2002) argued that synchrotron self-absorption is not the preferred absorption mechanism in a GPS sample because of the absence of a change of polarisation across the peak of the spectrum. However, we must remark that in GPS galaxies polarisation is extremely low and accurate measurements are not available.

It is possible that free-free absorption and synchrotron self-absorption dominate in different sources and that both absorption mechanisms play a role. However since the anti-correlation between turnover frequency and size can be accounted for quite naturally in terms of synchrotron self-absorption, we assume in the following that this is the dominant mechanism.

2.3.3 Turnover Frequency versus Largest Linear Size

The relationship between the turnover frequency and the projected linear size of the radio source constrains not only the mechanism for the turnover but also models for the source evolution.

In Figure 2.3 the CSS sample of Fanti et al. (1990) is plotted together with the GPS samples of Stanghellini et al. (1998) and Snellen et al. (1998c) in the turnover frequency (ν_{max}^{rest})-linear size (LS) plane. The line is the expected correlation (in the source frame) in the case of synchrotron self absorption (Fanti et al. 2002). This figure shows a remarkable continuity between GPS sources (upper left) and CSS sources (lower right), suggesting that the GPS and CSS sources are simply scaled versions of each other. The correlation is the same independently of optical identification of the sources (galaxies or quasars).

The best fit linear relationship in the log-log plane is (O'Dea & Baum 1997):

$$log(\nu_p) \sim -0.21(\pm 0.05) - 0.65(\pm 0.05) log(LS) \tag{2.3}$$

In the youth scenario, where the small linear size is related to the age of the source, this correlation means that the youngest objects have the highest turnover frequencies and that the peak frequency is expected to move towards lower frequencies as the source expands

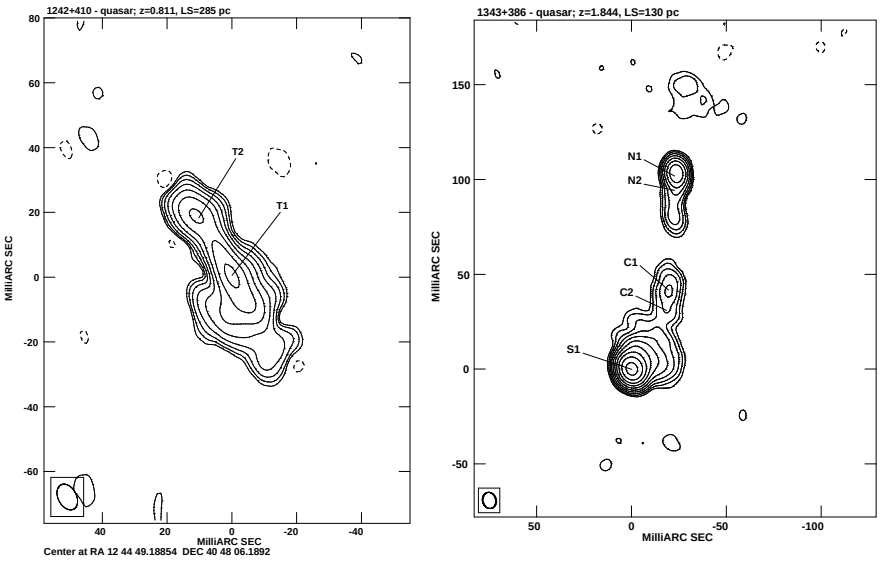

Figure 2.4: VLBA radio images of *quasars* from the B3-VLA CSS sample from Dallacasa et al. (2002)

and the energy density decreases. **In principle, the highest the turnover frequency, the youngest the radio source is.**

2.4 Radio Morphology

The development of a clear picture of the radio properties of GPS/CSS sources is related to the ability to image them with subarcsecond resolution.

In bright radio samples, GPS quasars are found to have core-jet or complex structure. In galaxies most of (if not all) the flux density is accounted for by two well separated steep spectrum components, often well resolved by VLBI observations and characterized by asymmetries in both size and flux density. Sometimes a much weaker, flat spectrum component is detected at high frequencies, clear a signature of the source core.

A large body of data on the radio structures of CSS sources have been accumulated (Spencer et al. 1989, Fanti et al. 1990, Sanghera et al. 1995, Cotton et al. 1997a, 1997b, Dallacasa et al. 2002). The CSS galaxies tend to be doubles and triples (see Fig. 2.5), sometimes asymmetric, while the quasars tend to be triple with a single bright jet (see

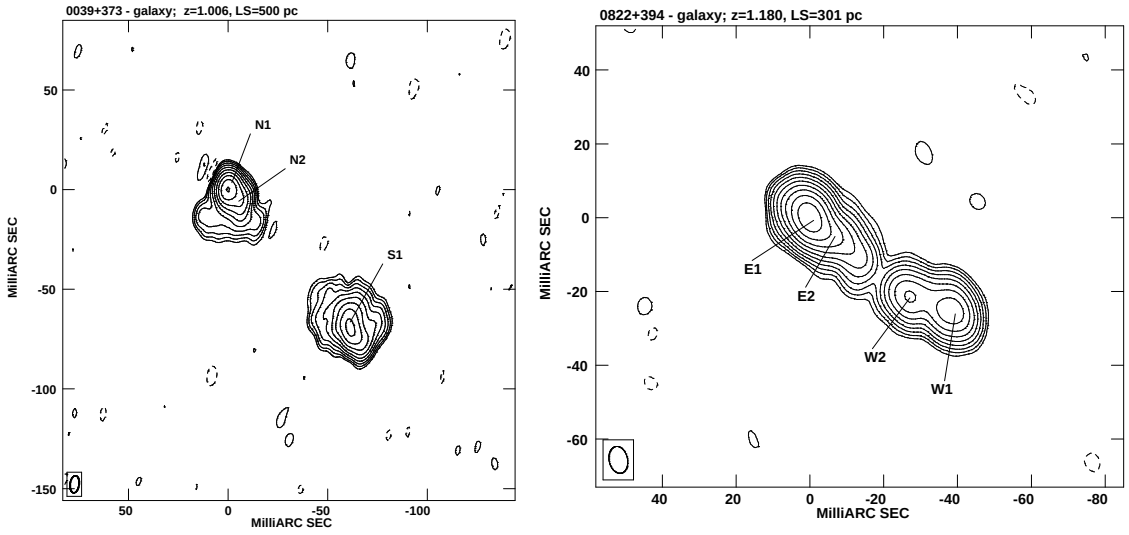

Figure 2.5: VLBA radio images of *galaxies* from the B3-VLA CSS samples from Dallacasa et al. (2002)

Fig. 2.4). Based on early low-fidelity images, the quasars were often thought to be core-jets, but new observations have shown that they are mostly triples. A similar situation may hold for the GPS quasars. The CSS quasars tend to have brighter jets and brighter cores than galaxies.

Some CSS sources have very distorted and asymmetric morphologies that can be due to interaction with dense clouds in their environment. Direct evidence for interactions between the radio jets and ambient gas has been found in some objects (Heckman et al. 1982, van Breugel et al. 1984, O'Dea, Baum & Gallimore 1994). However, in most cases the interaction is merely inferred from the distorted morphology.

The existence of two-sided GPS/CSS radio sources has two important implications. These structure are in contrast to the one-sided "core-jet" structures usually found in powerful compact radio sources (and thought to be due to relativistically boosted jets). On the other hand, there is a continuity in morphology between the GPS and CSS sources and the large-scale radio sources.

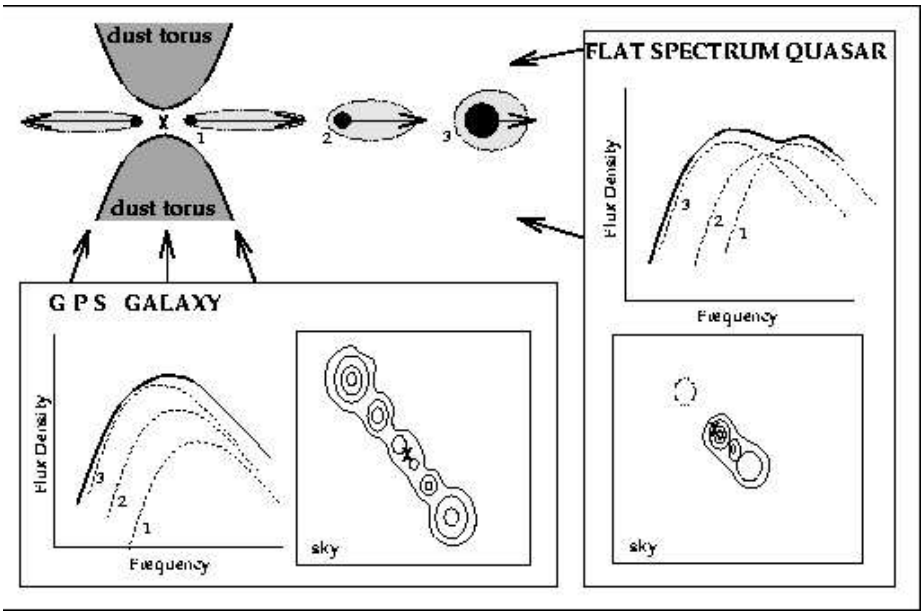

Figure 2.6: The decelerated component model combined with the orientation unification scheme from Snellen et al. (1998c)

2.4.1 Compact Symmetric Objects

The two sided radio structure is a very distinctive morphological property of intrinsically small radio sources. When selected from VLBI surveys they constitute a class of objects, named **Compact Symmetric Objects** (CSO) (Wilkinson et al. 1994). The large majority of CSOs exhibit a gigahertz-peaked spectrum. The overlap between CSO and GPS galaxies is large but not complete. Still, CSOs and GPSs can be the same class of objects since orientation effects can modify both the observed morphology and the radio spectrum in such a way that the objects cannot be formally classified as CSO or GPS respectively (Snellen et al. 1998a). Stanghellini et al. (1996) have shown that about 90% of the GPS sources identified with galaxies are CSOs. The main contributors to the overall radio spectrum are the synchrotron self-absorbed mini-lobes, located at the outer edges of most CSOs. They also produce the peak at about 1 GHz in frequency. However, if a CSO were oriented at a small angle to the line of sight, the contributions of the central core and of the fast moving jet feeding the approaching mini-lobe become important, producing a flattish and variable spectrum (Snellen et al. 1998c, see Fig. 2.6). Observed at such a small

viewing angle, the large contrast between the approaching and receding side of the radio source would make it also increasingly difficult to identify the objects as a CSO. The compact symmetric structure indicates that the relativistic boosting is relatively unimportant, otherwise only the radio emission on the side directed towards us would be visible. This implies that these components are not ejected from the nucleus at small angles to the line of sight or at highly relativistic speeds. However it is not excluded that the components move at highly relativistic speeds at large angle to the line of sight.

CSOs usually contain bright compact *hotspot* components located at the extremities of the source, representing the working surface as the jet propagates through the ISM. Using multi-epoch VLBI observations it is possible to measure or set limits on the rate of separation of these hotspots.

The first upper limits on the rate of hotspot separation in CSOs (Tzioumis et al. 1989) showed that their velocities were sub-relativistic and hence much smaller than for the core-jet objects. The first unambiguous detections of CSO expansion were reported in the CSOs 0710+439 (Owsianik & Conway 1998) and 0108+388 (Owsianik, Conway & Polatidis 1998) based on multi-epoch VLBI observations over a decade or more. Since then, detections or upper limits on expansion velocity have been determinated for 13 CSOs. Amongst the detections, the expansion rates range between $0.1h^{-1}c$ and $\sim 0.4h^{-1}c$, the unweighted mean value being $0.19h^{-1}c$ ($0.17h^{-1}c$ including the limits.) In several cases, motions have been detected for components which are not at the edges of the source. In these cases the outward velocities of the jet components are measured and, as expected for a jet origin, they are larger than for the hotspots components. In most cases these results are consistent with jet components moving with Lorentz factor γ between 2 and 5, but at relatively large angles to the line of sight.

Kinematic Ages of CSOs

The most direct result of the CSO expansion measurements are the low kinematics ages derived by dividing the projected source size (typically between few pc and 100 pc) by the measured projected separation velocities which are all $\leq \mathbf{3 \times 10^3}$ **yr**. Even if the exact values may be revised as new measurements are added, this implies that **CSOs are young**

objects. This constitutes so far the most direct way to estimate the age of an extragalactic radio source. The age estimates of some CSOs and the larger double sources (medium symmetric objects- MSOs) have been done via the detection of high frequency breaks in their spectra due to ageing of electrons in the lobes. Minimum energy and equipartition conditions are usually assumed (see Section 2.3.1). The estimated spectral ages are $10^3 - 10^4$ yr, in agreement with the kinematic ages (Murgia et al. 1999, 2003).

The close agreement between kinematic and spectral age estimates suggests that most CSOs are indeed young radio-loud sources and that particles and fields are probably close to equipartition in CSOs and that the standard model of radiative ageing is roughly correct.

2.4.2 Extended emission

An important point in the study of GPS/CSS sources is whether they are truly compact sources or whether they are just the inner parts of much more extended sources. The majority of the sources in the Fanti et al. (1990) CSS sample from the 3CR catalogue (Jenkins et al. 1977) and Peacock and Wall (PW) sample (1982) do not show any evidence for extended emission on scales larger than $\sim 10 - 20$ kpc up to $\lesssim 3\%$ of the compact emission (van Breugel et al. 1992). Only a few sources are now known to have larger scale structure; they are probably large doubles with radio axes at a small angle to the line of sight.

In 1990 Baum et al. reported the discovery of extended emission around the CSO 0108+388 and Stanghellini et al. (1990a, 1990b) reported extended emission associated with the candidate GPS sources 0201+113 and 1045+019. Both 0108+388 and 0201+113 were also associated with GPS-type spectra (Baum et al. 1990; O'Dea et al. 1990b). Moreover, the detection of arcsecond scale faint extended emission around $\sim 10\%$ of GPS sources (Baum et al. 1990; Stanghellini et al. 1990) motivated Baum et al. (1990) to suggest that the nuclear activity is **recurrent** in these sources. In this hypothesis, we see the relic of a previous activity as faint steep-spectrum diffuse emission surrounding the current young nuclear source.

Baum et al. (1990) also suggested another possible scenario: the *smothered* sources.

If the parsec-scale jet in a large-scale radio source is smothered and the jet propagation is halted on the scales of tens of parsecs, then the source would have both the still existing large-scale structure and the confined parsec-scale source with a GPS spectrum. The smothering could be produced by a large inflow of dense gas acquired in galactic cannibalism (Baum et al. 1990) or by distortion of the central torus causing the jet to ram into the dense torus gas (Gopal-Krishna 1995). Since the extended emission is no longer supplied by the jet, it would become faint and diffuse.

Recently, Stanghellini (2003) has examined all the sources of the complete sample of bright GPS radio sources selected by Stanghellini et al. (1998) where arcsecond scale extended emission has been detected around the compact component. Only one case (0108+388) is a good example of a radio source which has been reborn (in the framework of the youth scenario) or whose jets have been disrupted (in the framework of the "smothered sources"). The radio galaxy 1345+125 may also be explained in such a way, but in the other cases (all quasars) studied the most natural explanation is that we see a large radio source where the inner part of the jet is boosted because is pointed towards us. Taking into account the redshift distribution of the GPS quasars, the extended emission at the level of that detected around the closest quasar of the sample would be too weak to be detected for most of the other quasars in the sample. Therefore it seems from this analysis that the GPS quasars showing a core-jet or complex morphology at mas scales are likely large radio sources at high redshift where only the inner part of the jet is visible due to relativistic and projection effects. If this is true, most of GPS quasars are intrinsically more similar to the flat spectrum radio sources which dominate the radio surveys at cm wavelengths and are not related to the CSO phenomenon.

2.5 Radio Polarisation

Measurements of the polarisation state of the radio emission from GPS and CSS sources can give a great deal of information about the physical conditions inside and in front of the emitting region.

Intrinsically small sources are in regions close to the active nucleus where a sub-

stantial amount of high energy radiation is produced and where ionization and magnetic field strength are important. Consequently Faraday rotation is likely to be significant in GPS and CSS sources. The intrinsic polarisation angle is rotated by:

$$\Delta\Phi/rad = 8.1 \times 10^5 \lambda^2 \int n_e H_{\|} dl \qquad [\lambda/m, dl/pc] \tag{2.4}$$

where n_e is the electron density (m^{-3}) and $H_{\|}$ (G) is the component of the magnetic field parallel to the line of sight . The *rotation measure* is the amount of Faraday rotation expressed in $rad \cdot m^{-2}$. The Faraday rotation is proportional to the wavelength squared and can be determined from observations at a number of wavelengths, giving an integral along the line of sight of the thermal electron density times the parallel component of the magnetic field. Strong variations of Faraday rotation within the telescope beam will reduce the observed fractional polarisation producing depolarisation, which occurs when the inhomogeneities of the Faraday screen are not resolved by the observations. This effect can, and frequently does, completely depolarize regions of emission, especially at longer wavelengths.

Since GPS sources are very small, they reside in the inner regions of the host and are generally within the NLR with its relatively large column densities of ionized plasma. Strong Faraday effects are to be expected in these sources, likely completely depolarizing them at longer wavelengths.

CSS sources are still subgalactic in size but frequently exceed the size of the NLR, so Faraday effects in the outer parts of these sources should be less than in the inner regions. However, jet cloud interactions anywhere in the galaxy may give rise to local enhancements in the plasma density, hence local Faraday rotation. As jet-cloud interactions will likely deflect the jet, enhanced Faraday effects (either rotation or depolarisation) are expected near the bends that are common in CSS jets.

Rudnick & Jones (1982) first pointed out that the GPS sources tend to have low centimeter-wavelength polarisation. Further observations (O'Dea et al. 1990b; Aller, Aller, & Hughes 1992; Stanghellini et al. 1998b) have firmly established that GPS sources have very low integrated polarisation ($\sim 0.2\%$ at 6 cm). At present, there are not many high-frequency ($\nu \gtrsim 8.4$ GHz) measurements, so that the frequency dependence of the po-

larisation is not known. The low integrated polarisation could be due to:

- cancellation of polarisation due to vector averaging of polarisations with different orientations in different components;
- a very tangled magnetic field;
- large Faraday depths in or around the radio source.

The lack of high polarisation in individual components in the sources argues against the first hypothesis as an explanation. Cawthorne et al. (1993a) also favor high Faraday depths as the explanation for the low polarisation in the GPS galaxies.

The fractional polarisation of the CSS sources tends to be higher than those of the GPS sources ($\sim 1\% - 3\%$ at 6 cm) and higher still ($\sim 6\% - 7\%$) at higher frequencies (van Breugel et al. 1984a, 1992; Saikia, Singal & Cornell 1987; Mantovani et al. 1994, Sanghera et al. 1995; Akujor & Garrington 1995). The fact that the polarisation increases with increasing frequency (in the CSS sources) suggests that large Faraday depths are responsible for the depolarisation between 5 and 15 GHz rather than magnetic field geometry.

There is some evidence that the CSS quasars have higher polarisation than the CSS galaxies at 6 cm (Saikia et al. 1987; Sanghera et al. 1995). However, Akujior & Garrington (1995) find that quasars and galaxies have a similar distribution of fractional polarisation at 3.6 cm.

The GPS galaxies of the complete sample of Stanghellini et al. (1998) are undetected at 6 cm by the VLA below 0.3% and many below 0.1%. The GPS quasars instead have a mean fractional polarisation at 6 cm of 1.2%. In a sample of non-GPS quasars, chosen for comparison with GPS sources, Stanghellini et al. (1999, 2003) found an average fractional polarisation of 1.8% at the same frequency. Therefore there is some evidence that GPS quasars have a lower fractional polarisation than non-GPS quasars but they are significantly more polarised than GPS galaxies.

The polarisation properties of the GPS/CSO sources are in good agreement with the expectations of the young radio galaxy scenario: they are strongly depolarised. However, there is a number of sources, especially quasars, with GPS spectra showing significant

linearly polarised emission which may also be time variable. It is not clear whether these sources fit into the standard evolutionary picture as newly born radio galaxies or may simply be blazars with a single dominant component or intervening free-free absorbing screen.

The well-studied CSS sources have also polarisation properties in agreement with the general expectations of the evolutionary scenario; smaller sources are more depolarised than larger ones. However, this distinction does not appear to be a gradual increase in polarisation with source size but a discontinuity at total source size of about 6 kpc (Cotton et al. 2003). This needs further study but could be related to the outer boundary of the NLR. A number of CSS sources with bent jets appear to have enhanced Faraday rotation associated with the bends in the jets, supporting the hypothesis that much of the ionized plasma in these objects is produced by jet-ISM interaction.

2.6 Variability and Beaming

It is often stated in the literature that GPS radio sources have little variability and do not show superluminal motions in their pc-scale structures, namely the relativistic effects often seen in flat spectrum radio sources. These characteristics are attributed to the GPS class without distinction between galaxies and quasars. However, systematic studies are lacking, since flux density monitoring campaigns on large samples of GPS/CSS sources have never been carried out. Moreover, not much is known about variability at other wave bands. In the radio, GPS/CSS sources show only minor variations, e.g. $\sim 10\%$ over a timescale of ~ 1 yr. However, there are counter examples of sources (**all quasars**) that are much more variable.

Some CSSs are observed to vary at low frequencies; however, these cases are thought to be due to extrinsic effects, e.g. refractive scintillation or ionospheric Faraday rotation (see, e.g. Mantovani et al. 1992). Fanti et al. (1990b) and Saikia et al. (1995) have considered the orientation-dependent properties of CSS sources in order to determine whether beaming is significant. Fanti et al. concluded that the radio luminosity of the CSS sources was not strongly affected by Doppler boosting but that quasars seemed more asymmetric and distorted than expected purely on the basis of projection effects. Saikia et

al. has compared the fraction of total emission contributed by the core, projected linear size, misalignment angle, ratio of distances from the core to the lobes, and ratio of flux densities of the lobes for a sample of CSS sources and a sample of larger 3CR sources. They find that the distributions of these orientation indicators are consistent with the differences in the CSS galaxies and quasars being due primarily to orientation, i.e. CSS quasars are oriented at smaller angles to the line of sight than CSS galaxies. However, the CSS sources have more extreme values of these parameters than found in large scale sources (i.e., the CSS sources are more asymmetric than the larger scale sources). Saikia et al. suggest that this is due to an additional effect: interaction of radio emitting plasma with dense clouds in the environment.

Stanghellini et al. (2003) have compared the flux density measurements for the objects in common between the complete sample (Stanghellini et al. 1998, 1999) and the sources observed by Perley (1982). For the galaxies the mean variability has been found to be around 5%, which can be comparable to the uncertainties on the flux density calibrator, while for the confirmed GPS quasars it is 20%. For a comparison sample of flat spectrum radio sources the mean variability has been found to be $\sim 22\%$.

Jauncey et al. (2003) have monitored a sample of 34 southern hemisphere candidate GPS sources, drawn from the 2.7 GHz Parkes survey, during 65 observing sessions spread roughly uniformly over a 30-month period from 1990 through 1993 (King et al. 1993; King et al. 1994). These sources do not form a complete sample, but are collected from a variety of surveys. The majority of the sources have spectral peaks below ~ 3 GHz. This monitoring program on total flux density, together with VLBI monitoring data, shows that a small fraction of these sources ($\sim 10\%$) vary. Their variability corresponds to several categories: sources whose spectral classification is, at best, episodic on a timescale of years; sources with a stable GPS classification that vary; finally, a small number of sources that are affected by interstellar scintillation, but maintain a mean GPS spectrum. Existing data on GPS sources with higher frequency peaks, ≥ 3 GHz, reveals that many such sources vary. The variable GPS sources most likely represent the slow evolution of the usual month-to year variability commonly observed in flat spectrum sources, which exhibit GPS spectra.

2.7 Other bands properties

Although GPS and CSS sources are now receiving considerable attention in the radio band, there are no comprehensive studies other wavelengths. Here we have summarized the properties of GPS/CSS sources at different wavelength, putting together the available information from the literature:

Far-infrared properties

The infrared properties of the GPS and CSS sources can in principle give information on the properties of the central engine and on its immediate environment. In particular, the hypothesis that GPS/CSS are confined sources requires a rather dense interstellar medium (average density $n_{ISM} \gg 1$ cm^{-3} and total mass within 1 kpc $M_{ISM} > 10^8 M_\odot$; see De Young 1993; Fanti et al. 1995) which is in the path of the radio source. Even if the host galaxy contains a lot of gas, but it is distributed in a disk perpendicular to the radio source axis, it will have little effect on the radio source propagation. The *frustrating* gas has to be distributed over a large volume. If the nucleus in GPS sources is surrounded by gas and dust with a higher covering factor than in "normal" extended radio galaxies, a higher fraction of the optical-UV continuum light is expected to be reprocessed and to emerge as medium-far IR (MFIR) radiation. In this scenario, GPS sources should be brighter in the MFIR than "normal" radio sources.

Fanti et al. (2000) presented results from observations obtained with ISOPHOT, on board the ISO satellite, of a representative sample of seventeen CSS/GPS radio galaxies and of a control sample of sixteen extended radio galaxies spanning similar ranges in redshift ($0.2 \leq z \leq 0.8$) and radio luminosity ($P_{2.7GHz} \geq 10^{26}$W/Hz). These observations were performed at λ=60, 90, 174 and 200 μm. Even if the resulting performance of ISOPHOT was not very good they detected seven of the GPS/CSS sources and five objects of the comparison sample at $\geq 3\sigma$.

No evidence has been found that the MFIR luminosities of the GPS/CSS sources are different from those of the extended objects. For dust temperatures $\geq$ 30 K, they deduced masses of the interstellar gas much lower than required by the frustration scenario.

For lower dust temperatures larger masses would be allowed for by the data, but they would produce a larger amount of obscuration and reddening in the optical, which is not seen in the existing data.

All this argues against the GPS/CSS sources being "frustrated" by a dense ambient medium.

Optical properties

The study of optical properties of GPS/CSS radio sources gives information about the host galaxies of these powerful radio sources and their nuclear properties. The first important point is the optical identification and consequently the measurement of the **redshift distribution**. This sets the distance and absolute host galaxy luminosity. These quantities are necessary to compare sources on the same physical scale. Moreover, studies of the host galaxies magnitudes, morphology, colors, polarisations and emission line properties give information on the environmental properties that may trigger the radio activity (like clustering/grouping of galaxies, merger activity in the host galaxy, presence of gas reservoirs which may be tapped to fuel the AGN) and in which the radio source expands and interacts with.

Galaxies and quasars are almost equally represented in GPS samples (Stanghellini et al. 1998) while most CSS sources are galaxies (Dallacasa 2002b,c). Even if the optical identification of the GPS/CSS samples is often not complete their distributions reveal the trend of quasars and galaxies to have barely overlapping redshift ranges. Galaxies tend to be at redshifts $0.1 \lesssim z \lesssim 1$ while quasars are often found at very large redshift $1 \lesssim z \lesssim 4$ (O'Dea et al. 1990, O'Dea et al. 1996, Stanghellini et al. 1998). It is important to establish whether this dependence of optical host on redshift is genuine or if it is due to selection effects.

GPS galaxies are likely to be biased towards low redshift because it is increasingly difficult to measure their emission-line features. Moreover, the high-redshift GPS quasars are found to have substantially higher rest-frame radio peak frequencies than the GPS galaxies (Stanghellini et al. 1998, Snellen et al. 1998). If a population of low-redshift GPS quasars with similar peak frequencies as the high-redshift quasars exists, it would not have

been included in the radio-bright samples as a results of their too high observed radio peak frequencies. In order to investigate both these selection effects Snellen et al. (1999) studied a sample of **faint** GPS radio sources selected in such a way that is unlikely that a significant population of low-redshift GPS quasars has been missed because of selection effects. The redshift distributions of GPS galaxies and quasars is found to be different also in this radio-faint sample, not only in the bright samples (Stanghellini et al. 1998). Therefore it seems that this difference is genuine and not due to a redshift-luminosity degeneracy. Snellen et al. (1999) claimed that unlikely GPS quasars and galaxies are unified by orientation, because this would require the quasar opening angle to be a strong function of redshift. They therefore suggest that GPS quasars and galaxies are not related even if they have identical observed radio spectral properties and that GPS quasars are a subclass of flat-spectrum quasars.

X-ray Emission

Observations in the X-ray band could help in understanding the emission processes, the dynamics related to radio-emitting structures and in particular if the X-ray emission is directly connected to the expanding jet. Extended X-ray emission associated with local halo or cluster ($T \sim 10^7$ K) could help in studying the environment of GPS/CSS sources, and it could allow to detect the remnants of a merger event or a signature of interactions between expanding radio plasma and the IGM. In addition X-ray spectra can constrain the total absorbing column and if there is sufficient material to confine the GPS source. X-rays can also help in understanding any link between GPS and large scale radio sources and in particular whether there is sign of an intermittent activity and whether GPS sources grow into large radio galaxies.

During the last two decades there has been **no** systematic X-ray study of GPS/CSS sources and only a few X-ray observations have been performed. O'Dea (1998) lists 31 sources with available X-ray information, including seven sources with upper limits only. This sample shows that galaxies are less luminous than quasars in X-rays. Elvis et al. (1994) observed X-ray absorption in two out of three high redshift GPS quasars, suggesting that their environment might be different from other quasars. ROSAT upper limits for

a few GPS/CSS galaxies imply $L_X < 3 \times 10^{42}$ergs^{-1}, consistent with the X-ray emission expected from early type galaxies. O'Dea et al. (2000) presented the first X-ray with ASCA detection of a GPS galaxy, which had $L_X \sim 2 \times 10^{42}$ergs^{-1}. Before *Chandra*, observations at the highest spatial resolution were made with the ROSAT HRI, which revealed that two out of four GPS quasars showed traces of extended emission (Antonelli & Fiore 1997).

The *Chandra* X-ray Observatory has discovered many X-ray jets associated with radio structures in radio galaxies and quasars. *Chandra* is the only X-ray telescope which can resolve structure on $\sim$ arcsec scales, and this is suited for studying the environment of GPS/CSS sources. Siemiginowska et al. (2003) discovered X-ray jets in two GPS quasars, PKS1127-145 and B2 0738+313, indicating that X-ray emission associated with relativistic plasma is present at large distances from the GPS nucleus ($\sim$ 300 kpc projected). These structures can be too faint to be easily detected in the radio. In order to better investigate these issues, Siemiginowska et al. (2003) selected a sample of 14 GPS/CSS sources for a systematic X-ray study with the following characteristics: radio size $>$ 2 arcsec, redshift $<$ 2, low galactic hydrogen column. Their observations are compatible with the intermittent activity model, in which old electrons from previous activity are detectable in X-rays, via CMB Comptonization while new components expand into the medium formed by the previous active phase. However, six GPS sources show intrinsic absorption columns: $N_H > 10^{21} cm^{-2}$ that means a density $n_e > 0.03 - 0.3$cm^{-3} suggesting that the sources could be both confined and intermittent.

The discovery of extended X-ray jets associated with GPS quasars is in contrast with the *youthness* hypothesis. The available X-ray observations are compatible with both the confined and intermittent activity models. Alternatively GPS quasars can be simply be extended radio sources, whose core is boosted towards us (see Stanghellini 2003).

Chapter 3

The Sample of High Frequency Peakers

3.1 Introduction

As discussed in Chapter 2, the currently accepted model (the *youth scenario*) relates the small linear size of GPS/CSS sources to their age, implying that they are the progenitors of extended radio sources. In this framework, the well defined anti-correlation between the radio turnover frequency, ν_p, and the projected angular size, θ (O'Dea & Baum 1997; Fanti et al. 2002) means that the youngest objects have the highest turnover frequencies and that the peak frequency is expected to move towards lower frequencies as the source expands and the energy density decreases. In principle, the highest the turnover frequency, the youngest the radio source is. This provides a strong motivation for searches of "extreme" GPS sources, with spectral peaks at frequencies of tens of GHz, that may provide an opportunity to study radio sources very close to their birth. These objects, however, are likely to be very rare because their expansion rate, and therefore the rate of decrease of their peak frequency, is thought to be very rapid.

A complete sample of bright candidate GPS sources peaking above $\simeq 5\,\mathrm{GHz}$ has been obtained by Dallacasa et al. (2000), who termed such sources "High Frequency Peakers" (HFPs). As pointed out by these authors, only a fraction of their objects are expected

to be truly newborn sources since the sample is contaminated by beamed quasars (see also Snellen et al. 1999, Stanghellini et al. 2003); multifrequency observations at various epochs, polarimetric measurements and high-resolution imaging are necessary to assess the nature of the selected sources.

In this chapter I describe the observational work carried out so far in this direction.

3.2 Selection of the sample of High Frequency Peakers

The **bright** HFP sample of Dallacasa et al. (2000) was selected by cross-correlating the 87GB (Gregory et al. 1996) sources with $S_{4.9\mathrm{GHz}} \geq 300\,\mathrm{mJy}$ with the NVSS catalogue (Condon et al. 1998) at 1.4 GHz and picking out those with inverted spectra ($\alpha < -0.5$, $S \propto \nu^{-\alpha}$). The bright sample covered nearly the whole area of the 87GB (declination between 0 and 75°), excluding objects with $\mid b_{II} \mid < 10^{\circ}$ to avoid the Galactic plane. The constrains in declination and galactic latitude leave an area of 4.978 sr; however the effective area where the cross identification between the 87GB and the NVSS was made is 4.825 sr (i.e., 15840 square degrees).

Since the 87GB and the NVSS surveys were carried out at different epochs, this sample is contaminated by flat-spectrum sources that happened to be flaring when they were observed at 4.9 GHz. The sample was then "cleaned" by means of simultaneous multifrequency VLA observations at 1.365, 1.665, 4.535, 4.985, 8.085, 8.485, 14.96 and 22.46 GHz, leaving 55 sources whose single-epoch radio spectrum peaks at frequencies ranging from a few GHz to about 22 GHz. These "first epoch" observations were carried out in 1998–1999 (Dallacasa et al. 2000). The final number of HFPs represents a rather conspicuous fraction (3%) of the 1750 sources in the 87GB and NVSS catalogues and brighter than 300 mJy at 4.9 GHz.

This selection is independent of the optical identification. About half of the bright HFPs had already been identified in the literature and a project to complete such information is ongoing (Dallacasa et al. 2002a). The final sample of HFP candidates comprises 11 galaxies (including a type 1 Seyfert), 36 quasars, and 8 still unidentified sources (Dallacasa et al. 2002a). For comparison, galaxies and quasars are almost equally represented in

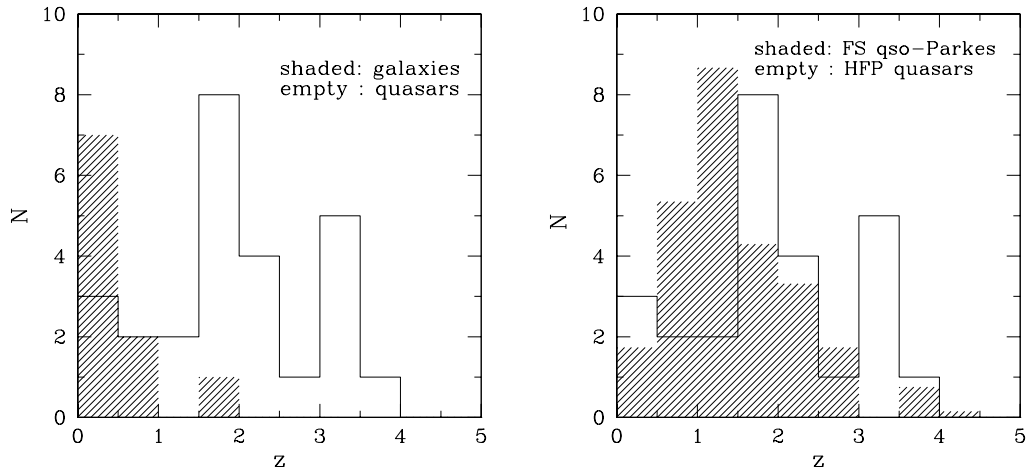

Figure 3.1: Distribution of measured redshifts for the sample by Dallacasa et al. (2000) (left-hand panel). Comparison between the redshift distributions of HFP quasars and flat-spectrum quasars in the 2.7 GHz Parkes quarter Jansky sample (Jackson et al. 2002) (right-hand panel).

bright GPS samples (Stanghellini et al. 1998) and most CSS sources are galaxies (Dallacasa 2002b,c). 36 objects out of 55 have known redshift and their distribution (Fig. 3.1, left-hand panel) confirms the trend of quasars and galaxies to have barely overlapping redshift ranges. The redshift distribution of HFP quasars is shifted to higher redshifts compared to the flat-spectrum quasars in the 2.7 GHz Parkes quarter Jansky sample (Jackson et al. 2002) with a similar flux-density limit, although at a slightly lower frequency (Fig. 3.1, right-hand panel). This difference can be due, at least partly, to the more favorable K-correction for high-z HFPs associated with their inverted spectra, and to the increasing variability amplitude with increasing frequency (Impey & Neugebauer 1988; Ciaramella et al. 2004), which also enhances the visibility of distant quasars.

3.3 VLA Observations and data reduction

In July 2002 we carried out multifrequency radio observations of the 45 (out of 55) candidate HFPs that were visible during the allocated observing time. We used the VLA in the B configuration, with a frequency coverage similar to that used for the sample

definition. This sub-sample comprises 10 galaxies (including the type 1 Seyfert), 28 stellar objects, henceforth referred to as "quasars" (including a BL Lac), and 7 unidentified sources. We used the intermediate frequencies (IFs) of 1.465 and 1.665 GHz in the L band, of 4.565 and 4.935 GHz in the C band, and of 8.085 and 8.465 GHz in the X band, while the standard VLA frequencies were used in the U band (14.96 GHz) and in the K band (22.46 GHz). The observing bandwidth was chosen to be 50 MHz per IF. Separate analysis for each IF in L, C and X bands was carried out in order to improve the spectral coverage of the data.

Each source was observed typically for 1 min in C, X, U and K bands, and for 9 min in L band in a single snapshot, cycling through frequencies. The flux density measurements can thus be considered as simultaneous.

Two scans were spent on the primary flux density calibrator 3C286, which was used also for the calibration of the absolute orientation of the polarisation vector. Secondary calibrators were observed for 1.5 min at each frequency about every 25 min; they were chosen aiming at minimizing the telescope slewing time. Accurate positions of the target sources were obtained from the JVAS catalogue (Patnaik et al. 1992; Browne et al. 1998; Wilkinson et al. 1998).

The data reduction followed the standard procedures for the VLA, implemented in the NRAO AIPS software. The L-band imaging has been quite complicated since a number of confusing sources fall within the primary beam, and an accurate flux density measurement could be obtained only once the confusing sources had been removed. Generally, at least one iteration of phase-only self-calibration has been performed before the final imaging, although a few sources required several iterations. Some radio frequency interferences affected the 1.665 GHz data, so that a few sources could not be imaged and flux densities could not be derived at this frequency. A Gaussian fit was performed on the final image by means of the task JMFIT for the compact component accounting for most if not all the source flux density, while the flux densities of the extended sources were determined with TVSTAT and IMSTAT.

The L band observations by Dallacasa et al. (2000) were not adequate to reveal possible extended emission given that were taken with the VLA in various configurations and were too short (1 min). The present deeper observations detected extended emission

for a considerable fraction of sources (see Sect. 3.3.2).

The r.m.s. noise levels in the image plane are relevant only for flux densities of a few mJy and are generally consistent with the expected thermal noise. For our bright sources the main uncertainty comes from the amplitude calibration error, conservatively estimated to be (1σ) 3% for the L, C and X bands, 5% for the U band, and 10% for the K band and therefore the r.m.s. noise has been considered for extended components only.

The new multifrequency measurements are listed in columns 6–13 of Table 3.1, together with the J2000 name (col. 1), the optical identification (column 2) taken from the NED database or by Dallacasa et al. (2002a), the redshift (column 3) taken from the NED database, the 4.9 GHz flux density (col. 4) measured by Dallacasa et al. (2000); the labels C and E in col. 5 stand for *compact* and *extended* sources, respectively, as seen in the L band images (see Sect. 3.3.2).

The time-lag between the present data-set and the previous observations is of about 3 to 4 years. The two data sets will be referred to as first and second epoch VLA observations. The epoch of each observation of every source is specified in Table 3.2.

3.3.1 Spectral analysis

In order to estimate the peak flux densities, S_p, and frequencies, ν_p, of the sources, we have fitted the simultaneous radio spectra at the two epochs using an hyperbolic function (Dallacasa et al. 2000) of the form:

$$\log(S) = a - \left[b^2 + (c\log\nu - d)^2\right]^{1/2} \tag{3.1}$$

with the optically thin and thick spectral indices as asymptotes. The parameters of this function are related to S_p and ν_p. The first derivative of Eq. (3.1) with respect to $\log\nu$ gives the relation between the peak flux frequency and the parameters of the function : $\log(\nu_p) = d/c$. If we substitute this value in Eq. (3.1) we obtain $\log(S_p) = a - b$. Finally, Eq. (3.1) can be rewritten as:

$$\log(S) = \log(S_p) + b - \left[b^2 + c^2(\log\nu - \log\nu_p)^2\right]^{1/2}. \tag{3.2}$$

The best fit values of ν_p and S_p, obtained minimizing the chi-square function with the Minuit package (CERN libraries), are reported, with their formal errors, in Table 3.2. The

J2000 Name	ID	z	$S_{5.0}^{\rm old}$ mJy		$S_{1.4}$ mJy	$S_{1.7}$ mJy	$S_{4.5}$ mJy	$S_{4.9}$ mJy	$S_{8.1}$ mJy	$S_{8.5}$ mJy	$S_{15.0}$ mJy	$S_{22.5}$ mJy
0003+2129	G*	0.4	265	C	102	120	250	253	234	227	140	86
0005+0524	Q	1.887	229	C	168	186	220	213	171	166	111	82
0037+0808	G?	>1.8	292	C	101	118	281	283	267	262	190	143
0111+3906	G	0.668	1324	E	476	594	1313	1286	978	937	507	315
0116+2422			243	C	110	124	254	258	252	248		149
0217+0144	Q	1.715	1862	E	810	802	743	745	810	810	856	838
0329+3510	Q*		770	E	442	462	560	555	608	613	659	702
0357+2319	Q*		560	C	139	133	131	130	143	144	154	168
0428+3259	G*	0.3	506	E	177	202	493	506	525	514	375	263
0519+0848			278	E	279	296	446	446	435	430	420	401
0625+4440	BL		442	C	172	184	231	231	238	238	219	210
0638+5933			591	C	277	301	590	606	668	667	620	567
0642+6758	Q	3.180	474	C	245	288	429	417	331	321	203	149
0646+4451	Q	3.396	1896	C	522	612	2580	2770	3709	3757	3691	3318
0650+6001	Q	0.455	1236	C	517	625	1142	1136	989	964	671	495
1335+4542	Q	2.449	735	C	294	366	797	785	613	592	359	234
1335+5844			723	C	319	396	734	725	680	671	531	253
1407+2827	G	0.0769	2362	C	910	1100	2469	2463	2114	2050	1139	604
1412+1334			330	C	205	236	345	337	275	267	185	130
1424+2256	Q	3.626	607	C	352	414	686	669	479	460	251	145
1430+1043	Q	1.710	910	C	326	402	885	882	770	752	546	385
1457+0749			241	E	360	367	262	251	194	188	141	109
1505+0326	Q	0.411	929	C	413	465	740	741	721	710	665	567
1511+0518	Sy1	0.084	536	C	90	115	568	607	848	861	843	617
1526+6650	Q	3.02	411	C	115	145	408	410	352	341	193	107
1603+1105			270	C?	182	188	214	214	225	225	234	217
1616+0459	Q	3.197	892	C	317	382	787	771	582	559	333	212
1623+6624	G	0.203	298	C	159	175	295	298	287	283	224	175
1645+6330	Q	2.379	513	C	303	315	510	526	615	618	596	493
1735+5049	G?		968	C	448		925	943	934	920	740	587
1800+3848	Q	2.092	791	E	313	331	702	748	1044	1063	1174	1076
1811+1704	Q*		691	E	545	530	494	491	508	509	499	418
1840+3900	Q	3.095	203	C	125	130	169	167	161	158	134	114
1850+2825	Q	2.560	1246	C	203	223	1096	1185	1540	1541	1318	1045
1855+3742	G*	0.5	364	C	193	191	362	345	222	212	124	91
2021+0515	Q*		477	C	260	302	450	441	377	368	267	191
2024+1718	S	1.050?	572	E	280	304	676	704	803	800	697	569
2101+0341	Q	1.013	920	E	553	610	694	678	593	583	499	478
2123+0535	Q	1.878	1896	E	1954	2006	2084	2111	2462	2482	2755	2560
2203+1007	G*	0.9	319	C	124	123	312	306	243	234	129	77
2207+1652	Q*		551	E	223		249	247	227	223	188	163
2212+2355	S		1182	C	601		963	979	1033	1028	975	915
2257+0243	Q	2.081	274	C	174		274	292	439	450	558	528
2320+0513	Q	0.622	1196	E	640		657	656	720	725	806	843
2330+3348	Q	1.809	558	C	370	383	407	407	457	463	532	548

Table 3.1: Integrated flux densities of candidates HFP sources at the 2002 epoch. * indicates the sources optically identified by Dallacasa et al. (2002a). The other identifications are taken from the NED database.

second epoch spectra of seven sources, all identified with quasars, turned out to be definitely flat and obviously S_p and ν_p could not be determined. Such sources are labeled as "flat" in column 9 of Table 3.2. The radio spectra of all sources are shown in Fig. 3.2, where the stars and the filled circles refer to the first and to the second epoch of simultaneous multifrequency VLA data, respectively, while the dashed and solid lines indicate the corresponding fits.

A Kolmogorov-Smirnov (KS) test did not detect any significant difference among the distributions of the observed turnover frequencies (shown in Fig. 3.3) and of the peak flux densities at the two epochs. This is not surprising since the time-lag is too short for an evolution of source spectra (see Chapter 4, Sect. 4.2.3) to be detected. The observed peak frequency distributions of candidate HFP galaxies and quasars are similar (left-hand panel of Fig. 3.4) as a consequence of the selection criterion, but quasars are found up to much higher redshifts (Fig. 3.1), implying much higher values of ν_p in the source frame (Fig. 3.4, right-hand panel). A similar behavior was already known for GPS sources (Snellen 1997; Stanghellini et al. 1998), whose peak frequencies are, on average, about a factor of 5 lower.

3.3.2 Extended emission

Within our sub-sample, 14 (31%) sources show some amount of extended emission (2 galaxies, 9 quasars and 3 objects without optical identification) on scales ranging from 6 to 35 arcsec. At the end of this paragraph we will comment on such sources, based on our own observations and on published VLBA/VLA data. Our images at 1.465 and 1.665 GHz are presented in Figs. 3.5 through 3.16. The flux density of the extended emission has been measured as the difference between the integrated flux density over the whole source extension and the flux density obtained using a point source model to fit the compact emission (see Table 3.3). The presence of weak emission below the surface brightness limit (~ 0.2 mJy/beam) of our maps cannot be excluded, and this may be particular relevant for high redshift objects.

The total projected linear size of all these sources exceeds the classical definition of a "compact" radio source, i.e. about 15-20 kpc (O'Dea 1998). The total flux density of the extended emission ranges between a few mJy and 80 mJy, with 1.4 GHz luminosities ranging from $\simeq 10^{24}$ W/Hz (close to the upper end of the range for FR I sources) to $\simeq 10^{27}$

Table 3.2: Peak frequencies and flux densities

Name			1998		1999		2002	
			S_p mJy	ν_p GHz	S_p mJy	ν_p GHz	S_p mJy	ν_p GHz
0003+2129	G*	C	272±5	5.7±0.1			257±5	5.4±0.1
0005+0524	Q	C			235±6	4.13±0.09	228±7	3.40±0.09
0037+0808	G?	C			287±5	5.9±0.1	287±6	6.2±0.2
0111+3906	G	E			1333±28	4.76±0.06	1303±28	4.68±0.07
0116+2422		C	245±4	5.1 ±0.1			266±9	6.3±0.3
0217+0144	Q	E			2557±105	18±3		flat
0329+3510	Q*	E	768±13	6.7±0.3				flat
0357+2319	Q*	C	637±15	12±1				flat
0428+3259	G*	E	545±10	7.3±0.2			539±11	6.8±0.2
0519+0848		E	>380	>22	>560	>22	448±7	7.4±0.6
0625+4440	BL	C	575±17	13±2			237±4	7.4±1.0
0638+5933		C	700±17	12±2			675±13	9.2±0.7
0642+6758	Q	C	481±11	4.5±0.1			431±10	4.08±0.08
0646+4451	Q	C	3371±118	15±2			3982±92	11.2±0.6
0650+6001	Q	C	1290±19	7.6±0.3			1143±27	5.2±0.2
1335+4542	Q	C	737±18	5.1±0.1			793±17	4.9±0.1
1335+5844		C	730±12	6.0±0.2			736±12	5.5±0.1
1407+2827	G	C	2320±36	5.34±0.05	2388±41	5.20±0.09	2484±49	5.01±0.08
1412+1334		C	337±7	4.7±0.1			345±8	4.18±0.09
1424+2256	Q	C	623±15	4.13±0.07			698±18	3.94±0.06
1430+1043	Q	C	905±14	6.5±0.2			887±39	5.7±0.1
1457+0749		E			239±4	5.4±0.3	367±12	1.7±0.3
1505+0326	Q	C			937±14	7.1±0.4	744±11	6.8±0.4
1511+0518	Sy1	C	778±18	11.1±0.4			903±20	10.6±0.4
1526+6650	Q	C	427±13	5.7±0.1			417±10	5.5±0.1
1603+1105		E			277±4	7.7±0.4	229±9	13±7
1616+0459	Q	C			897±20	4.7±0.1	782±17	4.63±0.09
1623+6624	G	C	291±5	6.0±0.2			302±8	6.0±0.2
1645+6330	Q	C	628±18	14±2			629±17	10.1±0.7
1735+5049	G?	C	972±18	6.4±0.2			955±16	6.3±0.3
1800+3848	Q	E			1392±65	17±3	1226±49	13±1
1811+1704	Q*	E			809±19	12±1		flat
1840+3900	Q	C			201±3	5.7±0.5	169±4	5.2±0.4
1850+2825	Q	C			1567±32	9.1±0.3	1591±32	9.5±0.3
1855+3742	G*	C			426±42	4.00±0.07	423±310	3.81±0.06
2021+0515	Q*	C			497±13	3.75±0.08	446±10	4.5±0.1
2024+1718	S	E			845±32	14±2	807±16	8.6±0.4
2101+0341	Q	E			1635±90	17±2	737±212	3.7±0.2
2123+0535	Q	E			2392±103	18±4		flat
2203+1007	G*	C			319±7	4.86±0.07	312±7	5.0±0.1
2207+1652	Q*	E			572±9	7.4±0.3	252±7	3.5±0.3
2212+2355	S	C			1379±13	13±2	1031±17	9±1
2257+0243	Q	C				>22		>22
2320+0513	Q	E			1176±20	5.4±0.2		flat
2330+3348	Q	C			558±9	5.6±0.3		flat

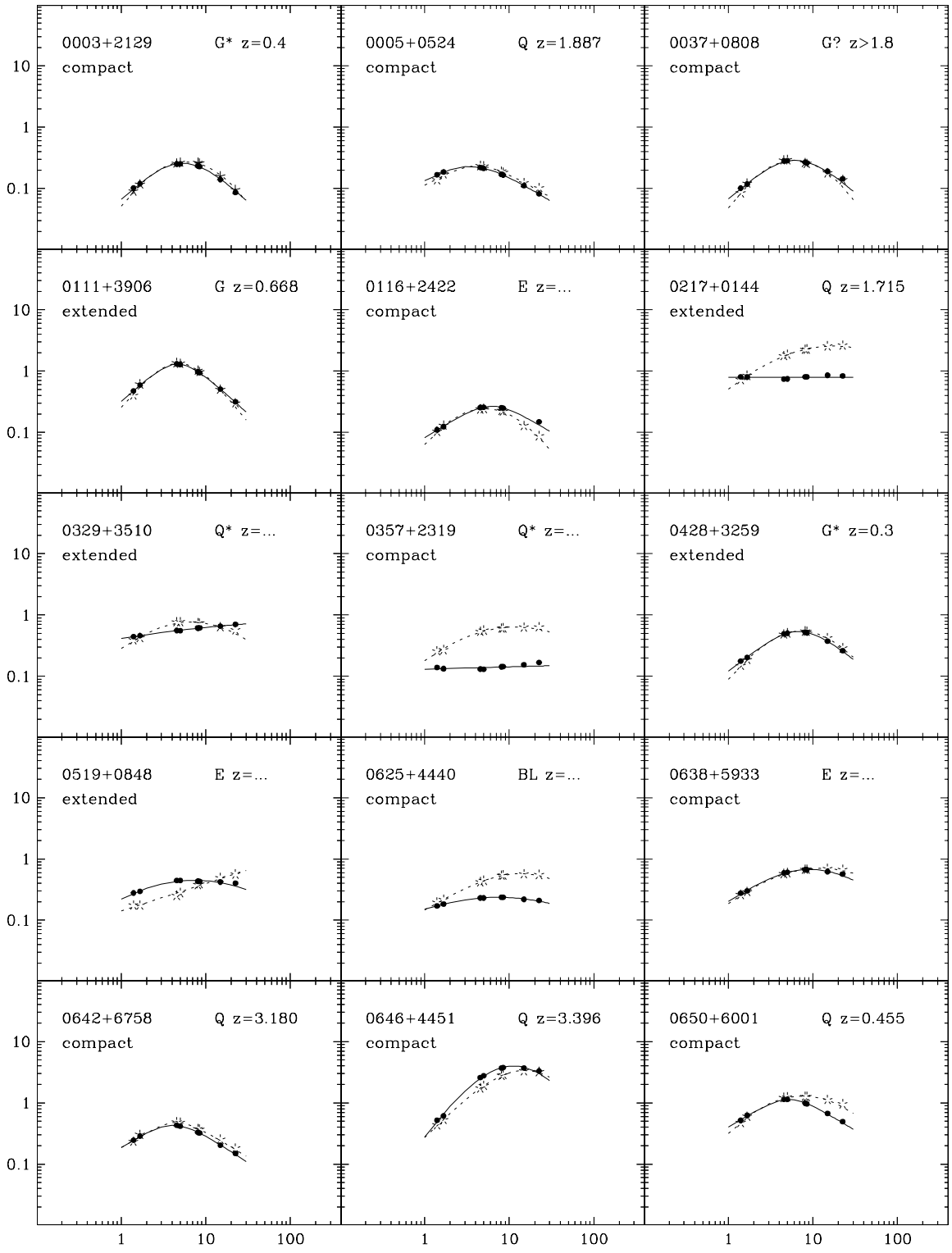

Figure 3.2: Radio spectra of sources [S_ν (Jy) vs ν (GHz)]. Stars and filled circles represent the first (Dallacasa et al. 2000) and the second (Tinti et al. 2005) epoch simultaneous multifrequency VLA data respectively; the dashed and solid lines show the corresponding polynomial fits.

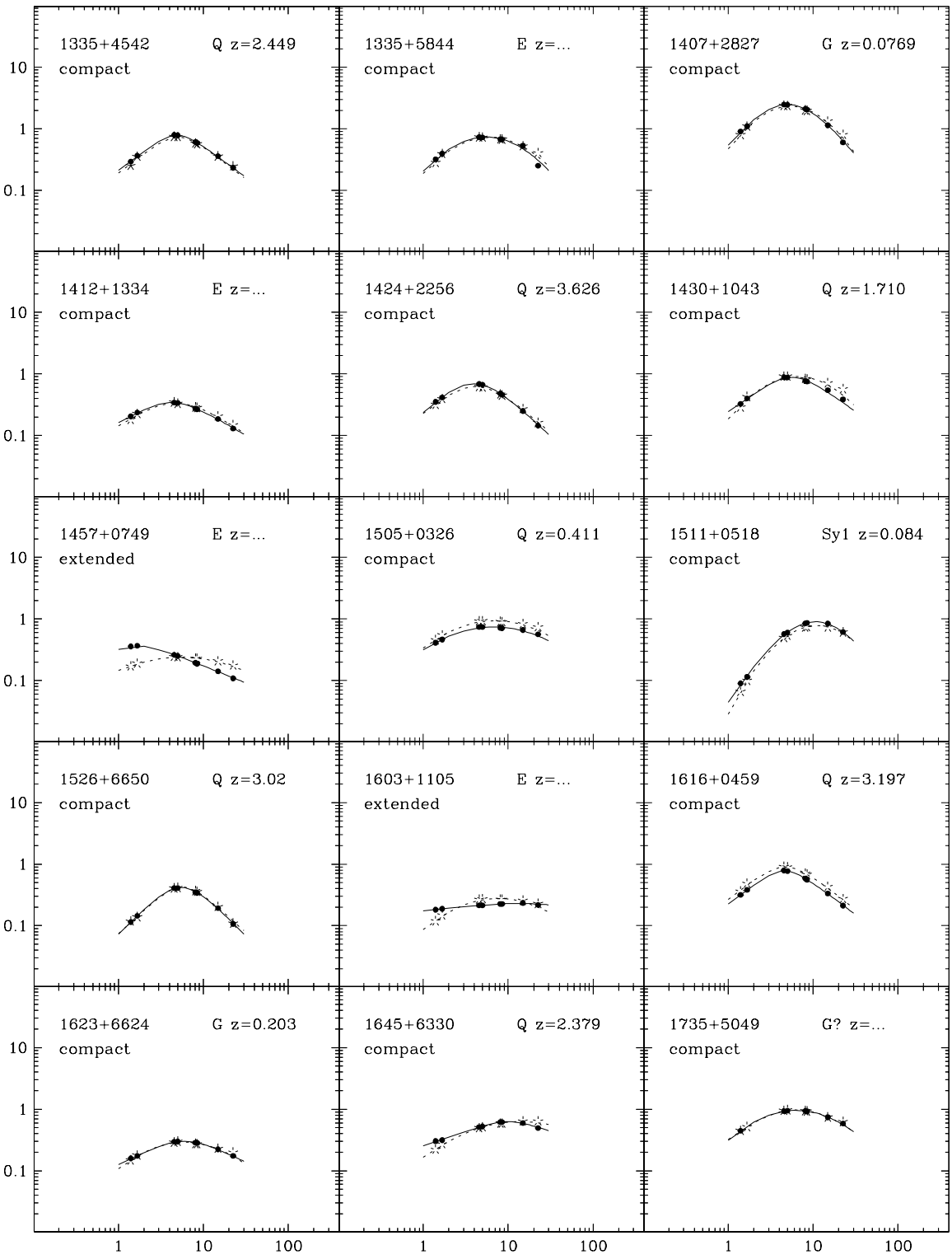

Figure 3.2: (continued)

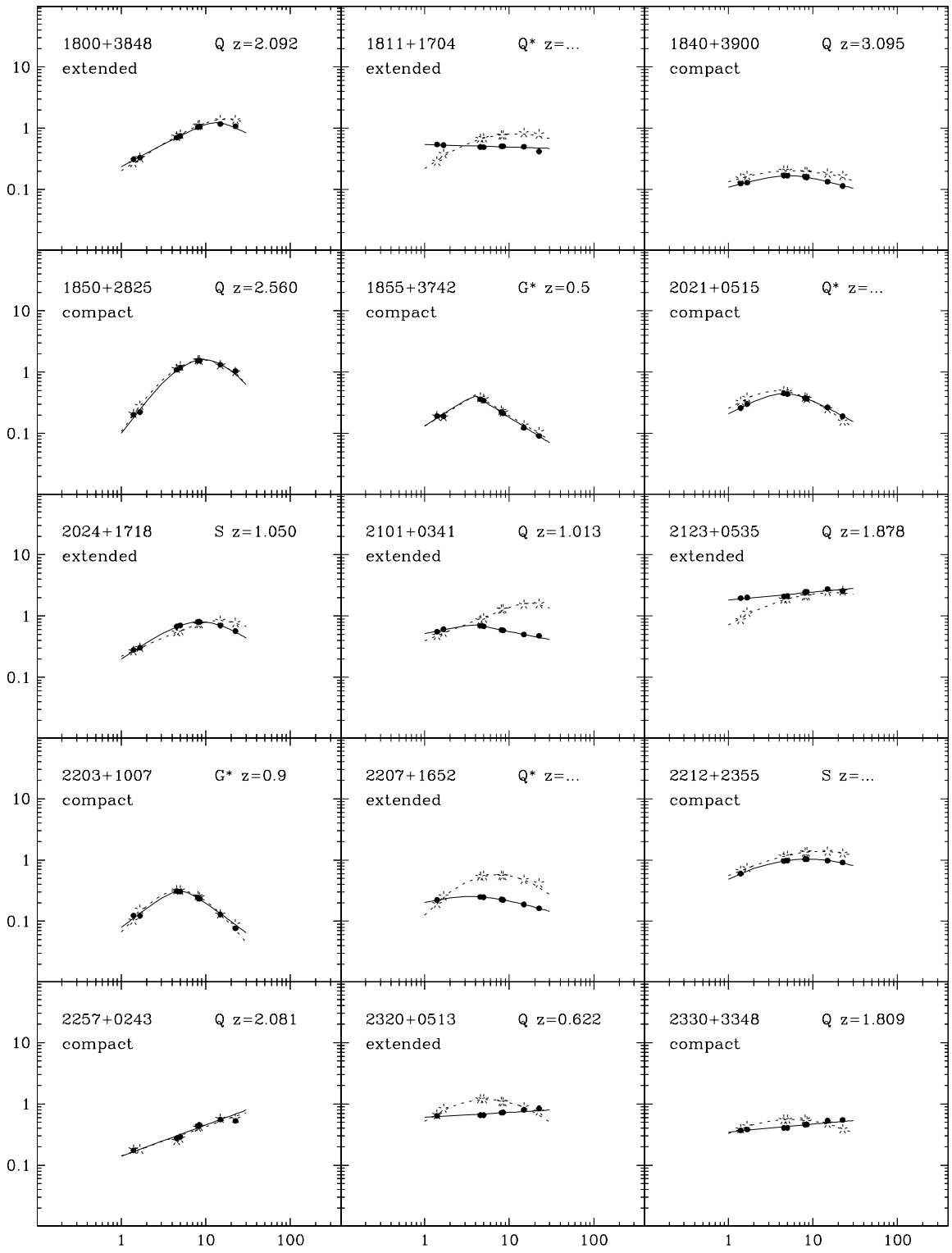

Figure 3.2: (continued)

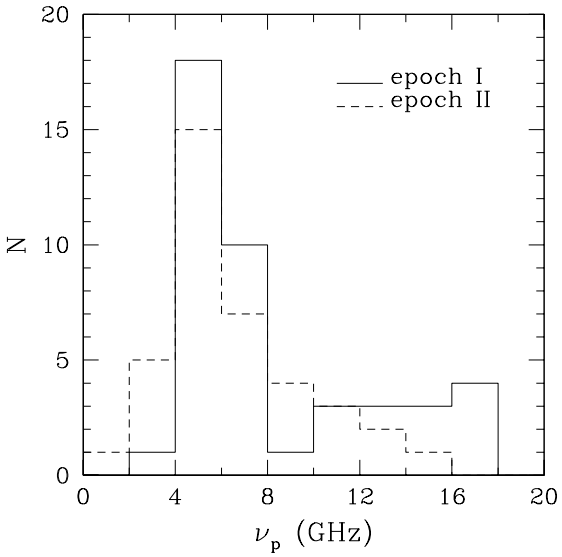

Figure 3.3: Histogram of observed turnover frequencies for the HFP sample at the two epochs.

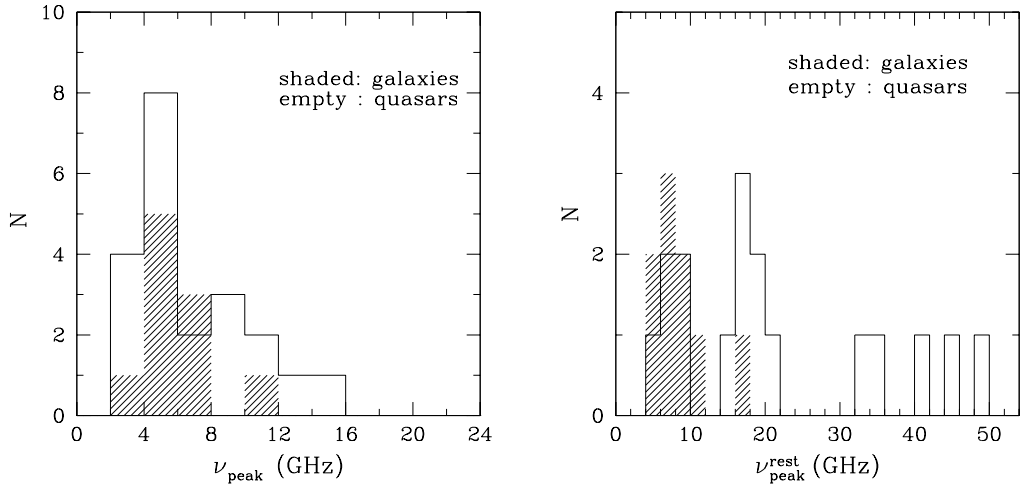

Figure 3.4: Observed (left) and rest frame (right) turnover frequency distributions for galaxies and quasars.

Table 3.3: Parameters of the extended objects

Name	$S_{1.4}$ (mJy)		$S_{1.7}$ (mJy)		$S_{\rm C\ band}$ (mJy)		$S_{\rm X\ band}$ (mJy)		LS (arcsec)
	peak	ext	peak	ext	peak	ext	peak	ext	
J0111+3906	477	10	594	7					17
J0217+0144	750	75	766	59	736	20	808	8	>6 (4.5 GHz)
J0329+3510	423	80	455	65	553	5			35
J0428+3259	167	12	198	8	492	3			>8 (4.5 GHz)
J0519+0848	268	17	287	15	444	4			10
J1457+0749	354	13	361	12					12
J1603+1105	170	27	175	26	213	2			94
J1800+3848	311	4	329	5					> 6
J1811+1704	537	15	523	18	488	4	494	6	22
J2024+1718	279	12	304	10					11
J2101+0341	550	15	609	14					22(EW)×14(NS)
J2123+0535	1949	14	1999	34					11
J2207+1652	215	50			248	12	225	6	11
J2320+0513	623	62			656	10	721	6	19 (4.5 GHz)

W/Hz, well within the luminosity range of FR II sources. The unresolved to extended luminosity ratios are in the range 4 to 78, when some amount of extended emission has been found.

The fraction of sources with detected extended emission ($\simeq 31\%$) is larger than in GPS samples, where it is found to be $\simeq 10\%$ (Stanghellini et al. 1990; Baum et al. 1990, Stanghellini et al. 2005). However, no dependence of the fraction of sources with extended emission on peak frequency can be found within our sample: if we split it into two roughly equally populated sub-samples (with $\nu_p > 5.5$ GHz and $\nu_p < 5.5$ GHz, ν_p being the second epoch peak frequency in the observer's frame), we find approximately the same fraction of sources with extended emission.

The presence of radio emission on scales of tens of kpc or even larger can indicate that we are really dealing with an evolved source but can also be reconciled with the youth scenario under the hypothesis of recurrent activity proposed by Baum et al. (1990), whereby a newly born source is propagating amidst the relic of previous large scale radio activity (see Chapter 2, Sect. 2.4.2). At low frequencies (hundreds of MHz) the extended emission

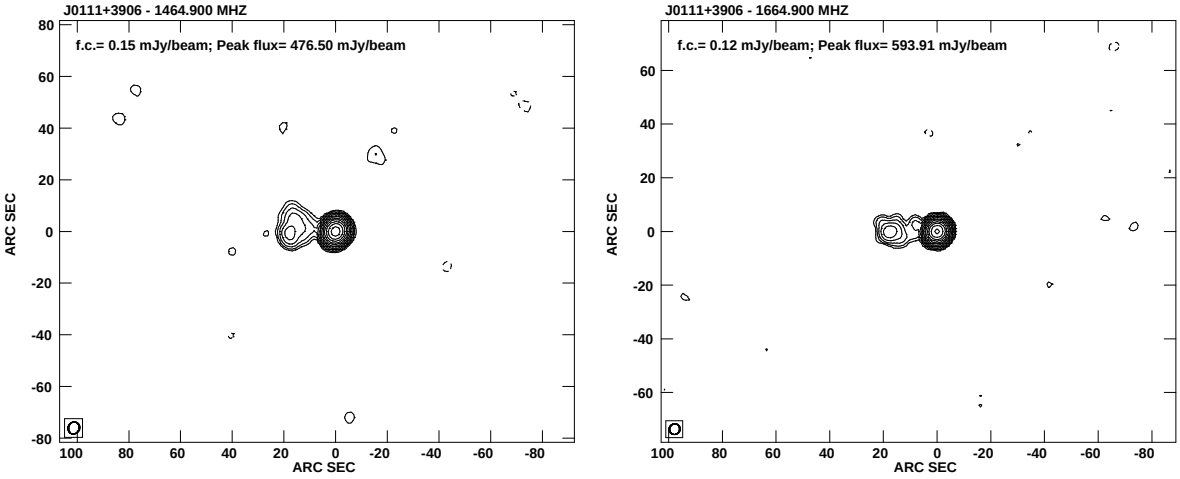

Figure 3.5: VLA L-band image of J0111+3906; the restoring beam is in the bottom left-hand corner of each figure, the contour levels are ±1, 2, 4, 8, 16, 32, 64, 128, 256, 512, 1024, 2048, 4096 times the first contour (f.c.) corresponding to 3 times the r.m.s. noise of the image.

should be dominant, because of its steep spectrum, while the contribution of the compact emission becomes progressively less important.

Seven out of the nine quasars with extended emission have strongly variable spectra. Five of them did not show anymore a convex spectrum (see Chapter 4, Sect. 4.3) when were re-observed, and therefore are not HFPs. On the other hand, the two galaxies with some amount of resolved emission on a kpc scale showed, at both epochs, the typical peaked spectrum. One is the well known J0111 + 3906 (B0108 + 388) for which Baum et al. (1990) proposed the recurrent activity hypothesis. The other is J0428 + 3259 for which we have analyzed high resolution VLBA observations to study its pc scale morphology (see Section 3.6)

Notes on individual sources:

J0111+3906: well known galaxy at $z = 0.668$. We have detected extended emission on kpc scale (see Fig. 3.5), already discovered and imaged by Baum et al. (1990), Taylor et al. (1996), Stanghellini (2003), at different resolutions. The extended emission is in contrast with a recent origin for the radio activity in this source but can be explained if the radio source is recurrent (Baum et al. 1990).

J0217+0144: quasar at $z = 1.715$. The source is slightly resolved in the NW-SE direction

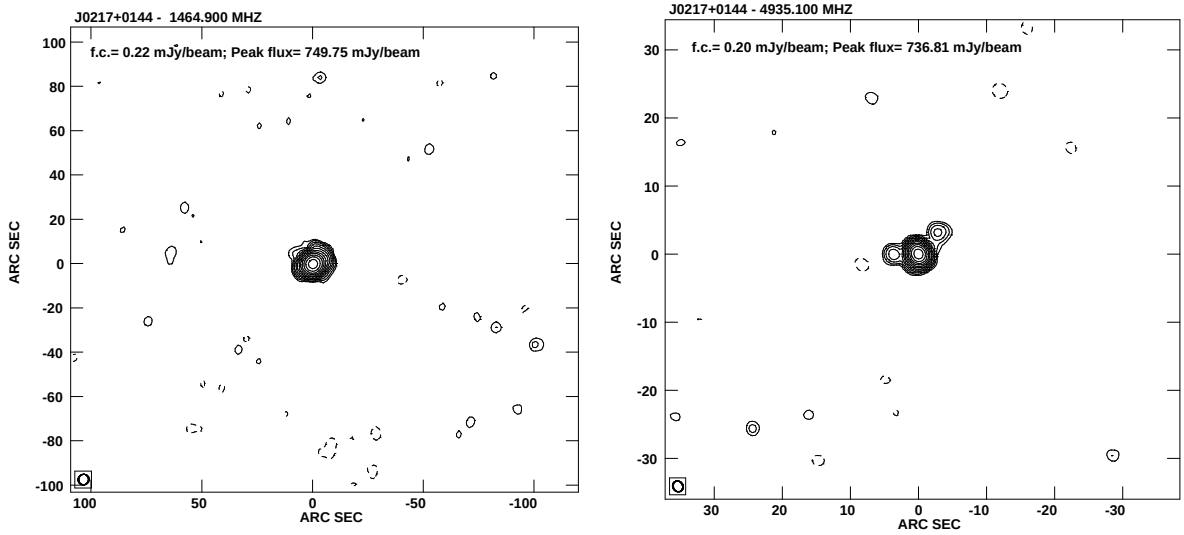

Figure 3.6: J0217+0144; see caption to Fig. 3.5

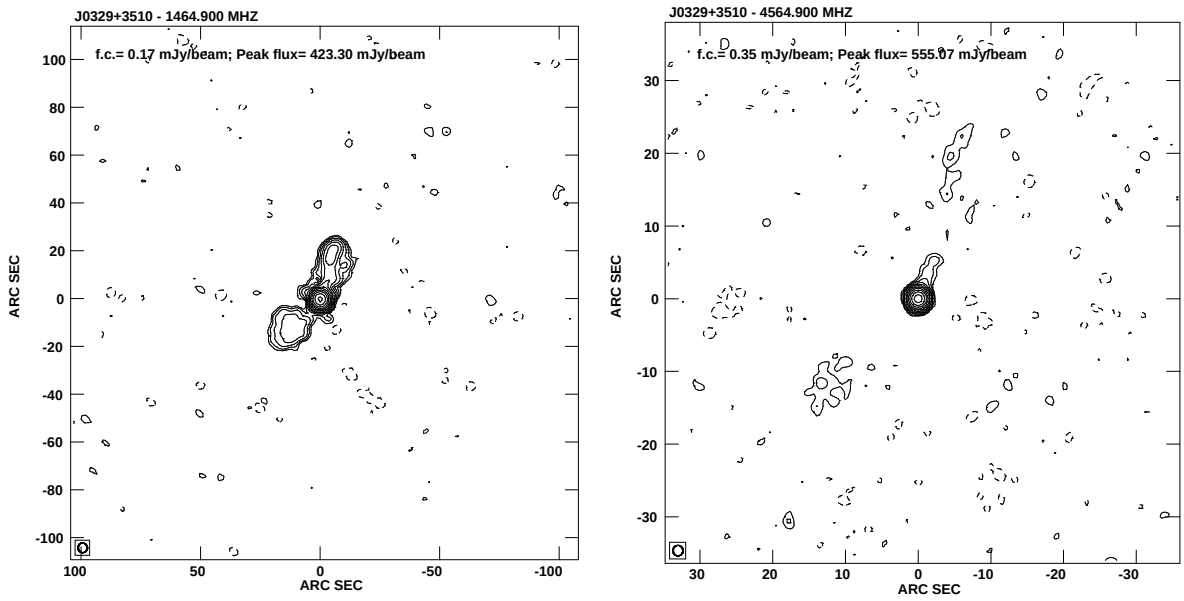

Figure 3.7: J0329+3510; see caption to Fig. 3.5

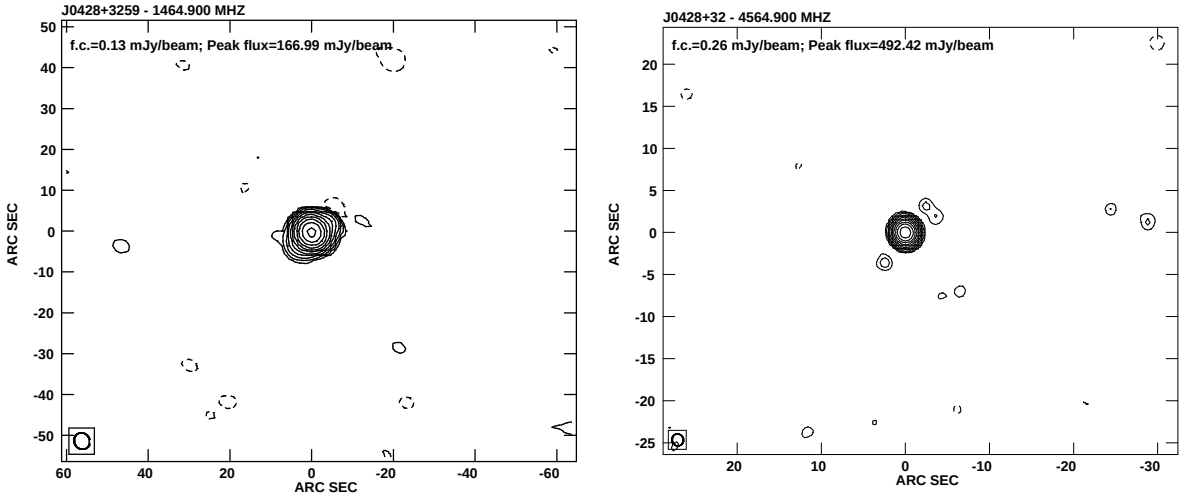

Figure 3.8: J0428+3259; see caption to Fig. 3.5

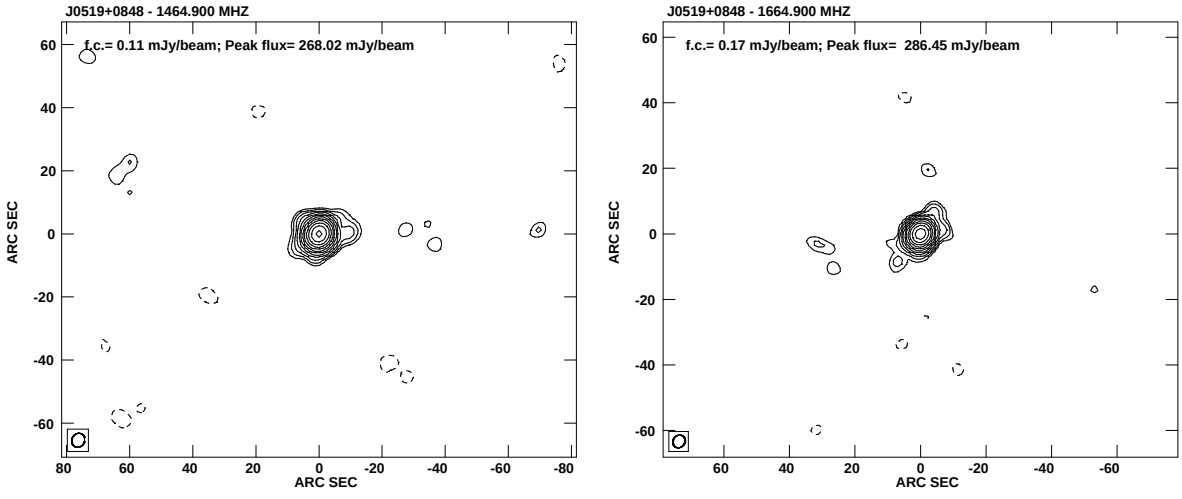

Figure 3.9: J0519+0848; see caption to Fig. 3.5

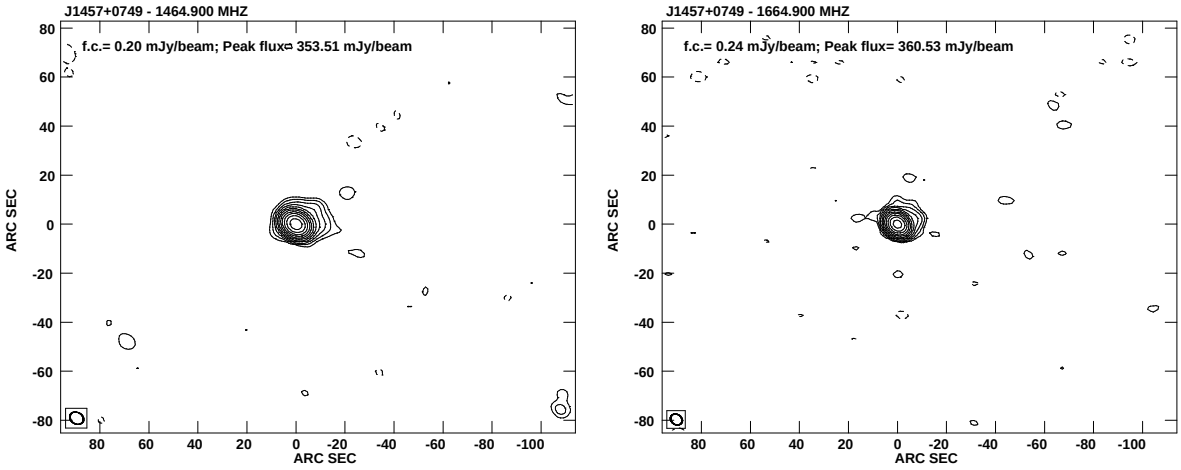

Figure 3.10: J1457+0749; see caption to Fig. 3.5

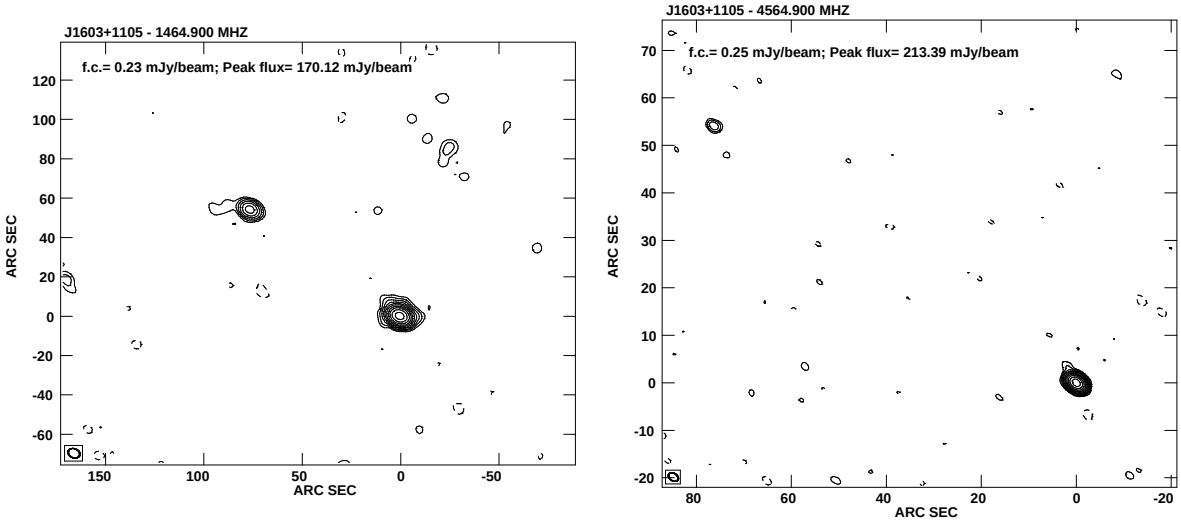

Figure 3.11: J1603+1105; see caption to Fig. 3.5

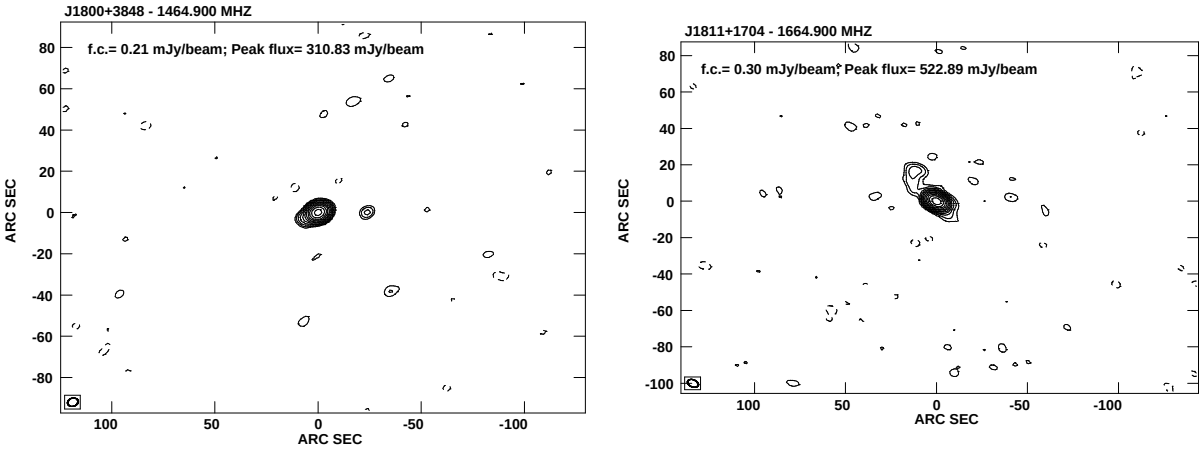

Figure 3.12: J1800+3848 (left) at 1.465 GHz and J1811+1704 (right) at 1.665 GHz; see caption to Fig. 3.5

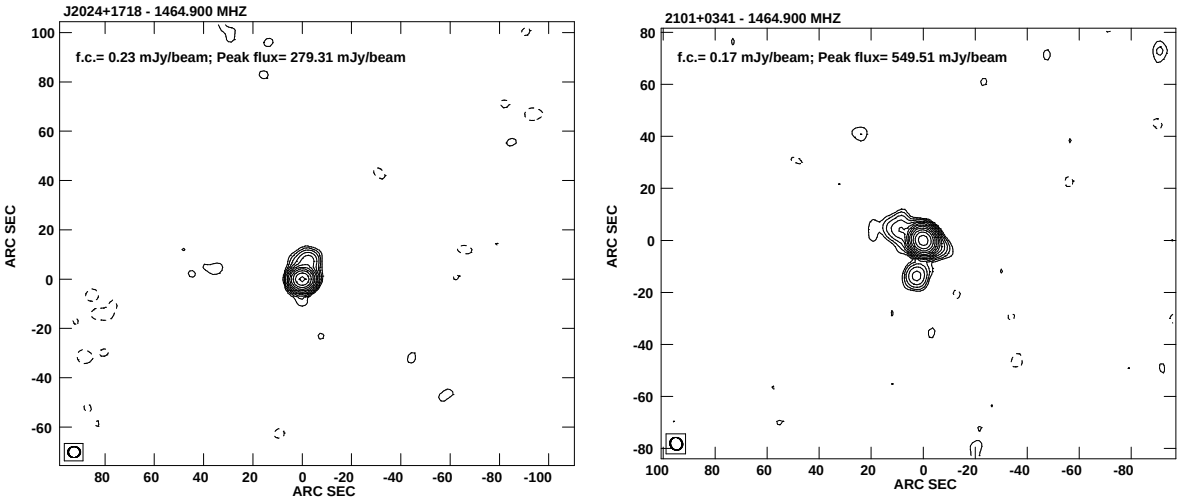

Figure 3.13: J2024+1718 (left) at 1.465 GHz and J2101+0341 (right) at 1.465 GHz; see caption to Fig. 3.5

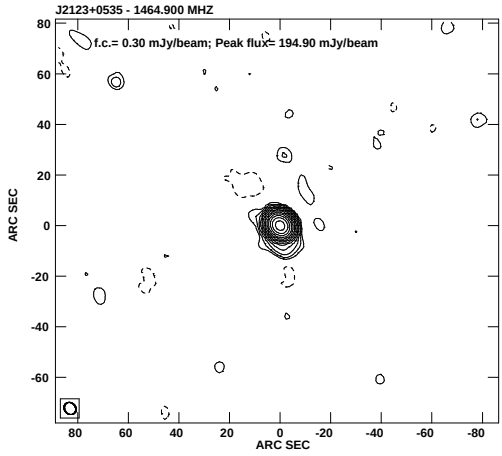

Figure 3.14: J2123+0535; see caption to Fig. 3.5

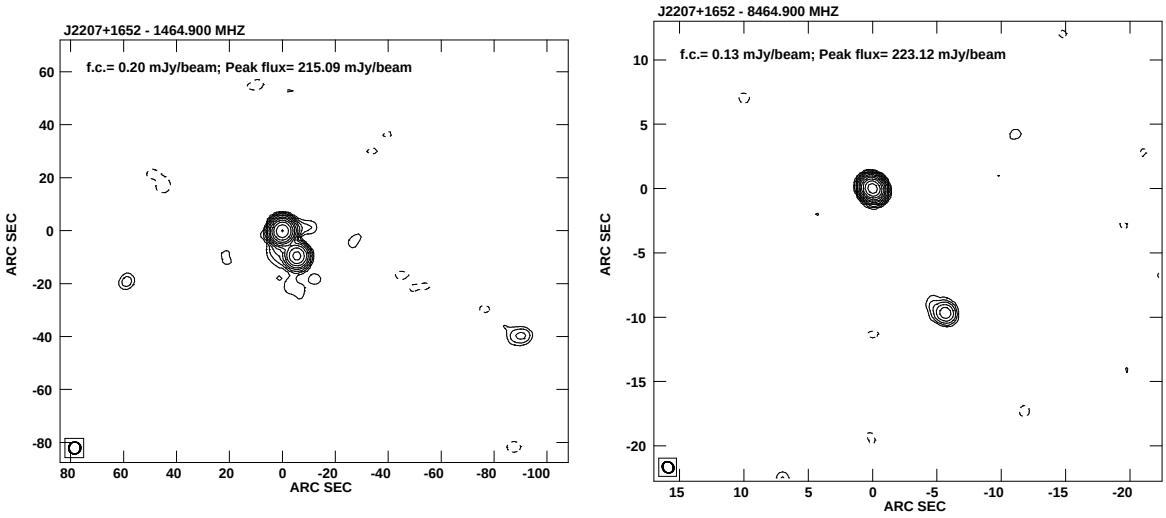

Figure 3.15: J2207+1652; see caption to Fig. 3.5

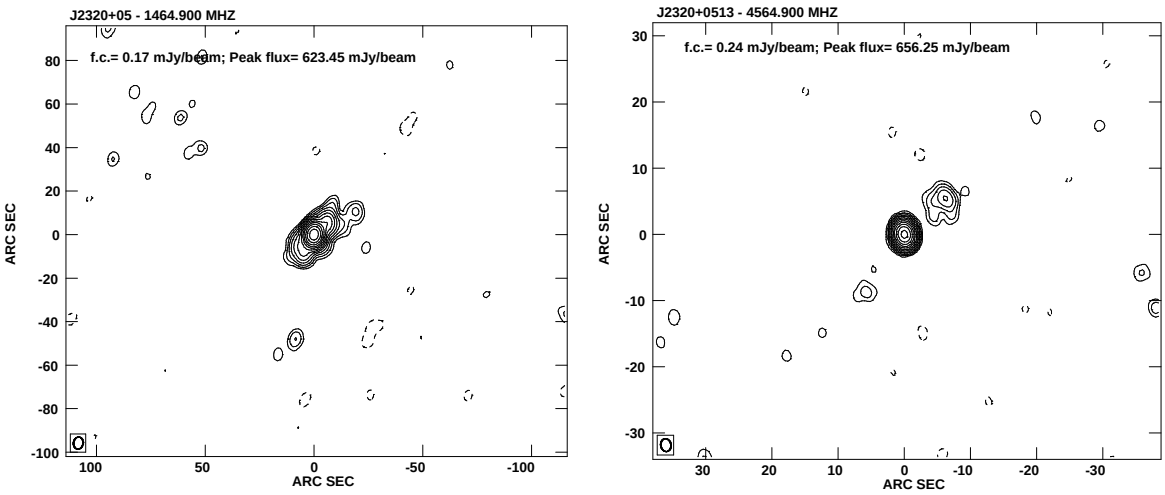

Figure 3.16: J2320+0513; see caption to Fig. 3.5

in the L band. At higher resolution, in the C and X bands, two opposite regions of emission with respect to the central compact component are detected (see Fig. 3.6).

J0329+3510: stellar object. On the arcsecond scale this source is characterized by a compact flat-spectrum core accounting for the vast majority of the flux density at all frequencies and with a two-sided roughly symmetric extended emission that can be regarded as the two steep-spectrum lobes of an FRII radio source. The extended emission is still detected, even if very weak, in the C band (see Fig. 3.7); a jet like feature is emerging from the core towards the brightest lobe.

J0428+3259: galaxy with estimated redshift $z = 0.3$ (Dallacasa et al. 2002), based on the Hubble diagram in Snellen et al. (1996). The source is slightly resolved along the NW-SE axis at both 1.465 GHz and 1.665 GHz (Fig. 3.8).

J0519+0848: no optical identification. It is slightly resolved with a hint of weak emission in the NW direction (see Fig. 3.9).

J1457+0749: no optical identification. It is slightly resolved in the NW direction (see Fig. 3.10).

J1603+1105: BLLac (Dallacasa, Falomo & Stanghellini, private communication). The NE component can be either associated with the central object or can be an unrelated source

(see Fig. 3.11); according to Snellen (1998) there is a 6% chance of finding an unrelated NVSS radio source with a flux density of > 5 mJy within a radius of 100 arcsec from the target source.

J1800+3848: quasar at $z = 2.092$. At 1.465 and 1.665 GHz the source appears slightly resolved but the estimated flux density of the extended emission is of a few mJy only (see Fig. 3.12).

J1811+1704: stellar object. A very weak component at NW is clearly visible both at 1.465 GHz and 1.665 GHz (see Fig. 3.12).

J2024+1718: stellar object at $z = 1.050$. The emission is extending from the core to the North for 11 arcsec (see Fig. 3.13).

J2101+0341: quasar at $z = 1.013$. This source has a very complex structure. Two components are aligned with the NS axis for a total angular size of 14 arcsec. Furthermore there is a diffuse low-brightness emission in the NE direction with angular size of 22 arcsec (see Fig. 3.13).

J2123+0535: quasar at $z = 1.878$. There is a very weak emission toward the South of the strong compact component (see Fig. 3.14).

J2207+1652: stellar object. On arcsec scales it shows two components, the southern one being weaker and smaller. This component is still clearly visible in the X band (see Fig. 3.15).

J2320+0513: quasar at $z = 0.622$. Extended emission is revealed in both the L and the C band. The maximum angular size in the NW-SE direction is of 19 arcsec. In the C band the extended emission has two components on both sides of the unresolved nucleus, the Southern one being weaker than the Northern one (see Fig. 3.16).

3.4 Polarimetric VLA observations

A common characteristic attributed to the GPS class is very low radio polarisation. GPS galaxies are found to be almost completely unpolarised (below 0.3% at 6 cm with the VLA for the complete sample of Stanghellini et al. 1998) while the mean fractional polarisation of GPS quasars is about 1.2% at 6 cm for the same sample which is consistent with

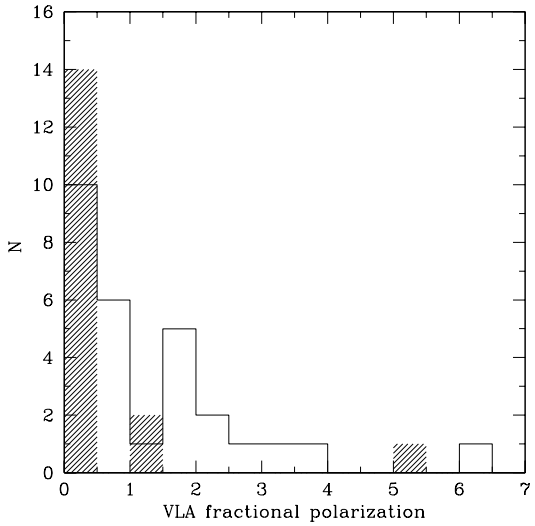

Figure 3.17: VLA fractional polarisation: galaxies and empty fields are represented by the shaded areas, quasars by the unshaded areas. All galaxies have a polarisation degree below 0.5%; the three objects with shaded areas at higher polarisation degrees are empty fields.

that of non-GPS quasars selected by Stanghellini (2003) for comparison with his sample. Therefore there is evidence in the literature that GPS quasars have a lower fractional polarisation than non-GPS quasars but they are significantly more polarised than GPS galaxies (see Chapter 2, Sect. 2.5).

For the bright HFPs, polarisation information was not available in a systematic way except in the NVSS catalogue, at frequency in the optically thick part of the spectrum of all sources. A preliminary analysis based on this information was done by Dallacasa (2003). He found that it is possible to distinguish the behavior of the HFP quasars from the other HFPs identified with galaxies or empty fields. The quasars span a wide range of fractional polarisation, with measured values up to 5%, while we have detected no fractional polarisation for the galaxies.

In order to investigate the polarisation properties of HFP sources, in particular the absorption mechanism (SSA or FFA) and the ordering and direction of the magnetic field, new polarimetric VLA multifrequency observations have been carried out on 03 July 2003 when the interferometer was in the B configuration. An appropriate source (J1927+739)

was observed at a wide range of parallactic angles to serve as instrumental polarisation calibrator. Generally the feed contamination was found between 1 and 3% for all the antennas with very low residuals. The absolute orientation of the electric vector was calibrated by means of the source 3C286 (1331+305) and residual errors can be estimated between 1° and 3°, based on the dispersion observed among the various scans on that source. Such dispersion was small for the X and C bands, while the largest discrepancy has been found for the L and K bands.

Once the "final" total intensity image have been produced from self-calibrated data, also Stokes' U and Q images have been obtained. Polarised intensity ($P=\sqrt{U^2+Q^2}$)) images have been then produced and finally also electric vector orientation ($\chi = 0.5 \times \arctan 2(U,Q)$) and fractional polarisation images have been obtained. The r.m.s. noise in the polarised intensity images was typically between 0.06 mJy and 0.20 mJy increasing from the L to the Q band respectively, allowing a 5σ limit as low as 0.1% for many unpolarised sources, depending on the total flux density of each object.

We considered independently the two IFs for the L, C and X bands where the frequencies used where spread across the allowed bandwidth. Therefore we have independent measurements of the polarised emission and of the electric vector orientation at 9 different frequencies, ranging from 1.365 to 22.3 GHz.

The analysis is still in progress. Only the data reduction in the C and X band has been completed. In Tab. 3.4 I have reported the fractional polarisation range estimated from the data in the C and X bands (column 3). On the basis of these data we classified a source as polarised (POL) if the fractional polarisation is greater than 0.5% otherwise the source is not polarised (NP) (see column 4 in the same table). Fig. 3.17 shows the mean fractional polarisation for the C and X bands. Galaxies and empty fields are represented by the shaded areas, while quasars by the empty histogram. The data confirms that HFP quasars have a wide range of fractional polarisation, with values up to 6%, while all the galaxies are not polarised. Three of the seven sources without optical identification (J0519+0848, J1457+0749 and J1603+1105) also have a significant polarisation level. Polarised emission is expected if HFP quasars are large-scale radio sources with the jet aligned close to the line of sight, so that the radiation comes from outside the region with high local ionization.

Therefore polarisation measurements provide further support to the hypothesis that most of quasars are blazars caught by during a flare at the time of the first epoch VLA observation. The complete analysis of polarisation measurements will be presented in Dallacasa et al. (in preparation).

3.5 OVRO Observations of HFP candidates

The VLA data give us information on a broad frequency range (1–23 GHz; Dallacasa et al. 2000, Tinti et al. 2005), but mostly sample the optically thick part of the spectrum. Higher frequency measurements are important to complete the information on the optically thin part and thus to better constrain the position of the turnover.

Two tracks of 2.4 hours at 3 mm and 2.3 hours at 1 mm, close in time (27 January and 29 January 2003), with the Owens Valley Radio Observatory Millimeter Array in L configuration have been allocated for a sub-sample of 10 HFPs. We have selected from the complete sample the sources that would have the highest 3 mm and 1 mm flux densities as extrapolated on the basis of the VLA spectrum and RA compatible with the local sidereal time (LST) range (16-01) allocated. The primary flux calibrators were Uranus and Neptune). Since most of these sources are quite bright, some of them are also present in the database of the OVRO calibrators over the last 2–3 years. However these data were taken in poor weather conditions so that they did not allow us to obtain useful constrains on the high frequency spectral index. Furthermore, the data selection criteria and reduction methods used to derive the flux densities entered in the database were inhomogeneous with unknown systematic effects.

All the observed sources are optically identified with quasars, since they are generally brighter than galaxies and have higher turnover frequencies. They are point-like at OVRO resolution, so imaging was not strictly necessary. We were able to measure flux densities for all the 10 sources at 3 mm while only 4 sources had signal-to-noise ratio SNR $\gtrsim 3$ at 1 mm. In Table 3.5 I have reported the J2000 name of the targets, the flux densities at 22.5 (VLA data), 101 and 222 GHz (OVRO data), the spectral indices between 22.5 and 101 GHz and between 101 and 222 GHz. Eight out of the ten sources have a steep spectral

Name	Id	Polarisation %	
0003+2129	G*	$< 0.5\%$	NP
0005+0524	Q	$< 0.5\%$	NP
0037+0808	G?	$< 0.5\%$	NP
0111+3906	G	$< 0.5\%$	NP
0116+2422		$< 0.5\%$	NP
0217+0144	Q	$1.5 - 2.5\%$	POL
0329+3510	Q*	$0.5 - 1.5\%$	POL
0357+2319	Q*	$1.5 - 3.0\%$	POL
0428+3259	G*	$< 0.5\%$	NP
0519+0848		$1.0 - 2.0\%$	POL
0625+4440	BL	$1.5 - 2.5\%$	POL
0638+5933		$< 0.5\%$	NP
0642+6758	Q	$0.5 - 1.5\%$	POL
0646+4451	Q	$1.6 - 3.6\%$	POL
0650+6001	Q	$< 0.5\%$	NP
1335+4542	Q	$< 0.5\%$	NP
1335+5844		$< 0.5\%$	NP
1407+2827	G	$< 0.5\%$	NP
1412+1334		$< 0.5\%$	NP
1424+2256	Q	$0.4 - 3.4\%$	POL
1430+1043	Q	$0.5 - 0.7\%$?	POL
1457+0749		$5.0 - 5.7\%$	POL
1505+0326	Q	$0.2 - 1.0\%$	POL
1511+0518	Sy1	$< 0.5\%$	NP
1526+6650	Q	$< 0.5\%$	NP
1603+1105		$0.8 - 1.7\%$	POL
1616+0459	Q	$0.2 - 2.9\%$	POL
1623+6624	G	$< 0.5\%$	NP
1645+6330	Q	$0.8 - 3.1\%$	POL
1735+5049	G?	$< 0.5\%$	NP
1800+3848	Q	$< 0.5\%$	NP
1811+1704	Q*	$1.8 - 2.7\%$	POL
1840+3900	Q	$< 0.5\%$	NP
1850+2825	Q	$< 0.5\%$	NP
1855+3742	G*	$< 0.5\%$	NP
2021+0515	Q*	$< 0.5\%$	NP
2024+1718	S	$0.1 - 0.8\%$?	POL
2101+0341	Q	$3.3 - 4.6\%$	POL
2123+0535	Q	$0.8 - 1.1\%$	POL
2203+1007	G*	$< 0.5\%$	NP
2207+1652	Q*	$1.0 - 1.5\%$	POL
2212+2355	S	$5.6 - 7.0\%$	POL
2257+0243	Q	$< 0.5\%$	NP
2320+0513	Q	$2.5 - 4.3\%$	POL
2330+3348	Q	$0.4 - 1.5\%$	POL

Table 3.4: The fractional polarisation range calculated between VLA C and X bands

J2000	$S_{22.5}$ (Jy)	S_{101} (Jy)	S_{222} (Jy)	$\alpha_{22.5}^{101}$	α_{101}^{222}
1645+6330	0.493±0.0493	0.248±0.051	0.376±0.174 *	0.5±0.2	-0.5±0.6
1751+0939	4.031±0.4031	4.438±0.331	3.342±0.395	-0.06±0.08	0.4±0.2
1800+3848	1.076±0.1076	0.624±0.068	0.469±0.150	0.4±0.1	0.4±0.4
1811+1704	0.418±0.0418	0.246±0.045	0.328±0.121 *	0.4±0.1	-0.4±0.5
2024+1718	0.569±0.0569	0.217±0.043	0.233±0.136 *	0.6±0.2	-0.1±0.8
2101+0341	0.478±0.0478	0.579±0.054	0.450±0.169 *	-0.13±0.09	0.3±0.5
2123+0535	2.560±0.2560	1.029±0.080	0.722±0.160	0.61±0.08	0.5±0.3
2136+0041	6.169±0.6169	1.731±0.142	0.733±0.167	0.9±0.1	1.1±0.3
2212+2355	0.915±0.0915	0.501±0.059	0.332±0.125 *	0.4±0.1	0.5±0.5
2257+0243	0.528±0.0528	0.237±0.045	0.363±0.180 *	0.5±0.1	-0.5 ±0.7

Table 3.5: OVRO flux densities and spectral indices. * indicates the sources with SNR<3 at 1 mm.

index between 22.5 GHz and 101 GHz ($\alpha_{22.5}^{101} \simeq$0.4-0.9). Since the errors on the flux densities at 222 GHz are quite large also the uncertainties on the spectral index between the two OVRO frequencies are large.

We have fitted the radio spectra using both the II epoch VLA data and the OVRO data using the hyperbolic function in Eq. 3.2. Two sources (J1751+0939 and J2136+0041) were not observed at the second epoch of VLA observations and therefore we have fitted the OVRO data combined with the first epoch VLA data. The radio spectra of HFPs using both VLA and OVRO data are shown in Fig. 3.18 and 3.19. Green triangles, red filled circles and blue crosses represent respectively the I epoch and II epoch VLA data and the OVRO data. The solid lines show the fit to the VLA+OVRO data while the dashed and dot-dashed lines are the polynomial fit to the II and I epoch simultaneous multifrequency VLA data, respectively. The best fit values of ν_p and S_p are reported, with their errors, in Table 3.6. The OVRO data have thus confirmed the presence of a peak in the frequency range 4.2–28 GHz.

Due to the strong variability of quasars it is very important to use simultaneous data to determine their spectrum. The time interval between the VLA and OVRO data is of about six months. In this time lag some sources can show quite strong variability both in the mean flux and the shape of the spectrum. The sources J1811+1704, J2101+0341,

Name		I epoch VLA		II epoch VLA		VLA+OVRO	
		S_p mJy	ν_p GHz	S_p mJy	ν_p GHz	S_p mJy	ν_p GHz
1645+6330	Q	628±18	14±2	629±17	10.1±0.7	632±17	10.2±0.7
1751+0939	BL	4325±89	11±0.9			5278±129	28±2
1800+3848	Q	1392±65	17±3	1226±49	13±1	1265±46	19±1
1811+1704	Q*	809±19	12±1		flat	532±11	1.5±1
2024+1718	S	845±32	14±2	807±16	8.6±0.4	813±16	8.9±0.4
2101+0341	Q	1635±90	17±2	737±212	3.7±0.2	671±18	4.2±0.4
2123+0535	Q	2392±103	18±4		flat	2372±35	7.0±0.5
2136+0041	Q	9731±146	6.4±0.2			9781±178	6.9±0.3
2212+2355	S	1379±13	13±2	1031±17	9±1	1038±19	9±1
2257+0243	Q		>22		>22	613±79	18±2

Table 3.6: Peak frequencies and flux densities of HFPs with OVRO observations.

J2123+0535 indeed reveal strong variability between the first and second epoch of VLA observations.

The OVRO flux densities of J2101+0341 are well above those expected from the second epoch VLA data and seem consistent with the extrapolation of the first epoch VLA data. This is obviously accidental; OVRO observations are detecting a different, high frequency, possibly flaring, emission component.

For the sources that show low variability between the first and the second epoch of VLA observations (J1645+6330, J1800+3848, J2024+1718, J2257+0243), the OVRO data confirm and in some cases (like J2257+0243) improve the determination of the peak frequency and flux density. We have no information on variability for the two sources observed only once with the VLA. For these too the OVRO flux densities are in agreement with the extrapolation of the VLA data and set a better constrain on the peak frequency and density.

3.6 VLBA Observations of candidate HFPs

High resolution VLBI images are very important to assess the nature of candidate HFPs and to study their properties. Intrinsically small and young objects are expected to

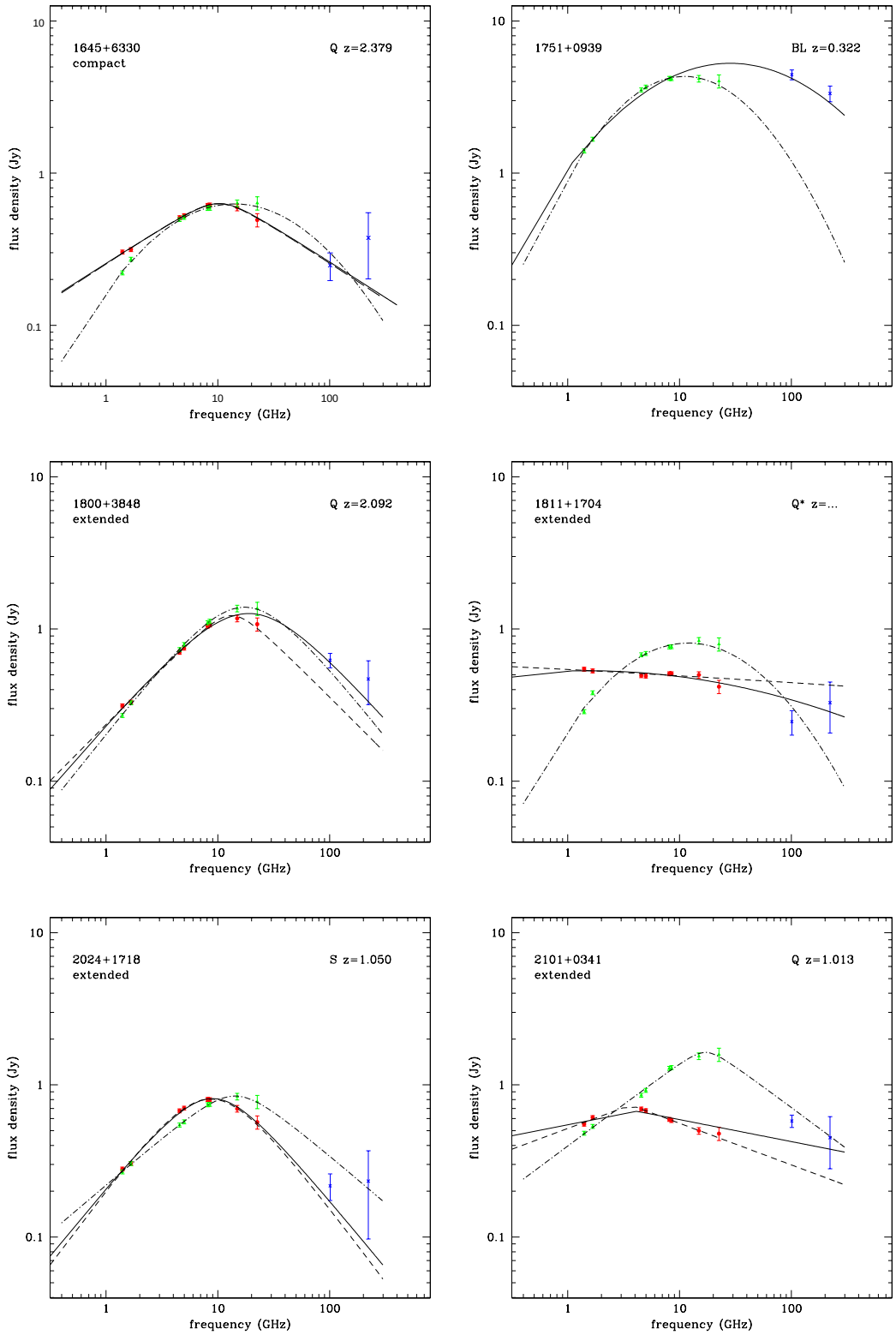

Figure 3.18: VLA+OVRO spectra. The lines are fits with the hyperbolic function (Eq. 3.2) of the OVRO+VLA data (solid), of the first epoch VLA data (dot-dashed), and of the second epoch VLA data (dashed). Green triangles, red filled circles and blue crosses represent respectively the I epoch and II epoch VLA data and the OVRO data.

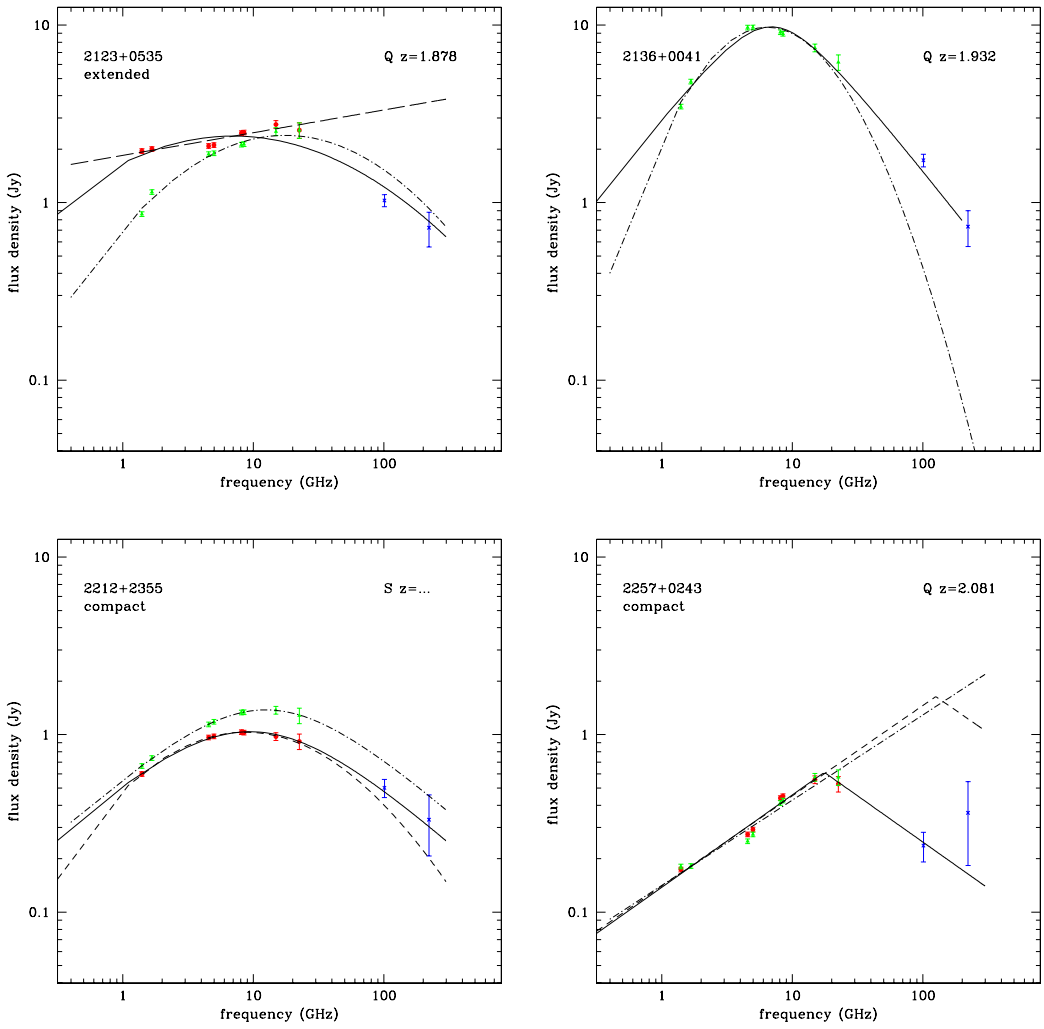

Figure 3.19: VLA+OVRO spectra. The lines and the data points have the same meaning as in Fig. 3.18.

have a CSO morphology, possibly asymmetric in flux densities. On the other hand, a core-jet (CJ) radio structure is typical of blazar objects and they are also known to possess some degree of flux density and spectral variability. A search of on-line databases/catalogues has shown that low sensitivity VLBI images, with typical resolution of a few milliarcseconds, are available for most of the HFP sources.

We found images for 41 objects in the VLBA Calibrator Survey (VCS) and 15 in the RRFID database. More sensitive images for 12 HFP candidates at 6/18 cm can be found in the Caltech-Jodrell Bank database and 9 objects appear also in the VLBA 2 cm survey (Kellermann et al. 1998). Three objects are included in the COINS sample (Peck & Taylor 2000, Peck et al. 2000). It is also evident from the images in these databases that there is a significant incidence of objects which look point-like in the 2.3 cm VLBA image, but show a relatively symmetric double morphology in the 8.4 GHz image, suggesting that they are very good candidates to be very small (a few mas in size) Compact Symmetric Objects, with dynamics ages of the order of 100 yrs. The literature information is quite inhomogeneous since it has yielded maps at various frequencies and with different resolutions. At least we need observations at two different frequencies in the optically thin region of the spectrum for each source to calculate the spectral indices of the different components which are required to establish the two-sided nature of the radio morphology.

To systematically investigate the milli-arcsecond morphology of the HFPs we have acquired in 4 experiments between January and May 2002, high resolution VLBA observations at 8.4, 15.3, 22.2 and 43.2 GHz, with a recording band-width of 32 MHz at 128 Mbps. Each target source was observed at two of these frequencies, selected to fall in the optically thin region of its spectrum, determined from the first epoch VLA observations (Dallacasa et al. 2000). The objects with turnover frequency above 15 GHz were necessarily observed at 22.2 and 43.2 GHz. Each target was observed at each frequency typically for 20 to 30 min spread over 4 to 7 short scans at various hour angles (HA) to improve the *uv* plane coverage.

The strong sources 3C 454.3, 3C 345 and J2136+0041 (a bright HFP quasar) were used as fringe finders and a few more calibration sources (including the bright HFP J1407+2827 alias OQ208) were observed to verify the system performance during each

experiment.

The data reduction has been carried out following the standard procedures for the VLBA, implemented in the NRAO AIPS software. A-priori amplitude calibration was derived using measurements of the system temperature and antenna gains. We estimate that the error on the absolute flux density scale is generally within 5% perhaps with a slightly larger value at 43.2 GHz. Fringe fitting was carried out on each source, with a short (down to 1 min) solution interval at 22.2 and 43.2 GHz in order to preserve the coherence. In general all sources were detected on all baselines, and the data turned out to have good quality at all frequencies with a few exceptions. The final radio images were obtained after a number of phase self-calibration iterations. A Gaussian fit was performed on the final image by means of the task JMFIT for marginally resolved components, and the flux densities of the extended ones were determined with TVSTAT and IMSTAT.

The results will be presented in detail in Orienti et al. (in preparation). In Tab. 3.7 I report the VLBA flux densities of candidate HFPs compared with the VLA flux densities at the same frequencies. Column 1 gives the source name (J2000), column 2 the optical identification, column 3, 4: VLA and VLBA 8.4 GHz flux density, respectively, column 5, 6: VLA and VLBA 15.3 GHz flux density, column 7, 8: VLA and VLBA 22.2 GHz flux density, column 9: VLBA 43.2 GHz flux density, column 10: the spectral index between the two frequencies available and, finally, column 11: morphological classification from VLBA images. In Fig. 3.20 we compare the flux densities of the sources detected with the VLA and the VLBA at three frequencies (8.4, 15.0 and 22.0 GHz). The lines correspond to equality of the two measurements. The two sets of observations have a maximum time gap of $\sim$6 months. The plots show that there are no significant differences in flux densities at 8.4 GHz while at higher frequencies the flux densities measured with the VLBA are increasingly lower than those measured by the VLA. The flux density differences are clearly systematic and can be partially ascribed to calibration errors. Probably the larger flux density losses can be explained by structures detected with the VLA but completely resolved out by the VLBA, given also the limited *uv*-covarage, unsuitable to map complex components with sizes of the orders of ten milliarcesecond.

The analysis of the data is still in progress. Of the 53 sources analyzed, 33 appear

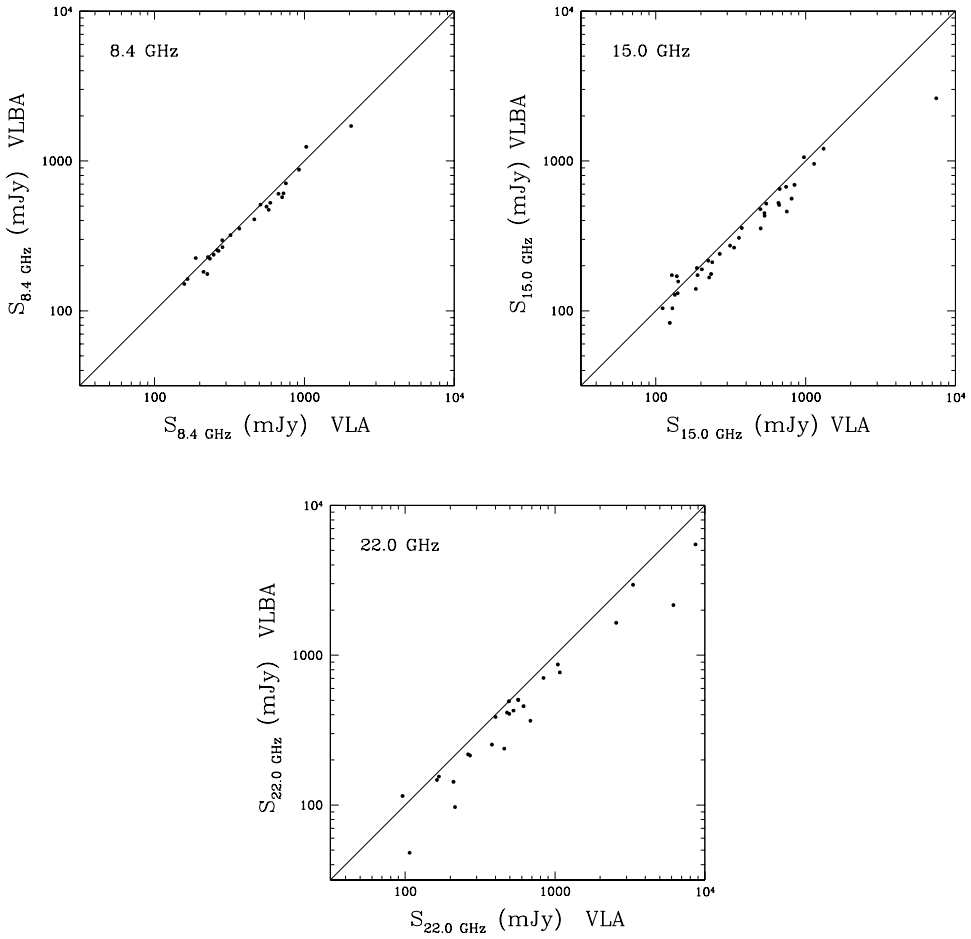

Figure 3.20: Comparison between the VLBA integrated flux densities and the VLA flux densities at 8.4, 15.0, 22.0 GHz. The lines correspond to equality of the two determinations.

resolved by the VLBA resolution; one (J1424+2256) is a gravitational lens. The images of the resolved sources are shown in Figs. 3.21–3.51.

We have performed a Gaussian fit to the resolved sources, at least at the highest frequency of observation (i.e. at the best resolution), to determine angular (linear) size and flux densities of two (or more) distinct components. These sources have been then classified as Compact Symmetric Objects (**CSO**) or Core-Jet (**CJ**) sources on the basis of the spectral indices of their components. If both the components are steep ($\alpha > 0.5$) we classified the object as a CSO. On the other hand sources with a strong flat or inverted spectrum component in addition to a weak, steep spectrum larger component are classified as core-jet objects. In this way we could reliably classify 25 of the 33 resolved sources (Tab. 3.7). Eight sources which require further investigation are labelled with a question mark in the latter table, where the twenty sources still unresolved at the higher VLBA resolution are marked as **Un**.

In Tables 3.8 and 3.9 I have reported the parameters of the components of the sources classified as CSO and CJ, respectively: columns 1 and 2 give the source name and sub-component label; columns 3, 4, 5 and 6 the VLBA flux densities at 8.4, 15.3, 22.2 and 43.2 GHz respectively; column 7 the spectral index between the two frequencies available.

Twelve sources (8 galaxies, 2 quasars and 2 empty fields) show a "double/triple" morphology and the spectral index of all the components is steep ($\alpha > 0.5$). Nine sources have a double structure and five are characterized by two well separated components which show large asymmetries in brightness. Some sources possess a more complex morphology: three distinct components are visible in J0428+3259 at both frequencies of observations and in J2203+1007 at 8.4 GHz; we have fitted J1855+3742 with two components but the morphology of the North component is quite broad and complex; in two sources (J0650+6001 and J1735+5049) the radio emission is dominated by two extended components that can be interpreted as radio lobes. Since the data do not have either the dynamic range or the resolution suitable to detect weak flat spectrum components, there is no core identification so far.

Thirteen objects (11 quasars and 2 empty fields) show a core-jet morphology. The core components are compact, with a flat or inverted spectrum and account for a large

fraction (about 70% and 80% at the lowest and highest frequency respectively) of the total flux density. Jet components are weaker and with a steep spectrum.

3.6.1 Radio structure and optical identification

The analysis of the data is still work in progress, however some interesting conclusions can be already drawn on the classified sources. There is a clear segregation in radio morphology between quasars and galaxies. The majority of galaxies ($\sim$80%) show a "Double/Triple" morphology and have been classified as CSO sources (56% if we consider also the empty fields), while quasars are generally either Core-Jet ($\sim$31%) or Unresolved ($\sim$ 40%).

This is consistent with the idea that the HFP spectrum in galaxies and quasars originates from intrinsically different emitting regions: mini-lobes and/or hot spots in galaxies, compact regions related to the core in quasars. This is in agreement with other results obtained comparing the properties of galaxies and quasars in GPS and bright CSS sample (Stanghellini et al. 1998; Fanti et al. 1990). Morphology is a strong support to the classification of the radio sources and this analysis confirms that it is likely that HFP quasars (as well as GPS quasars) have a morphological structure intrinsically similar to that of flat spectrum radio sources, and their convex radio spectrum is due to a single rather homogeneous component, like a knot in a jet, which dominates the radio emission. Nevertheless some HFP quasars can still be genuine young radio sources.

Source		$S_{8.4}^{VLA}$	$S_{8.4}^{VLBA}$	$S_{15.0}^{VLA}$	$S_{15.0}^{VLBA}$	$S_{22.0}^{VLA}$	$S_{22.0}^{VLBA}$	$SS_{43.0}^{VLBA}$	α	Morph.
		mJy	mJy	mJy	mJy	mJy	mJy	mJy		
J0003+2129	G	227	228	140	131				0.95	CSO
J0005+0524	Q	166	163	111	104				0.78	CJ
J0037+0808	G	262	254	190	173				0.67	CSO
J0116+2422	EF	248	237	128	173				0.50	Un
J0217+0144	Q					838	705	521	0.38	CJ
J0329+3510	Q	578	472	659	525				-0.17	CJ
J0357+2319	Q					168	155	110	0.50	Un
J0428+3259	G			375	357	263	218		1.32	CSO
J0519+0848	EF					401	387	349	0.15	Un
J0625+4440	Q					210	143	60	1.30	Un
J0638+5933	EF					567	505	340	0.59	CJ
J0642+6758	Q	321	320	203	189				0.88	Un
J0646+4451	Q					3318	2953	1938	0.63	CJ
J0650+6001	Q			671	650	495	406		1.26	CSO
J0655+4100	G			313	272	271	214		0.64	Un
J0722+3722	Q			138	170	96	115		1.05	CJ
J0927+3902	Q					8660	5488	3093	0.85	CJ
J1016+0513	Q					379	253	227	0.16	Un
J1045+0624	Q	284	266	238	211				0.32	CJ
J1148+5254	Q			501	355	458	238		1.00	?
J1335+4542	Q	592	526	359	307				0.93	?
J1335+5844	EF	671	604	531	449				0.51	CSO
J1407+2827	G	2050	1712	1139	957					CSO
J1412+1334	EF	267	251	185	140				0.97	CSO
J1430+1043	Q	752	709	546	519				0.56	CJ
J1457+0749	EF	188	225	141	157				1.09	Un
J1505+0326	Q	710	573	665	509				0.21	Un
J1511+0518	G			843	693	617	457		1.18	CSO
J1526+6650	Q					107	48	?		?

Table 3.7: The VLBA flux densities of candidate HFPs.

Source		$S_{8.4}^{VLA}$ mJy	$S_{8.4}^{VLBA}$ mJy	$S_{15.0}^{VLA}$ mJy	$S_{15.0}^{VLBA}$ mJy	$S_{22.0}^{VLA}$ mJy	$S_{22.0}^{VLBA}$ mJy	$SS_{43.0}^{VLBA}$ mJy	α	
J1603+1105	EF	225	176	234	176				0.00	Un
J1616+0459	Q	559	496	333	264				1.04	CSO
J1623+6624	G	283	296	224	216				0.53	Un
J1645+6330	Q					493	493	363	0.46	Un
J1717+1917	Q			227	167	215	97		1.50	Un
J1735+5049	G	920	875	740	672				0.44	CSO
J1800+3848	Q					1076	768	537	0.51	Un
J1811+1704	Q	509	511	499	477				0.11	CJ
J1840+3900	Q	158	151	134	128				0.28	Un
J1850+2825	Q			1318	1208	1045	867		0.81	?
J1855+3742	G	212	182	124	83				1.31	CSO
J2021+0515	Q	368	354	267	240				0.65	?
J2024+1718	Q					569	502	294	0.78	?
J2101+0341	Q					478	414	341	0.28	Un
J2114+2832	EF			749	460	685	365		0.62	CJ
J2123+0535	Q					2560	1645	1330	0.32	?
J2136+0041	Q			7443	2620	6169	2160	1502		CJ
J2203+1007	G	234	223	129	104				1.27	CSO
J2207+1652	Q			188	193	163	147		0.73	Un
J2212+2355	Q	1028	1242	975	1059				0.27	Un
J2257+0243	Q					528	427	272	0.67	Un
J2320+0513	Q	725	608	806	561				0.13	Un
J2330+3348	Q	463	408	532	431				0.09	CJ

Table 3.7: The VLBA flux densities of candidate HFPs (continued).

Name	Comp	$S_{8.4}$ mJy	$S_{15.0}$ mJy	S_{22} mJy	S_{43} mJy	α
J0003+2129	E	214.4	125.43			0.92
	W	7.5	3.9			1.13
J0037+0808	E	218.9	159.1			0.55
	W	32.6	13.2			1.6
J0428+3259	E		23.0	12.0		1.67
	C		233.0	168.0		0.87
	W		93.0	40.0		2.23
J0650+6001	N		488	327		1.04
	S		150	78		1.70
J1335+5844*	N	420.2	392.5			0.12
	S	159.7	36.0			2.5
J1407+2827	N	1712.4	916			1.08
	S	122.1	33.45			2.23
J1412+1334	N	157	100			0.75
	S	96	43			1.34
J1511+0518	E		416.2	293.53		0.91
	W		255.6	158.4		1.25
J1616+0459	N	390	204			1.08
	S	103	60			0.90
J1735+5049	N	177.4	83.4			1.30
	S	691.8	574.9			0.32
J1855+3742	N	173.2	79			1.35
	S	16.8	9.0			1.08
J2203+1007	E	155.2	89.3			0.95
	W	55.3	17.0			2.03

Table 3.8: The VLBA flux density of candidate CSOs' components. Columns 1 and 2: source name and sub-component label; Columns 3, 4, 5 and 6: VLBA flux density at 8.4, 15.3, 22.2 and 43.2 GHz respectively; Column 7: spectral index between the two frequencies available.

Source	Comp	$S_{8.4GHz}$ mJy	$S_{15.0GHz}$ mJy	S_{22GHz} mJy	S_{43GHz} mJy	α
J0005+0524	C	89.6	83.2			0.13
	J	77.3	33.4			1.4
J0217+0144	C			559	462	0.29
	J			147	37	2.07
J0329+3510	C	340	374			-0.16
	J	126	143			-0.21
J0638+5933	C			312.8	165.9	0.39
	J1			179.2	60.0	1.63
	J2				66.2	0.284
J0646+4451	C			2396	1338	0.87
	J			496.0	517	-0.06
J0722+3722	C	102	97			0.08
	J	67	20			2.01
J0927+3902	J1			1825	1215	0.61
	J2			3650	1857	1.02
J1045+0624	C	156	171			-0.15
	J	102	47			1.29
J1430+1043	C	546	363			0.68
	J	160	140			0.22
J1811+1704	C	342	367			-0.12
	J	176	119			0.68
J2114+2832	C		440.6	356.4		0.55
	J		10.0	9.5		0.13
J2136+0041*	C		2619.7	2160.9	1502	0.50
	J		2858	1775.3	979	1.24
J2330+3348	C	328	341			-0.06
	J	74	99			-0.49

Table 3.9: VLBA flux densities of core-jet source components. Columns 1 and 2: source name and sub-component label; columns 3, 4, 5 and 6: VLBA flux density at 8.4, 15.3, 22.2 and 43.2 GHz respectively; column 7: spectral index between the two frequencies available

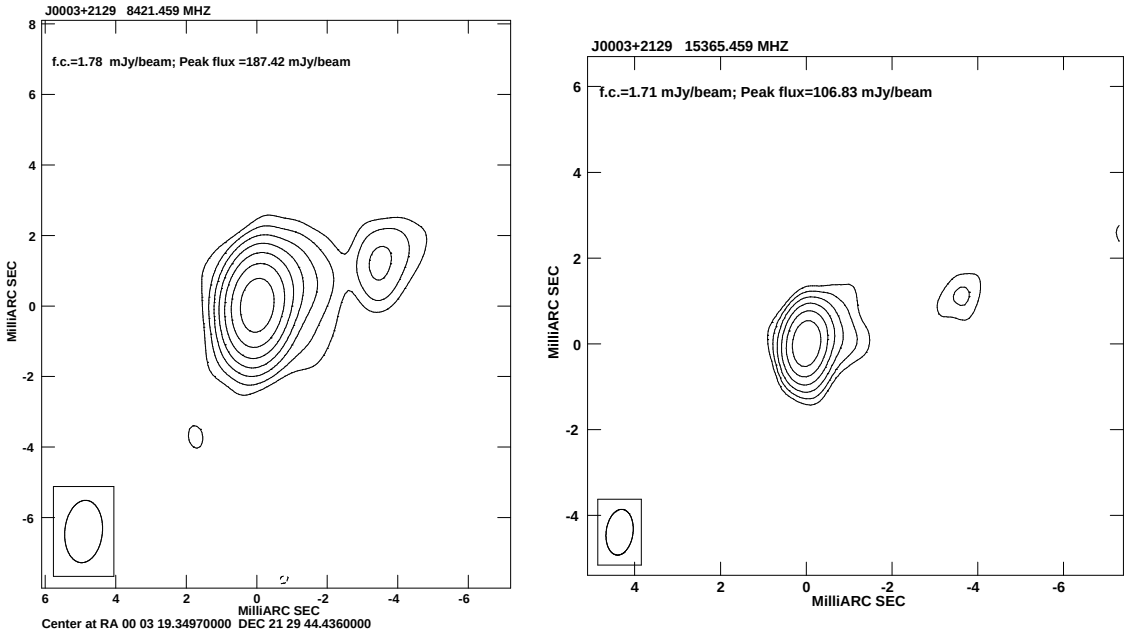

Figure 3.21: J0003+2129: classified as CSO

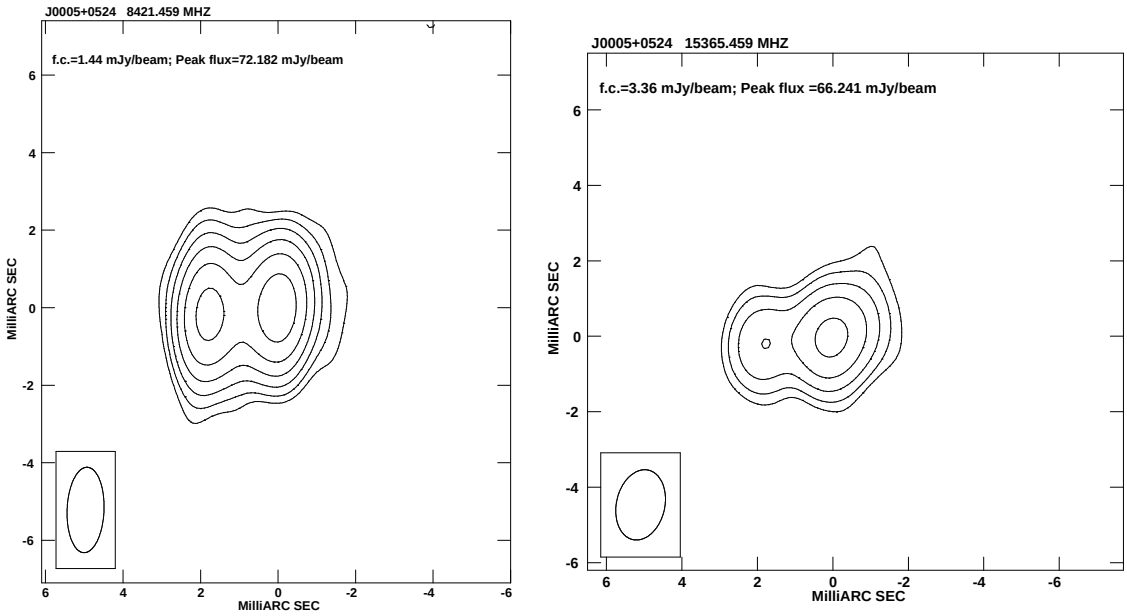

Figure 3.22: J0005+0524: classified as CJ source

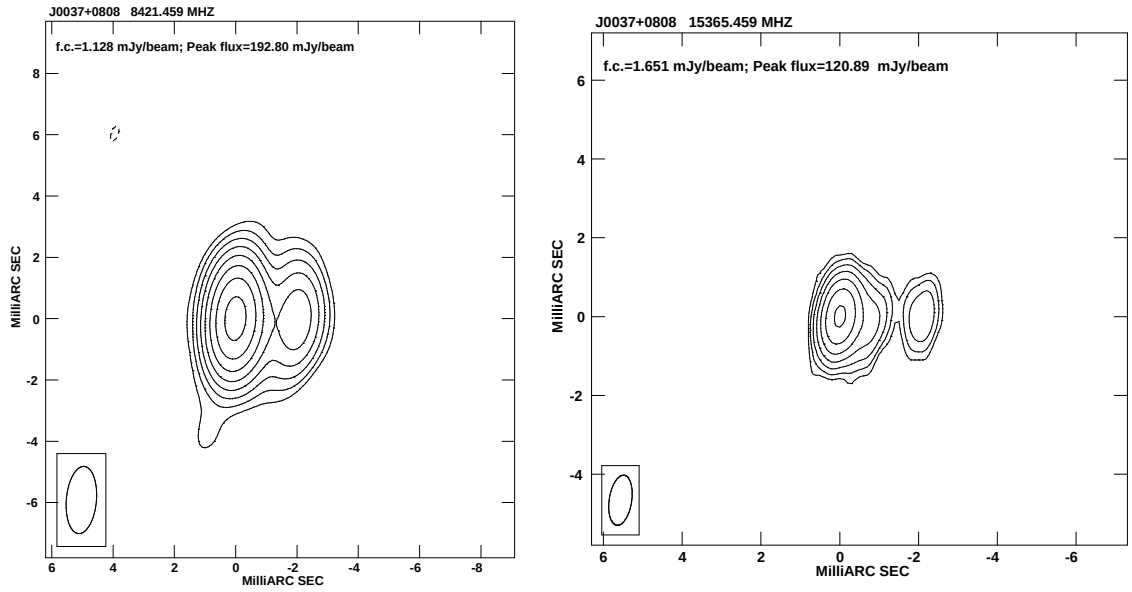

Figure 3.23: J0037+0808: classified as CSO

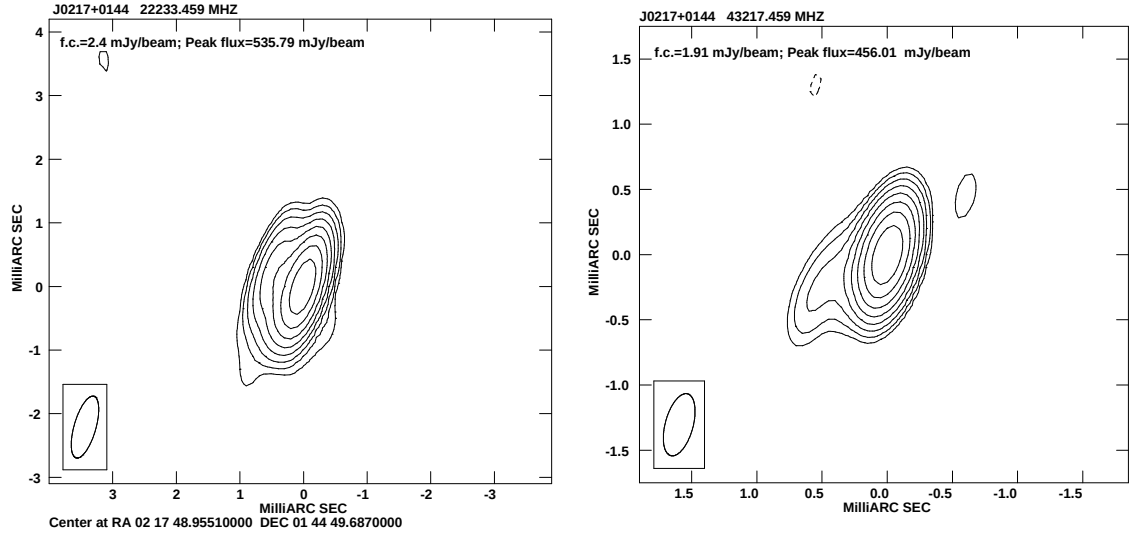

Figure 3.24: J0217+0144: classified as CJ source

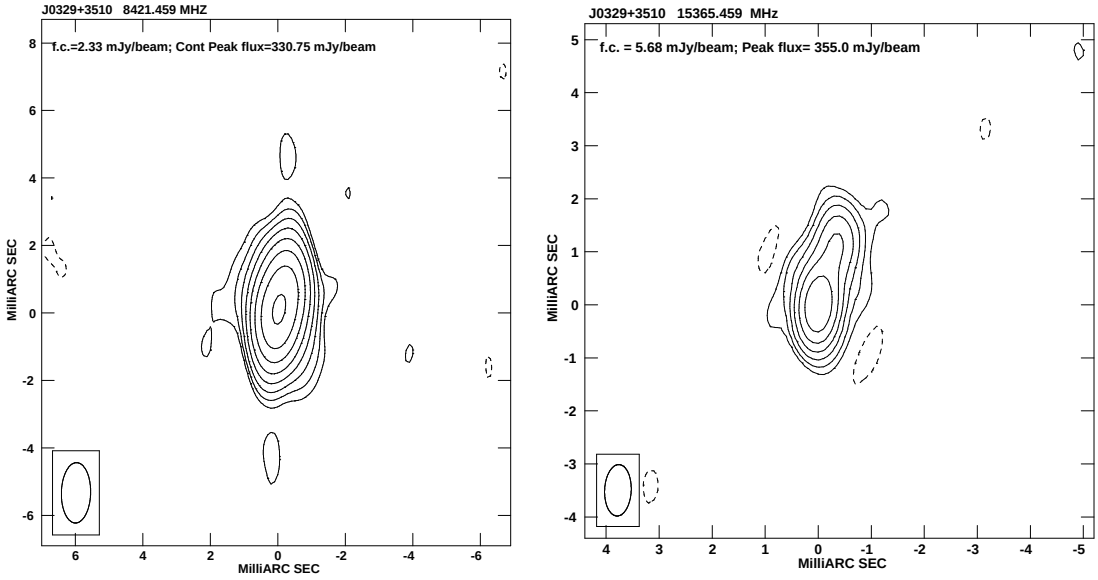

Figure 3.25: J0329+3510: classified as CJ source

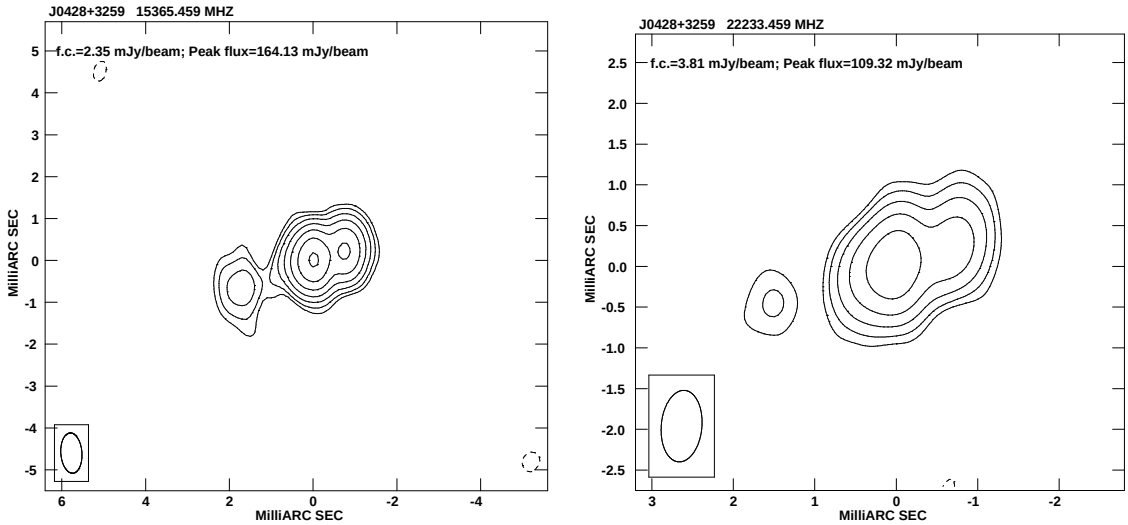

Figure 3.26: J0428+3259: classified as CSO

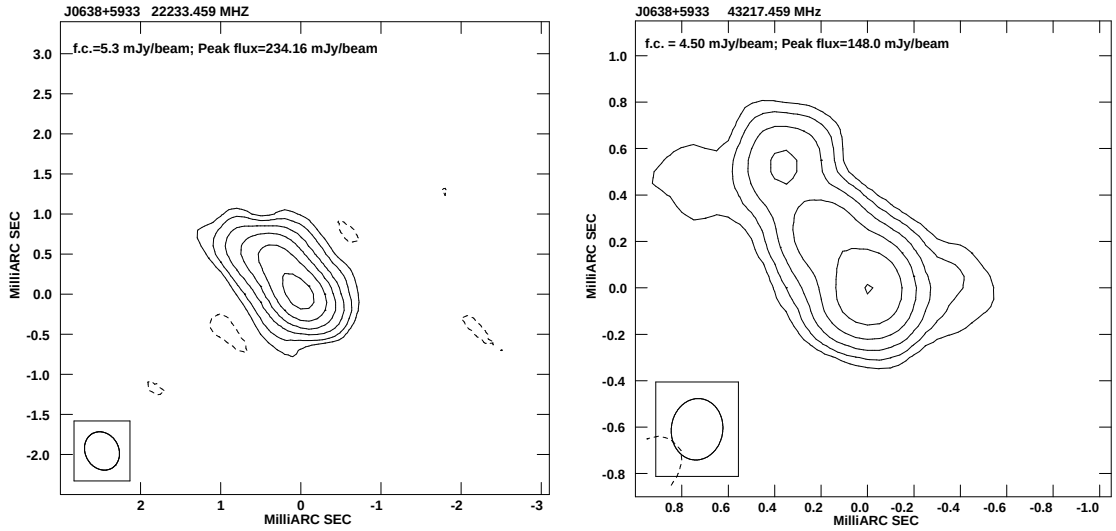

Figure 3.27: J0638+5933: classified as CJ source

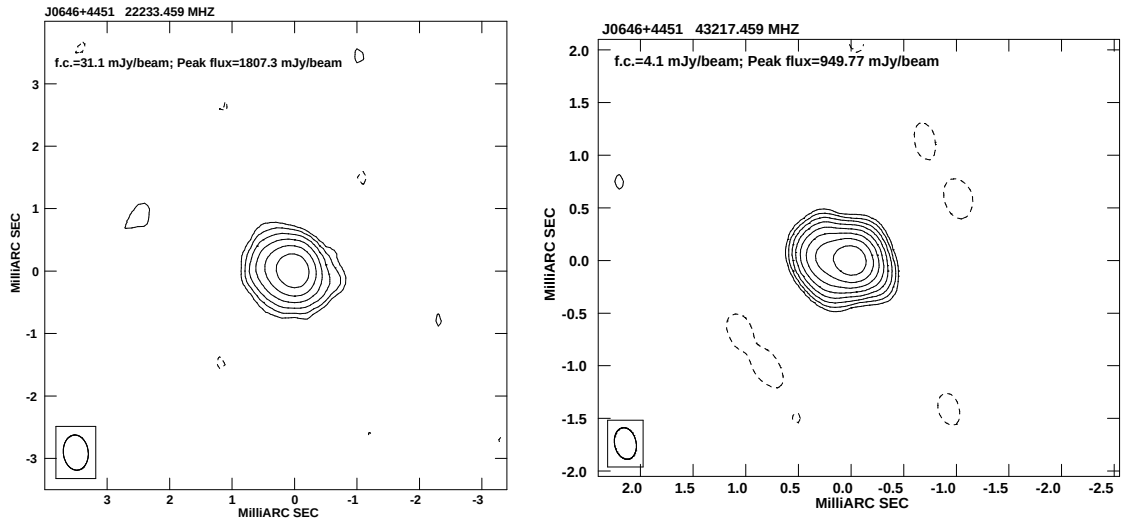

Figure 3.28: J0646+4451: classified as CJ source

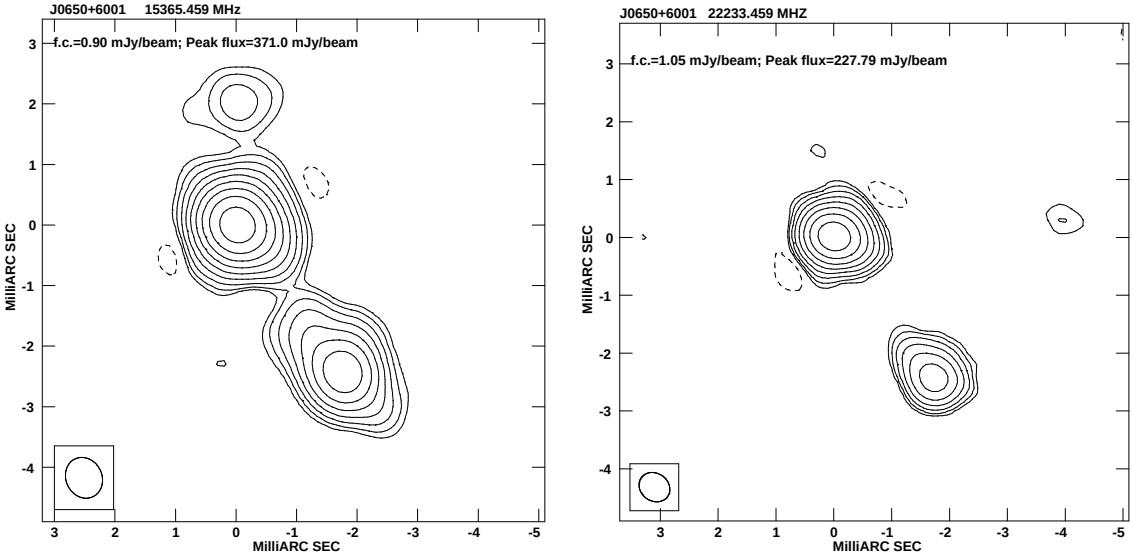

Figure 3.29: J0650+6001: classified as CSO

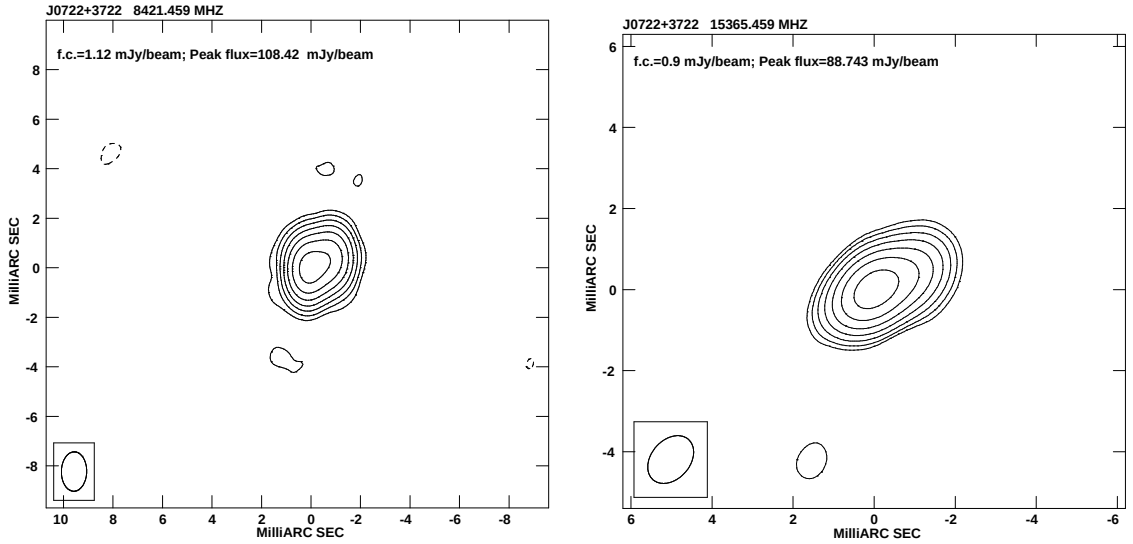

Figure 3.30: J0722+3722: classified as CJ source

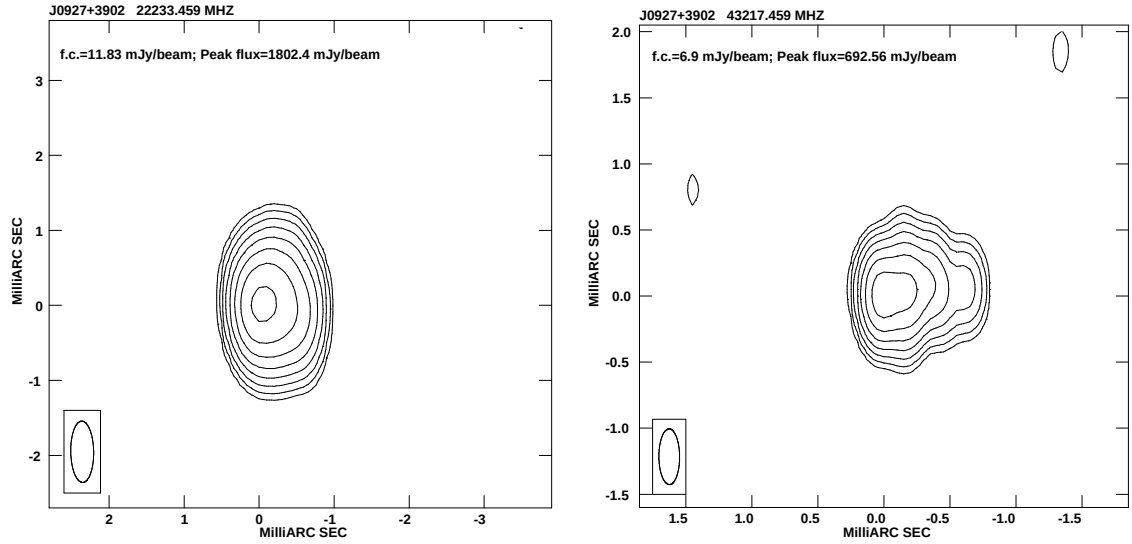

Figure 3.31: J0927+3902: classified as CJ source

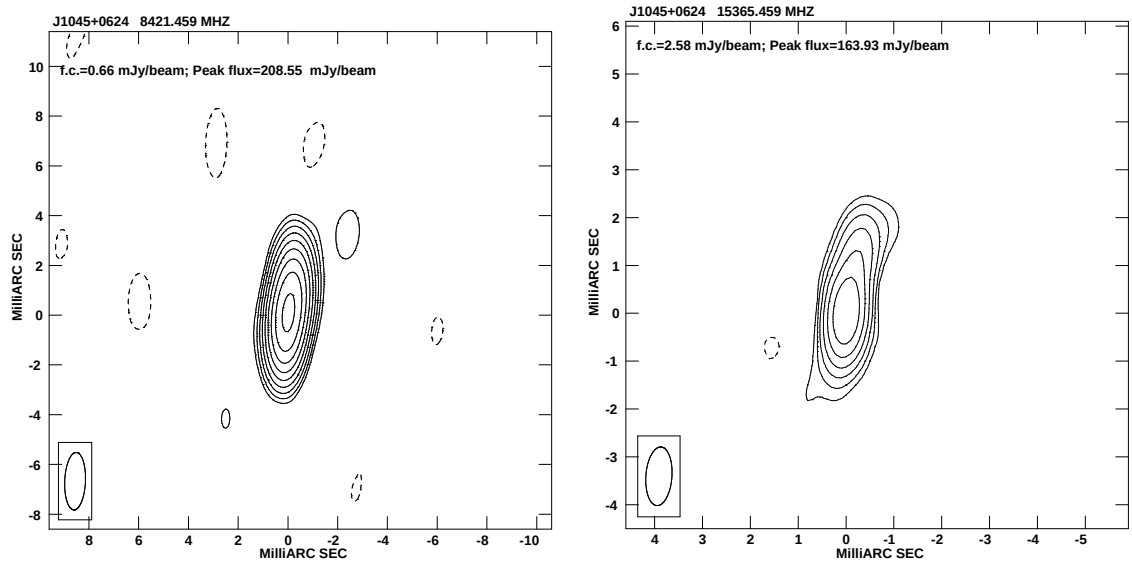

Figure 3.32: J1045+0624: classified as CJ source

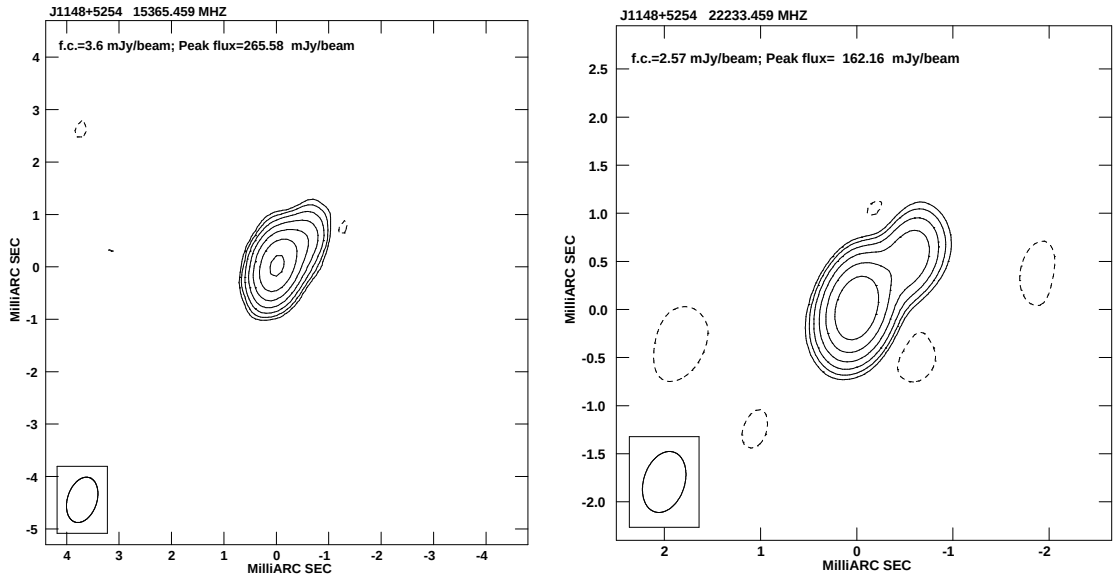

Figure 3.33: J1148+5254: classification uncertain (?)

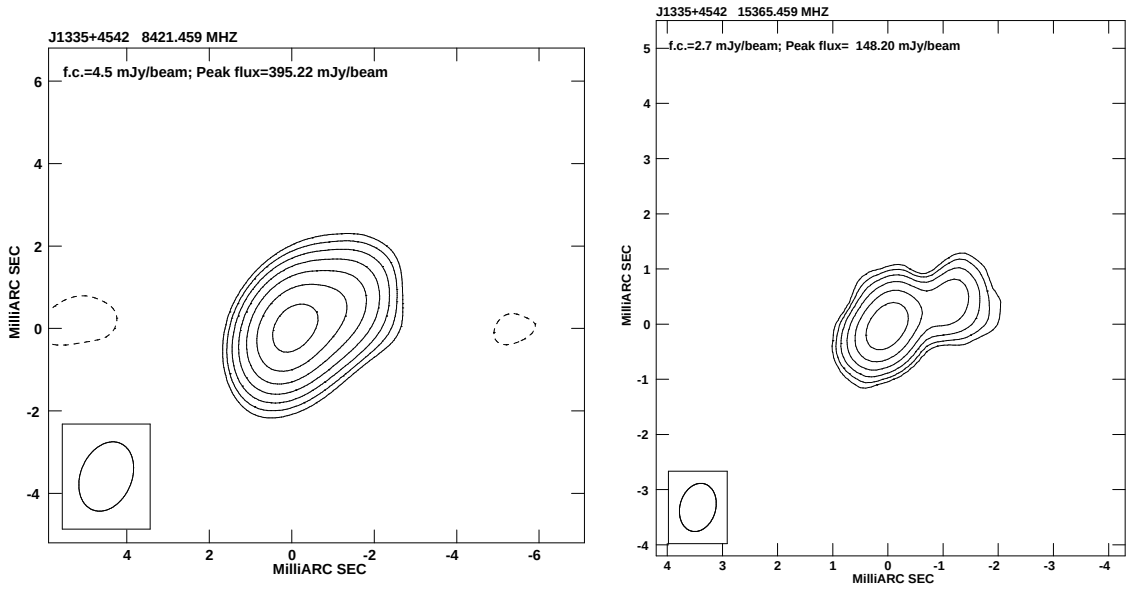

Figure 3.34: J1335+4542: classification uncertain (?)

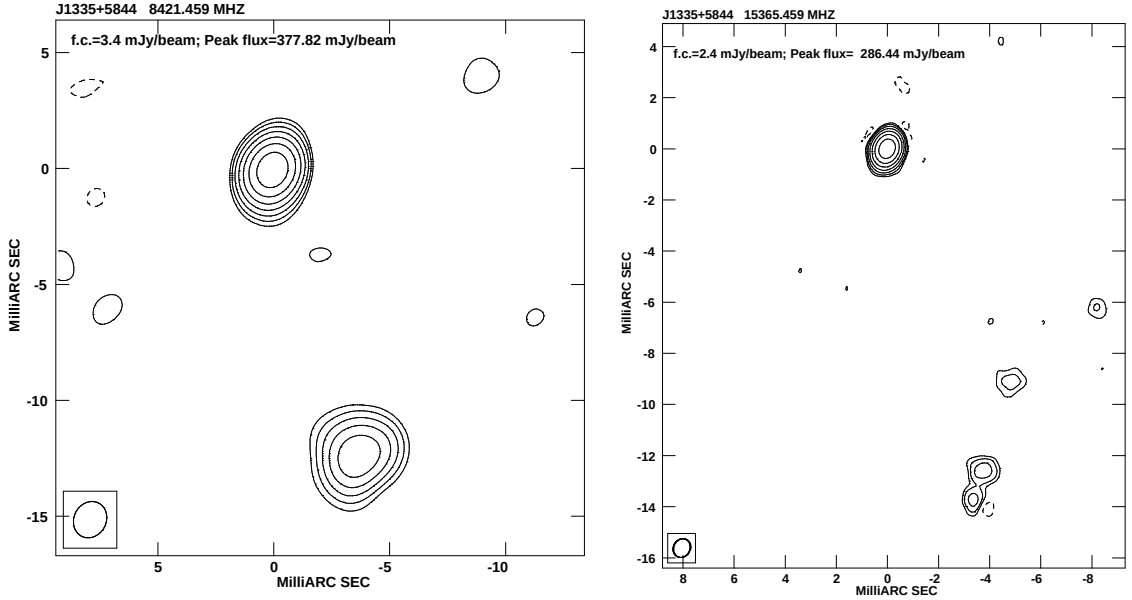

Figure 3.35: J1335+5844: classified as CSO

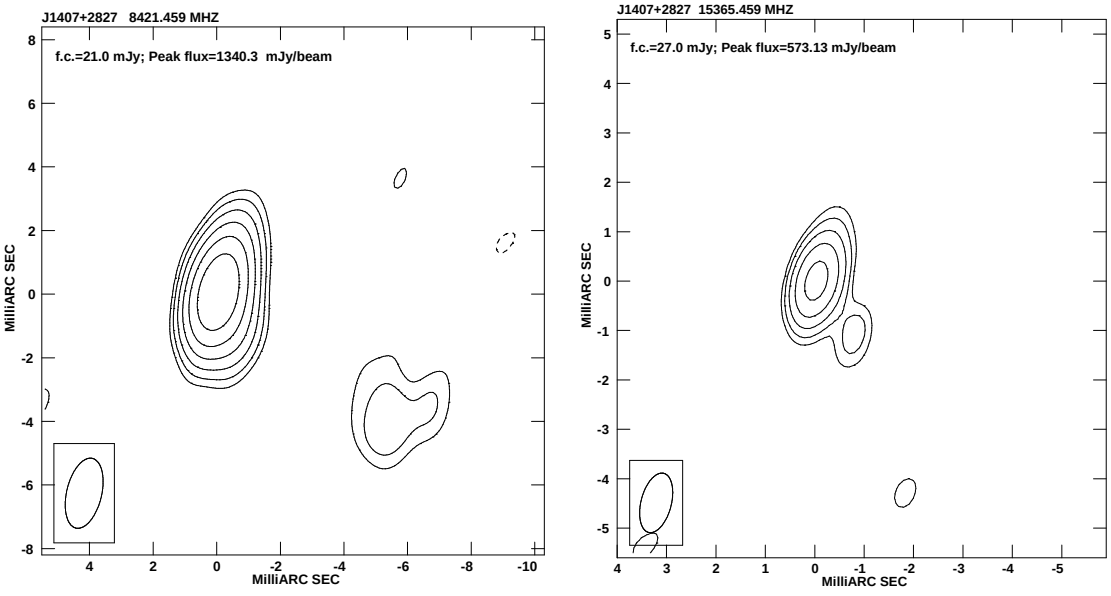

Figure 3.36: J1407+2827: classified as CSO

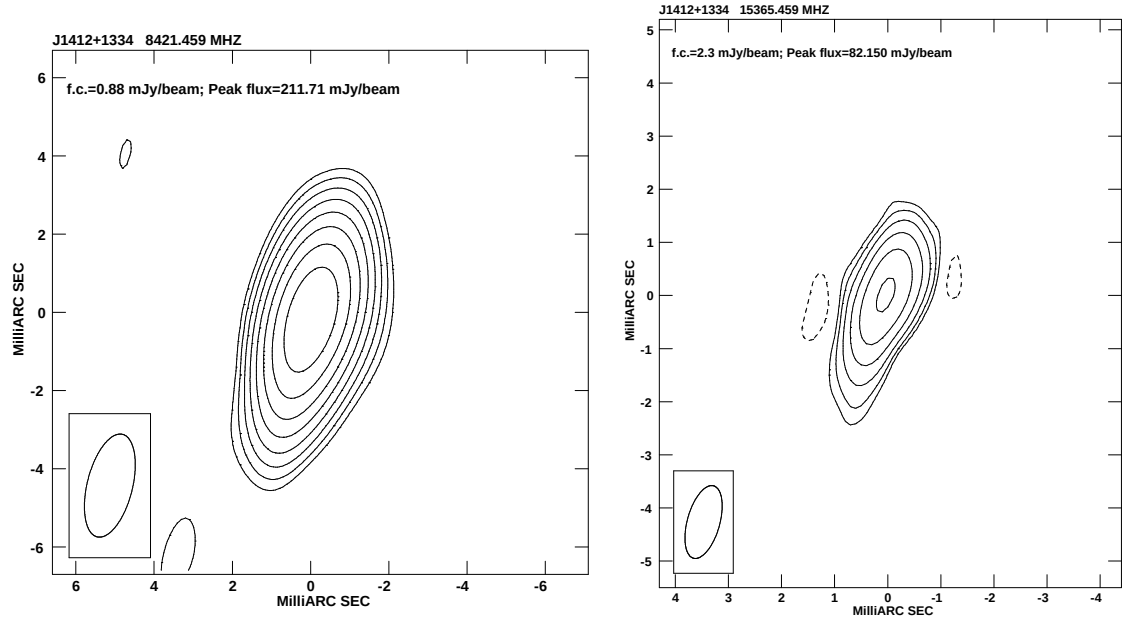

Figure 3.37: J1412+1334: classified as CSO

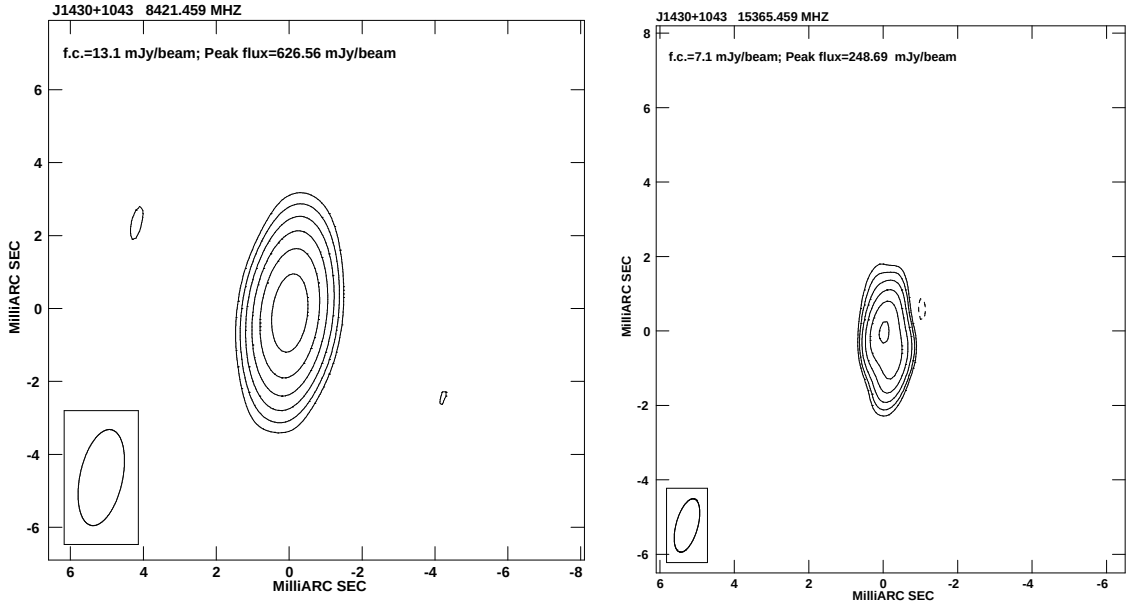

Figure 3.38: J1430+1043: classified as CJ source

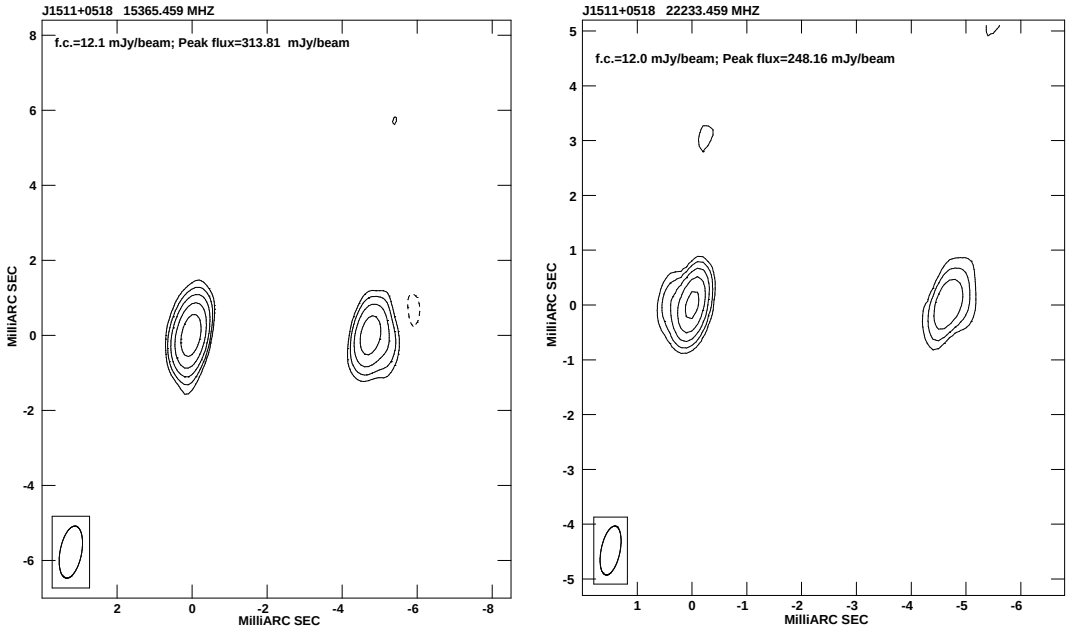

Figure 3.39: J1511+0518: classified as CSO

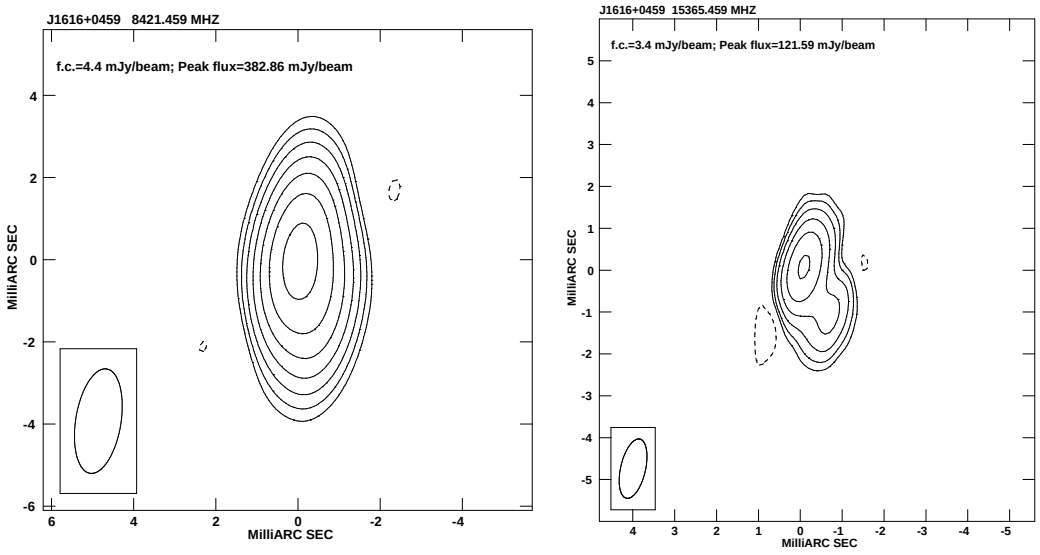

Figure 3.40: J1616+0459: classified as CSO

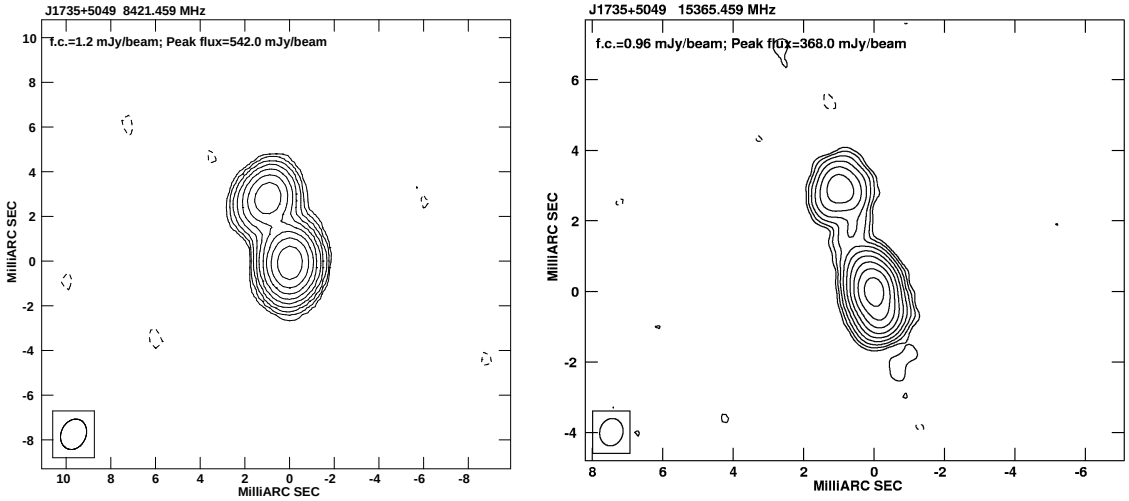

Figure 3.41: J1735+5049: classified as CSO

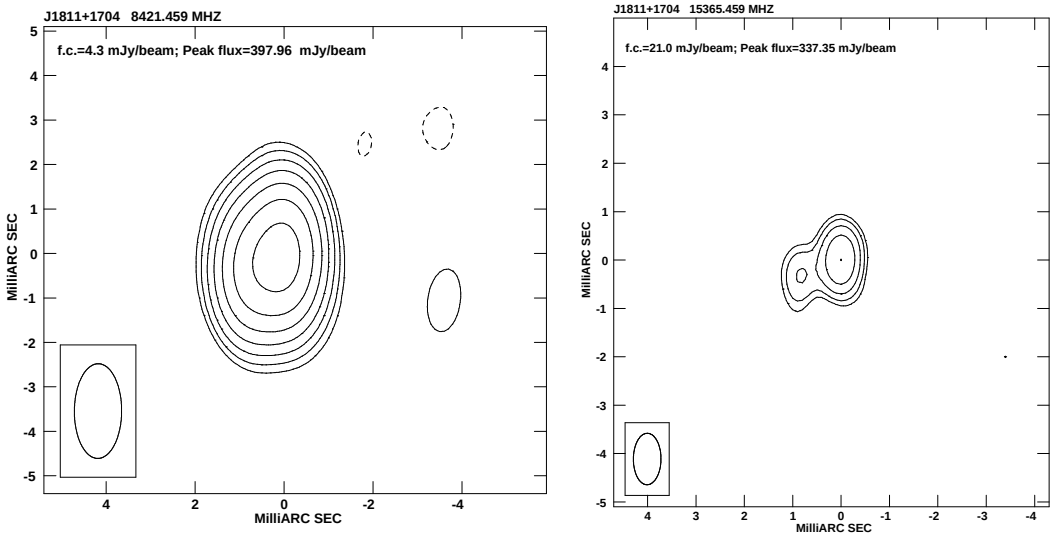

Figure 3.42: J1811+1704: classified as CJ source

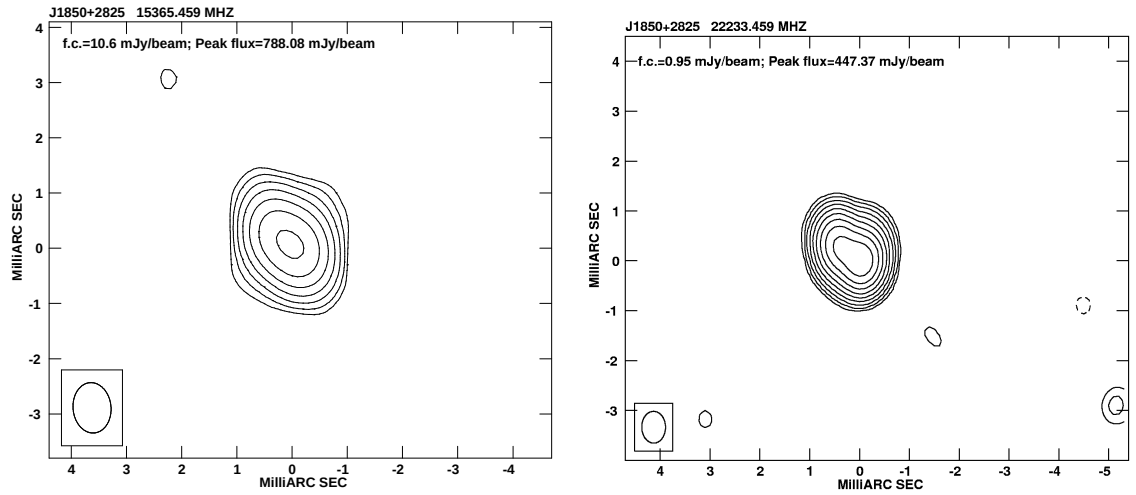

Figure 3.43: J1850+2825: classification uncertain (?)

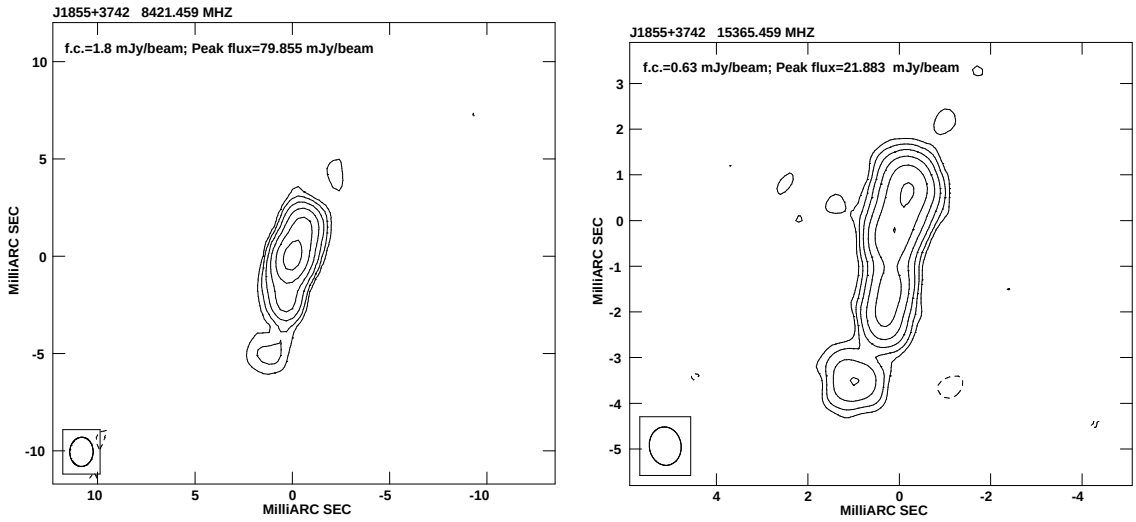

Figure 3.44: J1855+3742: classified as CSO

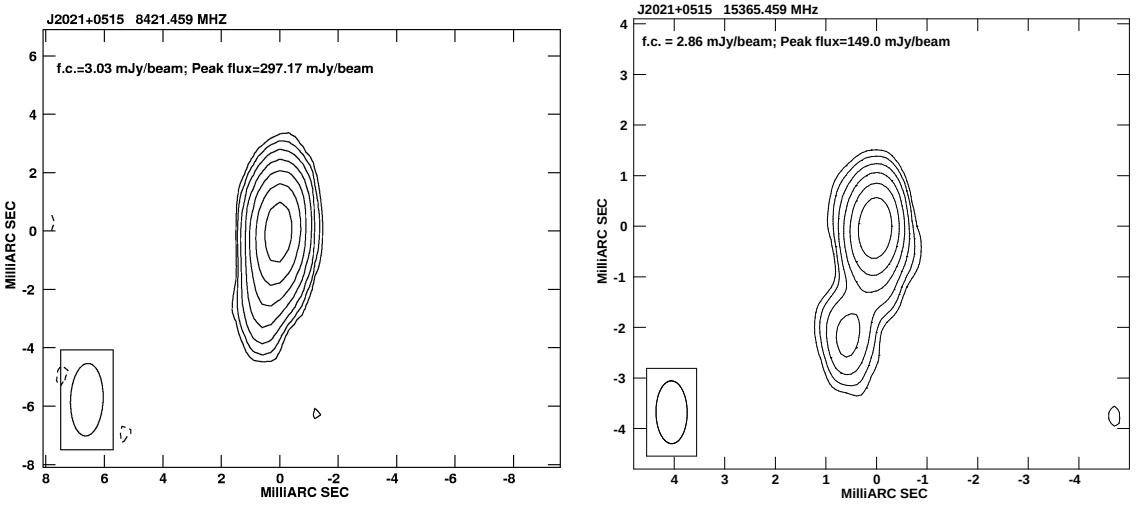

Figure 3.45: J2021+0515: classification uncertain (?)

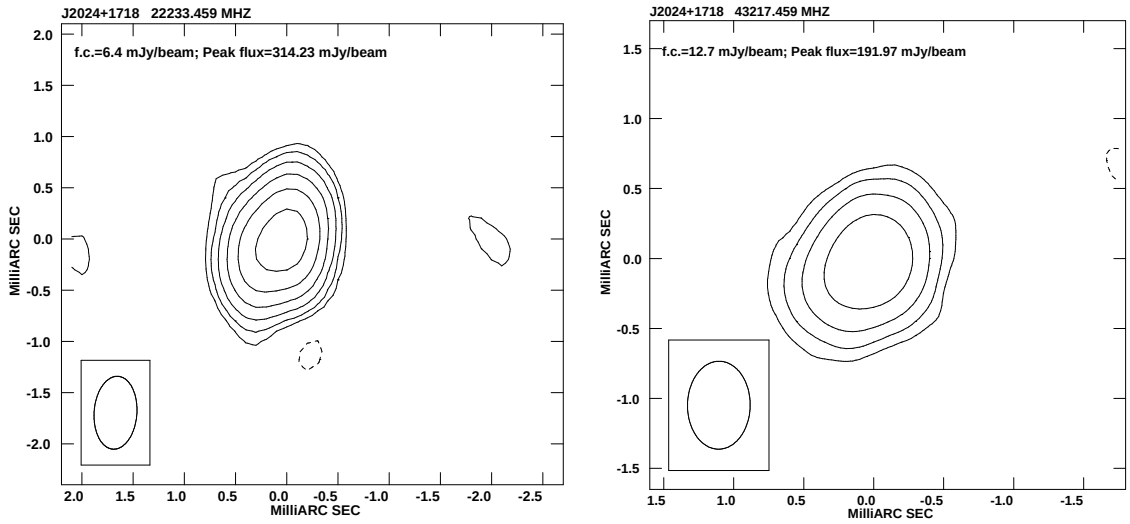

Figure 3.46: J2024+1718: classification uncertain (?)

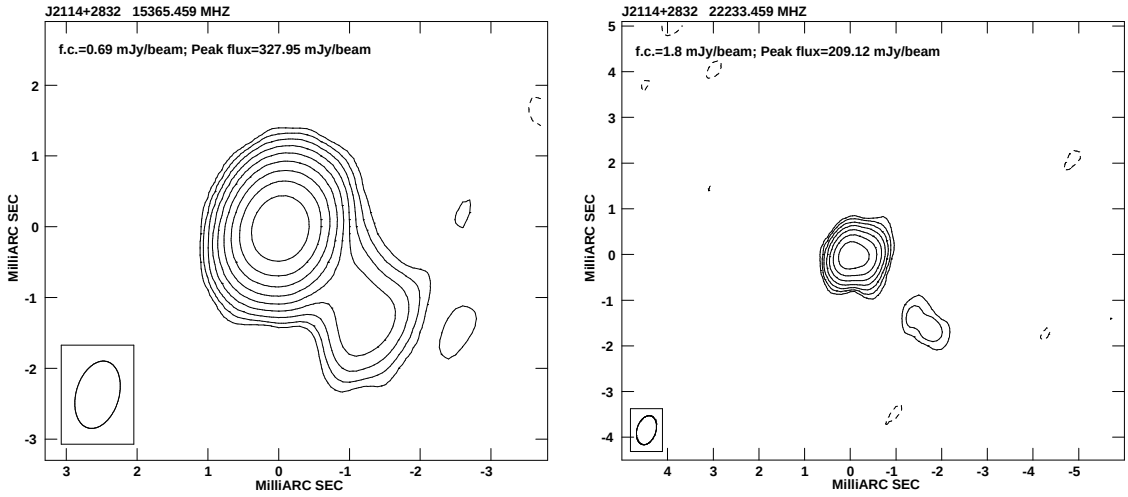

Figure 3.47: J2114+2832: classified as CJ source

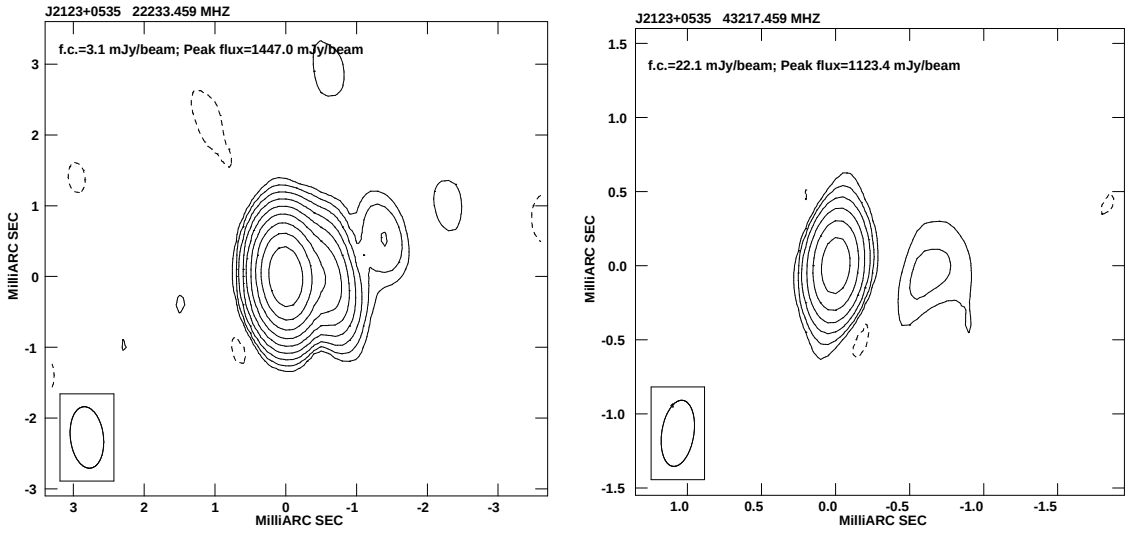

Figure 3.48: J2123+0535: classification uncertain (?)

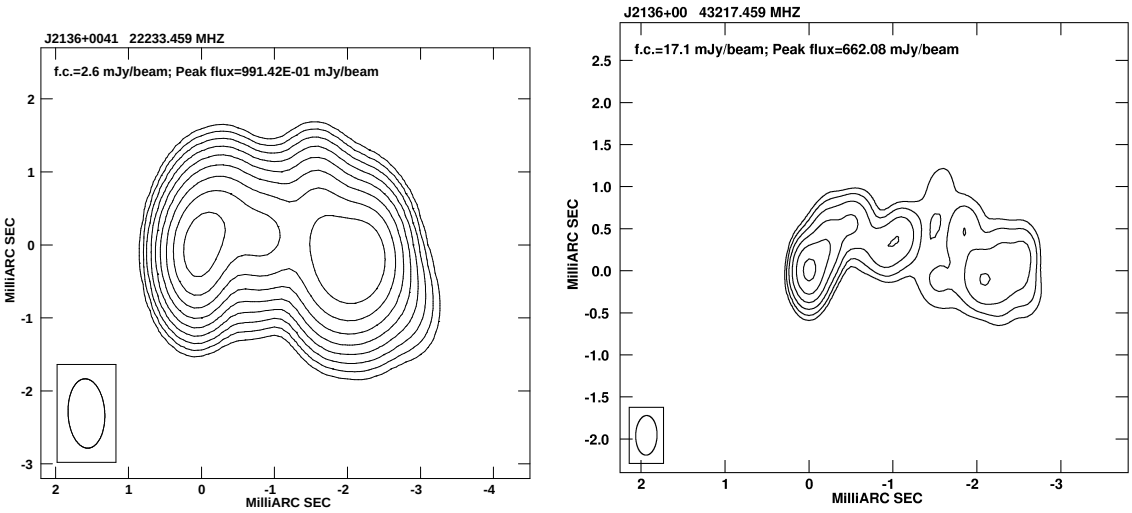

Figure 3.49: J2136+0041: classified as CJ source

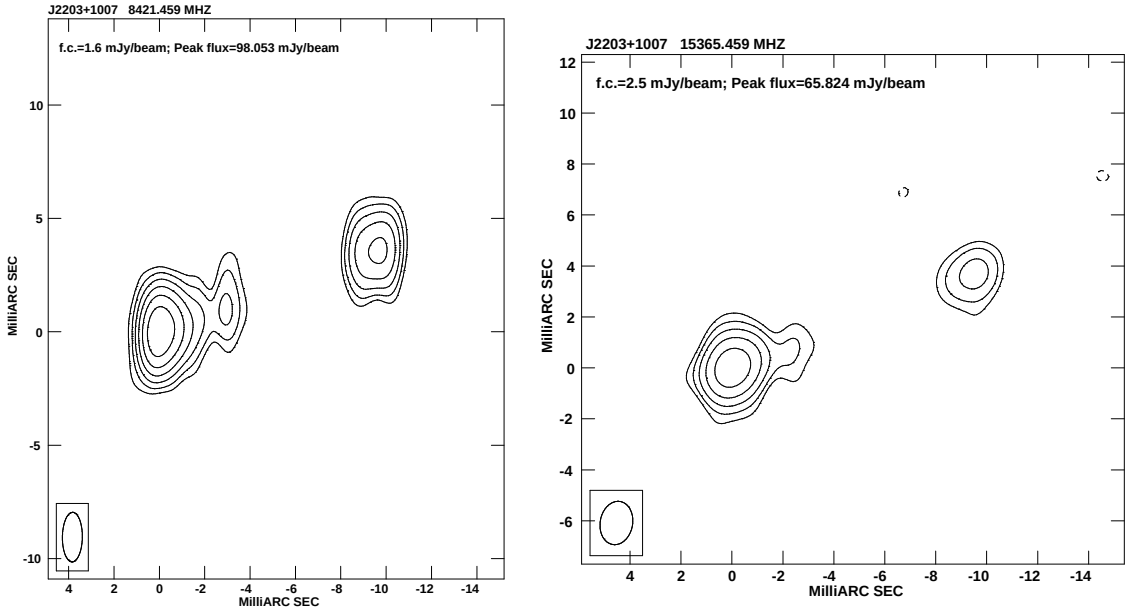

Figure 3.50: J2203+1007: classified as CSO

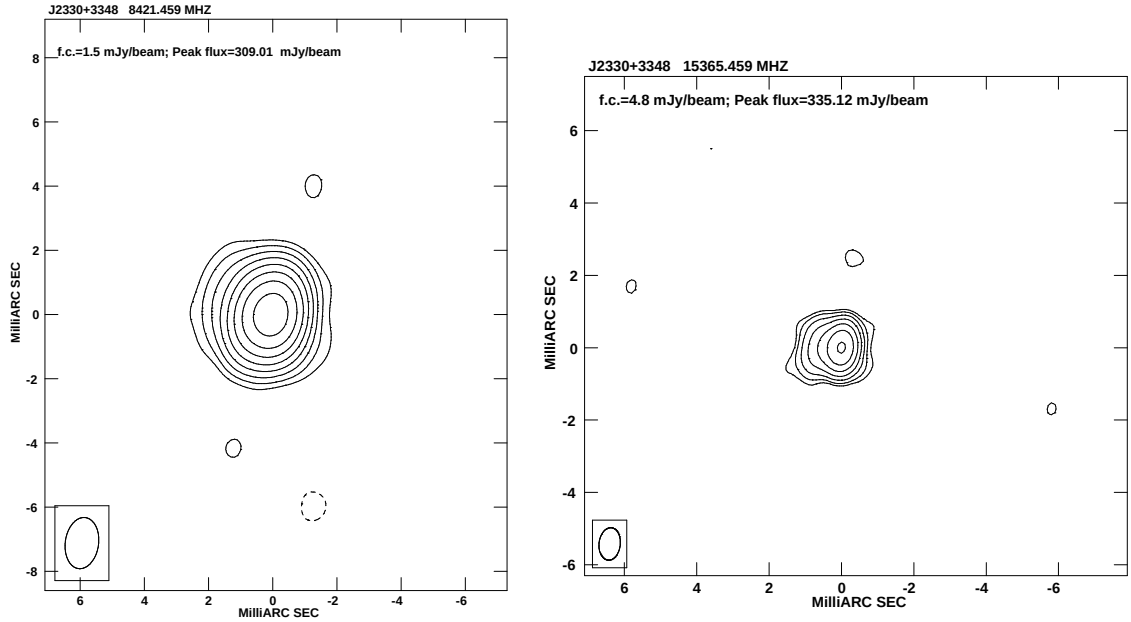

Figure 3.51: J2330+3348: classified as CJ source

Chapter 4

Young sources or Flaring Blazars?

4.1 Introduction

Since the process that characterizes both flaring blazars and young radio sources is the expansion of an emitting "blob" within the ISM, i.e. the lobes in the case of young sources, a knot of the jet that dominates the radio spectrum for blazars, it is quite difficult to distinguish the two phenomena. The information on flux density variability of HFP candidates, on their morphology at different resolutions and the polarimetric study have helped us to define criteria to discriminate between the two classes of objects.

Such criteria can be summarized as follows:

- **Variability properties:**
  - **Shape of the spectrum:** GPS/CSS sources have convex spectra that should be preserved during the growth of the source while the blazar spectra are generally flat, but with occasional convex shape when a source has a bright knot whose spectrum is self-absorbed.
  - **Flux density variability:** large Doppler factors in blazars boost the variability amplitudes while GPS/CSS sources are thought to expand at mildly relativistic velocities with marginal or no influence on the radio spectrum.
  - **Evolution of the turnover:** the turnover frequency, ν_p, is expected to decrease with increasing source age, so that the quantity $t_p \propto (d\nu_p/nu_p)/dt)^{-1}$ is an

Name	Id			V	$\Delta\nu/(\nu_p^I \cdot \Delta t)$	POL	Morph	
0003+2129	G*	C	peaked	3.02		NP	CSO	HFP
0005+0524	Q	C	peaked	3.18	0.170 ± 0.03	NP	CJ	?
0037+0808	G?	C	peaked	0.46		NP	CSO	HFP
0111+3906	G	E	peaked	0.46		NP		HFP
0116+2422		C	peaked	5.59		NP	Un	HFP?
0217+0144	Q	E	flat	238.27		POL	CJ	BL
0329+3510	Q*	E	flat	21.60		POL	CJ	BL
0357+2319	Q*	C	flat	420.12		POL	Un	BL
0428+3259	G*	E	peaked	1.20		NP	CSO	HFP
0519+0848		E	peaked	62.80		POL	Un	BL
0625+4440	BL	C	peaked	160.34		POL	Un	BL
0638+5933		C	peaked	0.83		NP	CJ	HFP?
0642+6758	Q	C	peaked	6.77	0.10 ± 0.03	POL	Un	BL
0646+4451	Q	C	peaked	36.91	0.3 ± 0.1	POL	CJ	BL
0650+6001	Q	C	peaked	19.92	0.11 ± 0.01	NP	CSO	?
1335+4542	Q	C	peaked	1.23		NP	?	HFP
1335+5844		C	peaked	1.50		NP	CSO	HFP
1407+2827	G	C	peaked	1.77	0.017± 0.005	NP	CSO	HFP
1412+1334		C	peaked	1.03		NP	CSO	HFP
1424+2256	Q	C	peaked	2.11		POL	?	?
1430+1043	Q	C	peaked	4.19	0.08 ± 0.02	POL	CJ	BL
1457+0749		E	peaked	39.74		POL	Un	BL
1505+0326	Q	C	peaked	19.65		POL	Un	BL
1511+0518	Sy1	C	peaked	8.28		NP	CSO	HFP
1526+6650	Q	C	peaked	0.53		NP	?	HFP
1603+1105		E	peaked	16.65		POL	Un	BL
1616+0459	Q	C	peaked	15.20		POL	CSO	BL?
1623+6624	G	C	peaked	0.47		NP	Un	HFP
1645+6330	Q	C	peaked	2.74		POL	Un	BL
1735+5049	G?	C	peaked	0.15		NP	CSO	HFP
1800+3848	Q	E	peaked	1.91		NP	Un	HFP
1811+1704	Q*	E	flat	58.74		POL	CJ	BL
1840+3900	Q	C	peaked	20.16		NP	Un	BL?
1850+2825	Q	C	peaked	4.86		NP	?	HFP
1855+3742	G*	C	peaked	1.32		NP	CSO	HFP
2021+0515	Q*	C	peaked	5.92		NP	?	HFP
2024+1718	S	E	peaked	9.58	0.26 ± 0.06	POL	?	BL
2101+0341	Q	E	peaked	119.87	0.53 ± 0.02	POL	Un	BL
2123+0535	Q	E	flat	27.49		POL	?	BL
2203+1007	G*	C	peaked	5.02		NP	CSO	HFP
2207+1652	Q*	E	peaked	228.45		POL	Un	BL
2212+2355	S	C	peaked	22.62		POL	Un	BL
2257+0243	Q	C	peaked	1.85		NP	Un	HFP
2320+0513	Q	E	flat	86.24		POL	Un	BL
2330+3348	Q	C	flat	21.42		POL	CJ	BL

Table 4.1: Properties of HFP sources relevant to distinguish between young sources and flaring blazars. In column 2, G stands for galaxy, Sy1 for type 1 Seyfert galaxy, Q for quasar, S for starlike source (taken as a quasar in the analysis), BL for BL Lac object

estimator of the source age (apart from a coefficient expected to be of order unity, depending on the evolution law; cf. Sect. 4.2.3); a too low value of t_p indicates the likely presence of a substantial Doppler factor.

- **Extended emission**: the presence of radio emission on scales of tens of kpc is in contrast with the young age hypothesis. Nevertheless if it is associated with sources with convex spectra without significant flux density variability, it can be reconciled with the youth scenario under the hypothesis of recurrent activity proposed by Baum et al. (1990).

- **Polarisation properties**: since very young sources reside in the innermost regions of the host galaxy, well within the narrow line region (NLR) with its relatively large plasma column densities, very strong Faraday rotation effects are to be expected and they are capable of producing complete depolarisation, except at very high radio frequencies. On the contrary, blazars generally have a significant polarisation degree at GHz frequencies.

- **Morphology**: intrinsically small and young objects are expected to have a Compact Symmetric Object (CSO) morphology, eventually asymmetric in flux density. On the other hand, a core-jet radio structure is typical of blazars.

As is clear from the above summary, there is no single clear-cut quantitative criterion allowing to determine which sources are truly young and which are not. It is thus necessary to use as many data as possible to ascertain the nature of candidates. In Table 4.1 I have reported the results of our measurements of variability, morphology and polarisation of HFP sources. Column 1 gives the source name (J2000), column 2 the optical identification, in column 3 'E' means that extended (on the arcsec scale) emission has been detected, while 'C' applies for the objects where only a compact component has been found (extended emission criterion), in column 4 the label *peaked* indicates the sources that preserve their peaked spectrum at both epochs of VLA observations while the label *flat* indicates the sources that have a flat spectrum at the second epoch (shape of the spectrum criterion), columns 5 and 6 report values of parameters estimating the flux density variability and the

evolution of the turnover frequency, respectively, column 7 indicates if a source is found to be polarised (POL) or not (NP) with the VLA at C and X bands, column 8 reports the morphological classifications at the VLBA resolution and, finally, column 9 indicates if the source is still classified as a candidate HFP or is more likely a blazar object (BL) according to the studied criteria. In the following sections I discuss the various data sets and the consistency of their indications on the source nature.

4.2 Variability properties of the HFP sample

4.2.1 The shape of the spectrum

A convex spectrum is the first property that should be preserved in the evolution of young sources. This is not observed for 7 sources (16% of the sample), all identified with quasars (25% of such objects), whose second epoch radio spectrum turned out to be flat. Five of them show also extended emission at 1.4 GHz (see Section 4.3). Such sources, labeled as "flat" in column 4 of Table 4.1, are therefore classified as blazars, caught by Dallacasa et al. (2000) during a flaring phase of a strongly self-absorbed component.

4.2.2 Flux density variability

Flux density variability also helps distinguishing between expanding young objects and aged beamed objects (blazars) whose radio emission is dominated by a single knot in the jet. While HFP/GPS sources are thought to expand at mildly relativistic velocities, the large Doppler factors characterizing blazar jets boost the variability amplitudes and decrease the corresponding observed timescales. We have analyzed the variability of our sources by studying the parameter V defined as follows:

$$V = \frac{1}{m}\sum_{i=1}^{m}\frac{(S_I(i) - S_{II}(i))^2}{\sigma_i^2} \ , \tag{4.1}$$

where $S_I(i)$ and $S_{II}(i)$ are the VLA flux densities at the i-th frequency, measured at the first and second epoch, respectively, σ_i is the error on $S_I(i) - S_{II}(i)$, and m is the number of the sampled frequencies. We have noted that the second epoch flux densities at 1.4 GHz are systematically higher by about 10% than the first epoch ones (based on the sources

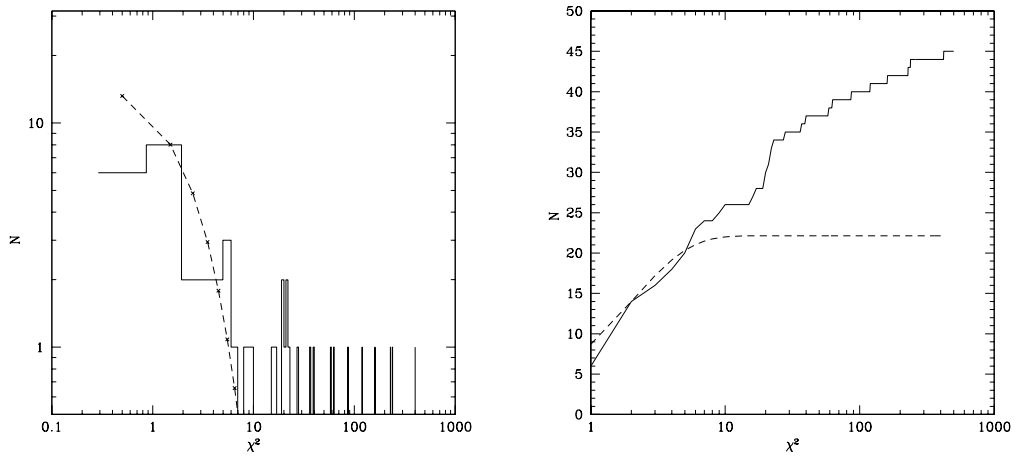

Figure 4.1: Differential (left) and cumulative (right) distribution of V, compared with the corresponding χ^2 distributions for 2 degrees of freedom (dashed lines). The bins of the differential distribution correspond to $\Delta\chi^2 = 1$.

found to stay stable at all the other frequencies), while the flux densities at 1.7 GHz at the two epochs appear to match. This may be related to an unidentified problem during the 1.4 GHz observation of the primary calibrator 3C286. We have therefore chosen to exclude the 1.4 GHz measurements, so that in the above equation $m = 7$. The values of V are reported in column 5 of Table 4.1.

For HFP sources, V depends essentially on only two free parameters, S_p and ν_p (since the spectral slopes are not expected to vary), and should therefore have a χ^2 distribution with 2 degrees of freedom. Figure 4.1 shows that indeed sources with low values of V obey such distribution. Since the probability that a source with $V > 9$ is extracted from such distribution is < 0.01, we conclude that sources with $V > 9$ are very likely blazars. On the other hand, blazars may well have small values of V, so that there is no guarantee that sources with $V < 9$ are all truly young. We must remark however that these conclusions rely to some extent on our error estimates, dominated by calibration uncertainties: any significant over- or under-estimate of errors would impair the match of the distribution of V with the χ^2 distribution with 2 degrees of freedom.

As shown in Table 4.2, all 10 galaxies, including the Seyfert 1, have $V < 9$, while

	N(tot)	N(V<9)	N(V>9)
Galaxies	10	10	0
Quasars	28	11	17
EF	7	4	3

Table 4.2: Number of galaxies, quasars and empty fields with $V < 9$ and $V > 9$.

most quasars (17 out of 28, including the 7 with flat second-epoch spectra) have $V > 9$; of the 7 unidentified sources, 4 have $V < 9$. Thus, if we confine ourselves to sources with $V < 9$, we have an almost equal number of galaxies and quasars, similarly to what is found for GPS samples. The quasars with $V < 9$ have higher median redshift ($z_{\rm median} \simeq 2.4$) than those with $V > 9$, whose median redshift ($z_{\rm median} \simeq 1.7$) is closer to that of flat spectrum radio quasars in the Parkes quarter-Jy sample ($z_{\rm median} \simeq 1.4$).

An alternative approach may be to consider as blazar candidates all sources with variability significant at more than 3σ. In this case the boundary between candidate HFP and likely blazars has to be set at $V = 3$ (as appropriate for a χ^2 distribution with 1 degree of freedom) rather than at $V = 9$. If so, 9 more sources (3 galaxies, including the type 1 Seyfert, 5 quasars and 1 unidentified source) add to the list of candidate blazars.

4.2.3 Evolution of the turnover frequency

According to the physical model for the evolution of young radio sources by Begelman (1996) (see Appendix A), a newly generated powerful jet injects energy into the ambient medium inflating a cocoon consisting of shocked jet material and shocked ambient matter. If the density of the surrounding medium scales with radius, r, as $\rho \propto r^{-n}$, the linear size, l_c, of the cocoon increases with the source age, t, as $l_c \propto t^{\epsilon}$, with $\epsilon = 3/(5-n)$. The best determined relationship for GPS/CSS sources relates the radio turnover frequency to the projected linear size $\nu_p \propto (l_c)^{-\delta}$ (O'Dea & Baum 1997). It follows that ν_p decreases with time as $\nu_p \propto t^{-\lambda}$, with $\lambda = \delta \cdot \epsilon$. The expected decrease of ν_p in a time interval Δt in the source frame (corresponding to $\Delta T = \Delta t(1+z)$ in the observer frame) is then:

$$\frac{\Delta \nu_p}{\nu_p} = -\lambda \frac{\Delta t}{t}. \tag{4.2}$$

Name		$\Delta\nu/(\nu_p^I \cdot \Delta t)$
0003+2129	G*	0.018 ± 0.009
0005+0524	Q	**0.170 ± 0.03**
0037+0808	G?	-0.05 ± 0.04
0111+3906	G	0.01 ± 0.01
0428+3259	G*	0.02 ± 0.01
0642+6758	Q	**0.10 ± 0.03**
0646+4451	Q	**0.3 ± 0.1**
0650+6001	Q	**0.11 ± 0.01**
1335+4542	Q	0.03 ± 0.02
1407+2827	G	**0.017± 0.005**
1424+2256	Q	0.05 ± 0.03
1430+1043	Q	**0.08 ± 0.02**
1505+0326	Q	0.02 ± 0.04
1511+0518	Sy1	0.01 ± 0.01
1526+6650	Q	0.04 ± 0.03
1616+0459	Q	0.02 ± 0.04
1623+6624	G	0.00 ± 0.01
1645+6330	Q	0.2 ± 0.1
1800+3848	Q	0.2 ± 0.2
1840+3900	Q	0.1 ± 0.2
1850+2825	Q	-0.05± 0.06
1855+3742	G*	0.02 ± 0.01
2024+1718	S	**0.26 ± 0.06**
2101+0341	Q	**0.53 ± 0.02**
2203+1007	G*	-0.02± 0.02

Table 4.3: Time evolution of the turnover frequency

The slope of the observed correlation for CSS/GPS sources is $\delta \simeq 0.65$ but O'Dea & Baum (1997) showed that the evolution of ν_p with l_c may be steeper than the statistical relation. Based on Begelman's model, they found $\delta \simeq 1.2$ for n=2. The typical uncertainties associated with our estimates of $\Delta\nu_p$ are at the several percent level. For n ranging from 0 (uniform density) to 2 (isothermal distribution) and $\Delta T = 3$–4 yr, a clear measurement of the peak frequency decrease due to the source expansion could be achieved for source ages well below 100 yr. Taking into account that our sources were selected from the GB87 catalogue, based on observations carried out in 1986–1987, and therefore they must be older than 15–16 yr when our second set of observations were done, we conclude that sources with

$\Delta\nu_p/[\nu_p\Delta t(\mathrm{yr})] > 0.05$ are unlikely to be HFPs (because too young ages would be implied). We propose to classify them as blazars, whose observed evolution timescale are decreased by the Doppler factor. Note that $\Delta\nu_p/[\nu_p\Delta t(\mathrm{yr})]$ can be computed (and is reported in Table 4.3) only for sources with measured redshift and measured peak frequencies at both epochs.

Seven star-like sources (highlighted in boldface in Tab. 4.3) show a variation of the peak frequency, significant at a $> 3\sigma$ level, larger than expected if HFP/GPS sources expand at mildly relativistic velocities ($\Delta\nu_p/[\nu_p\Delta t(\mathrm{yr})] > 0.05$), suggesting the presence of relativistic beaming effects. The only galaxy (1407+2827 in boldface in the same table) with a peak frequency variation significant at $> 3\sigma$ level has $\Delta\nu_p/[\nu_p\Delta t(\mathrm{yr})] = 0.017$. For the comparison with the other criteria we have used only the values found for these eight sources with a variation of the peak frequency significant at a $> 3\sigma$ level and therefore only their values are reported in column 6 of Table 4.1.

In principle, an estimate of source ages could be derived from Eq. (4.2). In practice, however, given the large uncertainties on $\Delta\nu_p$ and the additional uncertainties on λ (due to the poor knowledge of the parameter n characterizing the density profile of the medium), only rather uninteresting lower limits of a few tens of years can be set. On the other hand, interesting constraints would be provided by more accurate multifrequency measurements with a 2 or 3 times longer time-lag.

Although the Kolmogorov-Smirnov (KS) test does not detect any significant difference in the distribution of turnover frequencies at the two epochs, it is clear from the value of $\Delta\nu_p/[\nu_p\Delta t(\mathrm{yr})]$ reported in Table 4.3 that most sources have a smaller ν_p at the second epoch, consistent with a rapid evolution towards lower optical depths and lower luminosities.

4.3 Extended emission

The deeper VLA observations at 1.4 GHz of the sub-sample of 45 HFP candidates have revealed the presence of some amount of extended emission in 14 objects (2 galaxies, 9 quasars and 3 objects without optical identification) (see Chapter 3, Sect. 3.3.2). Seven out

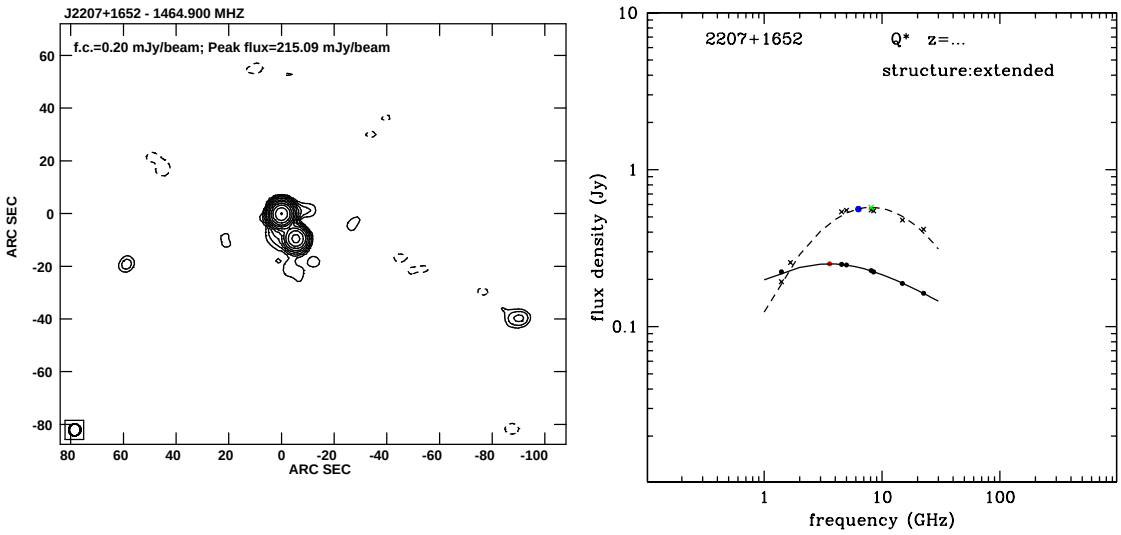

Figure 4.2: VLA image and spectra at the two epochs of the quasar J2207 + 1652, classified as a blazar in view of its morphology and strong variability.

of the nine quasars with extended emission have strongly variable spectra. I have reported in Fig. 4.2 as an example the VLA image at 1.4 GHz of one of them (J2207+1652) and its associated strongly variable spectrum (V=228.45). Five of them did not show anymore a convex spectrum when were re-observed, and therefore are not HFPs.

On the other hand, the two galaxies (J0111+3906 and J0428+3259) with some amount of resolved emission on kpc scales showed, at both epochs, the typical peaked, non-variable spectrum. One is the well known J0111 + 3906 (B0108 + 388) for which Baum et al. (1990) proposed the recurrent activity hypothesis. In Fig. 4.3 I have reported the VLA image at 1.4 GHz of the source J0428+3259 and its peaked, non-variable (V=1.20) spectrum. High resolution VLBA observations (see Fig. 3.26) have revealed a triple structure at mas scales; the components have all steep spectral indices ($\alpha > 0.8$) and this source is therefore classified as a CSO. Its fractional polarisation is smaller than 0.5% (see Tab. 3.4 in Chapter 3) and therefore it is also classified as a unpolarised object. All these elements support the hypothesis that this is indeed a reborn source.

According to Begelman's model (see Appendix A) the synchrotron emission decreases with source age t as $L \propto t^{-\eta}$ with $\eta = (n+4)/[4(5-n)]$, where n is the slope of

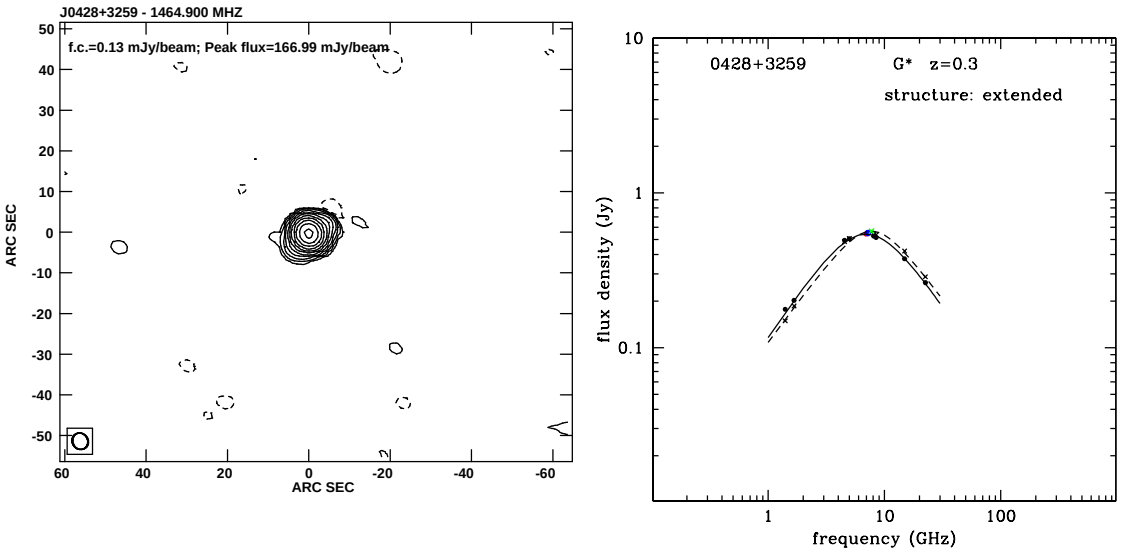

Figure 4.3: VLA image and spectra at the two epochs of the galaxy J0428 + 3259, classified as a recurrent GPS source

the density profile of the surrounding medium. In the case of recurrent activity, the HFP to extended emission age ratio can then be estimated as $t_{\rm HFP}/t_{\rm ext} = (L_{\rm ext}/L_{\rm HFP})^{1/\eta}$, where $L_{\rm ext}$ and $L_{\rm HFP}$ are the total *emitted* radio luminosities, that can be taken as proportional to the *emitted* flux densities at 1.4 GHz. In the case of a HFP component, the latter can be estimated extrapolating to 1.4 GHz the peak flux density, adopting the typical spectral index ($\alpha = 0.75$) of the optically thin synchrotron emission. The age ratio derived from Begelman's model depends on the slope n. Adopting $n = 2$ we get, for J0111 + 3906, $t_{\rm ext}/t_{\rm HFP} \simeq 9 \times 10^4$, and for J0428 + 3259 $t_{\rm ext}/t_{\rm HFP} \simeq 2 \times 10^4$, consistent with the intermittency timescales suggested by Reynolds & Begelman (1997). Although any conclusion at this stage is premature, this illustrates the potential of deeper low frequency observations to shed light on the nature of radio activity.

On the other hand, the most natural explanation for the sources with strongly variable spectra (7 quasars and 2 empty fields) is that we are seeing the Doppler boosted flaring inner parts of the jets of large radio source, closely aligned with the line of sight.

4.4 Polarisation properties of the candidates

As mentioned in Sect. 4.1 a characteristic property of young sources is a very low radio polarisation. In fact very strong Faraday depolarisation is expected for sources that reside in the innermost regions of the host galaxy (typically inside the NLR) with relatively large column densities of plasma. On the other hand significant and variable linear polarisation is generally detected in compact, flat-spectrum sources (blazars). The monitoring of the polarisation variability of some blazars at mm/submm wavelengths, i.e. in the core regions of the jets close to its origin, has shown that the polarisation is low during quiescent periods (0.7%-1.4%) while during flares the polarisation gets high (6%-7%) (Stevens et al. 1998, Nartallo et al. 1998).

Polarimetric VLA observations in the C and X bands of the HFP candidates have revealed some amount of polarised emission ($> 0.5\%$, corresponding to 3σ level for weak sources and 5σ for the brighter ones) in 22 objects out of 45 (see Chapter 3, Sect. 3.4). All the galaxies are not polarised while 19, out of a total of 28, quasars have a significant polarisation degree. Four out of the 7 sources without optical identification are polarised. All the seven sources that do not show anymore a peaked spectrum at the second epoch are polarised. This property gives further support to the classification of these objects as blazars.

A comparison with the classification based on variability has shown that 21 of the 25 sources with $V < 9$ are not polarised (and 2 of the 4 polarised sources have $V < 3$) while 18 of the 20 sources with $V > 9$ are polarised. Also, 5 of the 7 sources with $\Delta\nu_p/[\nu_p\Delta t(\mathrm{yr})] > 0.05$ are polarised while the only galaxy with a peak frequency variation significant at $> 3\sigma$ level and $\Delta\nu_p/[\nu_p\Delta t(\mathrm{yr})] < 0.05$ is not polarised. Given the large uncertainties on $\Delta\nu_p$, the classification criterion based on the value of $\Delta\nu_p/[\nu_p\Delta t(\mathrm{yr})]$ can be applied only to a few objects.

The median polarisation degree at 6 cm and 3.6 cm of HFP candidates with detected polarisation is 1.7%; if we consider only the sources with V>9, the median increases to 1.8%. The latter value matches perfectly that for a sample of non-GPS quasars brighter than 1 Jy at 6 cm (1.8%; Stanghellini 1999), and is higher than the mean polarisation of

GPS quasars in the bright sample by Stanghellini et al. (1998), estimated to be 1.2%, while polarisation of GPS galaxies is undetected at the 0.3% (in several cases at the 0.1%) level (Stanghellini 1999).

4.5 Morphological classification

Compact, flat-spectrum blazars show a core-jet morphology in very long baselines interferometry images, with a sequence of synchrotron self-absorbed knot-like structures combining to give the overall flatness of the radio spectrum. On the other hand, a two sided compact structure is the morphology expected for young radio sources. However, a Compact Symmetric Objects observed at a small viewing angle is difficult to identify since there is a large contrast between the approaching and receding side of the radio source.

As discussed in Section 3.6 of the previous Chapter, the morphological classification of the HFP candidates at mas resolution based on VLBA observations at two different frequencies in the optically thin part of the spectrum is still incomplete. So far, it has been obtained for 37 (9 galaxies, 21 quasars, 7 empty fields) out of the 45 HFP candidates with multifrequency observations at 2 epochs. Moreover 17 sources are unresolved also by the VLBA. Of the 9 galaxies, one is J0428+3259 that is resolved also at 1.4 GHz with the VLA and has a CSO morphology at the VLBA resolution. As discussed in Section 4.3 all the properties of this object seem to indicate that it is a good candidate to be a reborn radio source. The remaining 8 galaxies are compact at the VLA resolution; seven of them have a CSO morphology and one is unresolved also by the VLBA. On the other hand, of the 21 quasars we have already analyzed, 7 have a core-jet morphology, 2 are CSOs, but the majority (i.e. 12) are still unresolved. We have a morphological classification for 6 of the 7 sources that have a flat spectrum at the second epoch of VLA observations; 4 have a CJ morphology and 2 are unresolved.

Nineteen objects out of the 37 for which we have a morphological classification have $V < 9$. Ten of them show a CSO morphology, 3 are core-jet sources and 6 are unresolved. On the other hand, of the 18 sources with $V > 9$, 5 are core-jet sources, 2 are CSO (one of them is polarised, the other is not) and 11 are unresolved.

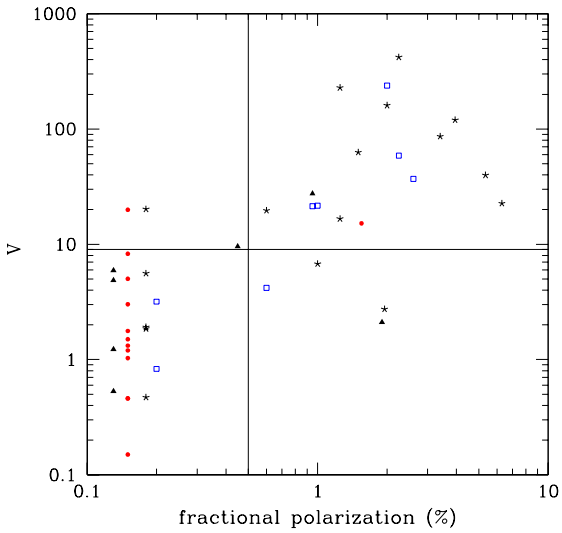

Figure 4.4: Variability index V vs fractional polarisation. Different symbols represent different VLBA morphologies. Red filled circles indicates CSO morphology, blue open squares core-jet, stars the unresolved objects and filled triangles the sources for which we have not a morphological classification at mas resolution. For clarity, unpolarised sources (polarisation degree $< 0.5\%$) have been attributed 3 slightly different polarisation degrees, thus avoiding superpositions of the points.

Of the 12 sources with a CSO morphology, 11 are not polarised; 6 out of the 8 sources with a core-jet morphology are polarised, and 11 of the 17 unresolved objects are polarised.

Even if the analysis is not complete, the majority of the sources with a core-jet morphology or unresolved are both polarised and show a strong flux density variability, while most of the sources with CSO morphology are not polarised and show little or no variability, as expected for truly young radio sources.

4.6 Comparison between the criteria

The consistency of the classification (HFPs vs blazars) yielded by the different criteria turns out to be rather good. The most complete information comes from the variability index V and from the fractional polarisation. In Fig. 4.4 we compare the consistency

of these two criteria plotting the variability index versus the fractional polarisation. The young source candidates populate the bottom left-hand part of the plane, where V is less than 9 and the fractional polarisation is smaller than 0.5%. On the other hand, candidate blazars, whose properties are strong variability and high polarisation, should be in the top right-hand part of the plane. Different symbols have been used to distinguish sources according to their VLBA morphology: red filled circles are CSOs, blue open squares are core-jet sources, stars indicate the unresolved objects, and filled triangles the sources still missing a morphological classification. Except for a few cases, discussed in the notes at the end of this Section, we found a substantial agreement among the classifications yielded by the variability and by the polarisation criteria for 87% of the sources. Also in 70% of the cases, the observed morphology corresponds to that expected on the basis of the polarimetric and variability classification.

In the notes below we give some additional details on sources for which different criteria point to different classifications. Some sources like J0650+6001 (Q), J1840+3900 (Q), J2024+1718 (S) are characterized by strong variability and low polarisation. On the contrary J1430+1043 (Q), J0642+6758 (Q), J1645+6330 (Q), J1424+2256 (Q) have weak variability and high polarisation. In some other cases [J0005+0524 (Q), J1616+0459 (Q), J0638+6001 (EF)] the morphology or the evolution of the turnover frequency differ from expectations from variability and polarisation properties. These situations are indeed expected since none of the criteria can ensure an unambiguous classification. For example, a weakly variable source may be a blazar observed during a quiescent phase; some blazars have very low polarisation; young sources expanding in a direction close to the line of sight can be classified as core-jet objects or may be unresolved, and so on.

However, the criteria relying on variability and on polarisation appear to be remarkably successful. Since the variability properties of this sample have been studied and analyzed in detail while the polarisation and morphological studies are still in progress, we adopt, in the following analysis, the variability criterion as our baseline to discriminate among candidate blazars and HFPs.

Notes on individual sources:

J0005+0524: the classification of this source is uncertain since the variability ($V = 3.18$) and polarisation properties ($< 0.5\%$) are those of a young objects, while its core-jet morphology and the $\Delta\nu_p/[\nu_p\Delta t(\mathrm{yr})] > 0.05$ point to a blazar classification.

J0638+5933: even if it shows a core-jet morphology we have classified this object as an HFP candidate since its variability is small (V=0.83) and it is not polarised.

J0642+6758: apart from the relatively low variability ($V = 6.77$), all the properties of this object (evolution of the turnover, polarisation and morphology) are those of a blazar probably caught in a quiescent phase.

J0650+6001: this object has a CSO morphology and it is not polarised, but it shows strong variability ($V = 19.92$) and $\Delta\nu_p/[\nu_p\Delta t(\mathrm{yr})] > 0.05$ at more than 3σ level; its classification is therefore uncertain.

J1424+2256: this source shows quite a strong polarisation (0.4-3.4%) but low variability (V=2.11); the morphological classification is still missing. It may be a blazar in a quiescent phase at the two epochs of observations.

J1430+1043: it is weakly polarised (0.5-0.7%), and has a low variability ($V = 4.19$), but it shows a core-jet morphology and $\Delta\nu_p/[\nu_p\Delta t(\mathrm{yr})] > 0.05$ at more than 3σ level. It may be a blazar in a quiescent phase.

J1616+0459: this is a variable object ($V = 15.20$) with strong polarisation (0.2-2.9%) and therefore it has been classified as a blazar even if it has a CSO morphology. The morphological classification needs confirmation since the source is well resolved only at the higher frequencies of our observations.

J1645+6330: it has been classified as a blazar even if its variability is small ($V = 2.74$) since it is unresolved by the VLBA and is polarised (0.8-3.1%).

J1840+3900: even if it is unpolarised, it has been classified as a blazar because of its strong variability ($V = 20.16$) and its very compact morphology, unresolved by the VLBA.

J2024+1718: it is weakly polarised (0.1-0.8%) in the C and X bands and has V just above threshold ($V = 9.58$), but it has $\Delta\nu_p/[\nu_p\Delta t(\mathrm{yr})] > 0.05$ at more than 3σ level; it has therefore been classified as a blazar.

4.7 Peak luminosity versus Peak Frequency

Another interesting issue is the relationship between peak frequencies and peak luminosities, L_p. Opposite trends are predicted by current models for GPS sources: while Begelman's (1996) model implies a decrease of L_p with decreasing ν_p, Snellen et al. (2000) and Alexander (2000) predict an increase during the HFP/GPS phase of the source evolution. In both cases, however, the dependence of L_p on ν_p is weak, and therefore easily swamped by variances in both quantities. In the case of relativistic beaming with Doppler factor δ, the observed peak luminosity scale as δ^3, while the observed peak frequency scale as δ, so that sources with equal intrinsic L_p and ν_p, but different δ's are observed to have $L_p \propto \nu_p^3$; this relation is much steeper than the L_p–ν_p relation predicted by both Begelman's and Snellen's models.

We have investigated this relationship for all objects (see Fig. 4.5), using first epoch data, when all sources but two had a well defined spectral peak. Although a clear correlation seems to be present, we must beware of the effect of the redshift distribution: as an example, the solid line in Fig. 4.5 shows the distribution in the L_p–ν_p plane of sources with equal observed $S_p = 300\,\mathrm{mJy}$ and $\nu_p = 5\,\mathrm{GHz}$ at different redshifts. Clearly the shape of the correlation is not far from that induced by the effect of redshift. Nevertheless, Kendall's partial correlation coefficient indicates a statistically significant positive correlation between L_p and ν_p after the influence of redshift has been eliminated. The probability of no correlation is 0.44% if we consider only stellar objects with $V > 9$ (which are probably blazars; we have 12 such objects with redshift, but for one of them the peak frequency is undefined). For stellar objects with $V \leq 9$ the probability of no correlation increases to 6% so that the correlation is only marginally significant. For galaxies there is no indication of a significant correlation (probability of no correlation 38%). This is not surprising given the smaller range spanned by both quantities (compared to the case of quasars) and the weaker dependence of L_p on ν_p expected for GPS/HFP sources is easily swamped by intrinsic dispersions of both quantities.

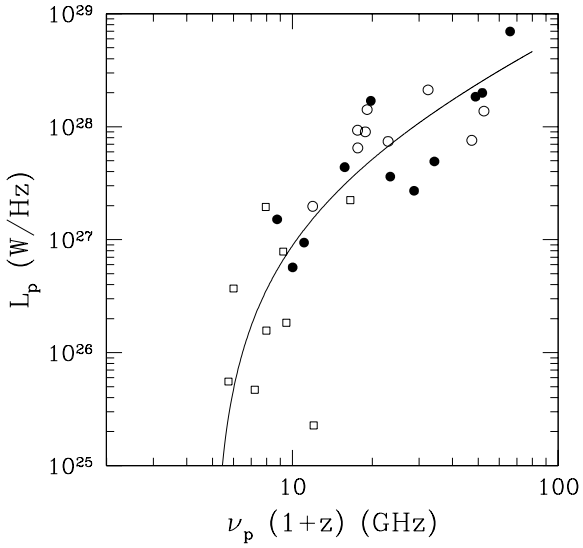

Figure 4.5: Peak luminosity versus peak frequency for all objects with measured redshift. Circles: quasars, squares: galaxies. Open symbols refer to sources with $V \leq 9$, filled symbols to sources with $V > 9$. The solid line shows the distribution in the L_p–ν_p plane of sources with equal observed $S_p = 300\,\mathrm{mJy}$ and $\nu_p = 5\,\mathrm{GHz}$ at different redshifts.

4.8 Variability properties of the candidate blazars

The analysis of the HFP sample has led to the conclusion that a large fraction of HFP quasars are actually beamed sources. According to the variability criterion, the 20 sources having $V > 9$ are candidate blazars; 17 of them (including the 7 with flat spectrum at the second epoch and 4 of the 7 with $\Delta\nu_p/[\nu_p \Delta t(\mathrm{yr})] > 0.05$) are star-like and 3 are unidentified. In order to test this classification, we have compared the properties of our candidates blazars with those of the known blazars:

- The median r.m.s. variations for our candidates blazars are $\simeq 30\%$ (27% for quasars only), close to those found for blazars ($\simeq 32\%$; Ciaramella et al. 2004).

- The variability timescales in the frequency range 5–15 GHz of bright blazars, derived from their structure function, are $\simeq 2\,\mathrm{yr}$ in the source frame (Hughes et al. 1992; Ciaramella et al. 2004). To convert the time-lag between the two sets of observations into the mean time interval in the source frame, we need to divide it by $(1 + z_{\mathrm{mean}})$.

Only 11 of the 17 starlike sources with $V > 9$ have measured redshift, with a median value of 1.7. We may thus expect that $\sim 50\%$ of blazars flaring at the moment of the first set of observations have recovered their baseline flat spectrum by the epoch when they where re-observed. For comparison, 7 out of 17 (i.e. $\simeq 41\%$) were indeed found to have a flat spectrum in the second observing run.

- There is evidence of a positive correlation between V and ν_p (probability of no correlation ~ 0.01), indicating that the fraction of blazars is higher among objects with higher peak frequency. This is not surprising because young objects become increasingly rare since their lifetimes decrease with increasing ν_p.

- We have found a statistically significant positive correlation between the peak luminosity and rest-frame peak frequency of quasars, after having removed the effect of the redshift distribution (Kendall's partial correlation test). A relationship among these two quantities is expected both in the case of GPS/HFP sources and of blazars, but with a much steeper slope for the latter sources. While previous studies enlightened a S_p–ν_p correlation for a few individual blazars (e.g., Stevens et al. 1996) our analysis indicates that it holds for flaring blazars as a class.

There are thus various pieces of evidence, albeit circumstantial, that most quasar HFP candidates are actually objects where the effects of beaming are relevant (blazar like) even if this does not necessarily imply that they are evolved/old objects.

4.9 Discussion and conclusions

The spectral selection adopted by Dallacasa et al. (2000) is independent of optical identification and redshift. As a result, both galaxies and star-like objects ("quasars") are present in the original sample of bright HFP candidates. Quasars are almost three times more numerous than galaxies, consistent with the previously noted decrease of the galaxy to quasar ratio in GPS samples selected at increasing turnover frequency (Fanti et al. 1990; O'Dea 1998; Stanghellini et al. 1998, 2003). Indeed, our new multifrequency observations, with a time lag of 3 to 4 years, indicate that the sample of candidate HFP quasars is

likely to be strongly contaminated by beamed objects, with variability, polarimetric and morphological properties consistent with those of blazars.

We have considered six different criteria to discriminate between young sources and flaring blazars and we found that in most cases they yield consistent indications on the source nature. For the statistical analysis of the sample we have referred to the variability index V [Eq. (4.1)], since, at present, this is the quantity on which we have the most complete information. The distribution of V for the less variable sources is close to the χ^2 distribution with two degrees of freedom, as may be expected since variations of spectra of young sources are controlled by two parameters, S_p and ν_p. If so, sources with $V > 9$ have a probability < 0.01 of being extracted from such a distribution and are therefore likely blazars. If we set the boundary between HFP candidates and blazars at $V = 3$ (see Sect. 4.2.2), 9 sources (3 galaxies, 5 quasars and 1 unidentified source) add to the list of blazar candidates, so that these would include 3 of the 10 galaxies, 22 out of the 28 starlike sources and 4 out of the 7 unidentified sources.

The candidates young radio sources in the HFP sample are 25 (10 galaxies, 11 quasars and 4 unidentified objects) if we select them with the limit $V < 9$ and 16 (7 galaxies, 6 quasars and 3 unidentified sources) if $V < 3$. Of the 25 objects with $V < 9$, only four (16%) are polarised; of the 19 of them with VLBA morphology only 3 (16%) are core-jet and 6 are unresolved. If we consider only the 9 objects with $3 < V < 9$, 2 (22%) sources are polarised, 2 out of 7 with known morphology have a core-jet morphology and 2 (29%) are unresolved. Finally, 2 (12.5%) sources are polarised among the 16 with $V < 3$ and 1 out of 13 (8%) have a core-jet morphology and 4 (31%) are unresolved at the VLBA resolution.

If we consider only our most reliable criteria, i.e. the variability and polarisation ones, we find that if we pass from the criterion $V < 9$ to the stricter one with $V < 3$ we reject 2 polarised objects, and the global fraction of polarised sources (i.e. possibly blazar objects) is reduced from 16% to 12.5%. On the other hand, we would lose 7 of the 9 objects (78%) with $3 < V < 9$ that are not polarised (i.e. good young-source candidates). For 3 of these 7 objects, the young-source classification is also supported by the CSO morphology.

Candidate blazars have a median variability amplitude $\simeq 22\%$ if we adopt the

criterion $V > 3$, and $\simeq 30\%$ if $V > 9$. The latter value is remarkably close to that found for a blazar sample ($\simeq 32\%$; Ciaramella et al. 2004).

In conclusion, while sources with $V > 9$ are likely blazars there is no guarantee that those with $V < 9$ are truly young radio sources. The stricter criterion $V < 3$ does not grant the rejection of blazars in a quiescent phase and may reject some truly young sources. It is thus necessary to complement variability studies with polarisation measurements and high-resolution imaging. As for the HFP sample, all the galaxies are consistent with being truly young, possibly recurrent, sources, while most quasars are consistent with being blazars.

Chapter 5

Constrains on Evolutionary Properties of GPS Galaxies

5.1 Introduction

The self-similar evolution model by Begelman (1996, 1999) implies that the evolution of the radio power as the source expands, depends on the radial profile of the external density. To test this scenario and to constrain the birth rates and the evolutionary properties of these sources, a detailed comparison of the model predictions with survey data is necessary. An exploratory study in this direction was presented by De Zotti et al. (2000), who showed that this kind of models may account for the observed counts, redshift and peak frequency distributions of the samples then available, but for rather unexpected values of the parameters. De Zotti et al. (2000) considered the available information from the samples of GPS galaxies and quasars by Snellen et al. (1998) and Stanghellini et al. (1998). They also used the counts reported by Grainge & Edge (1998) as an additional constraint. They have considered GPS galaxies and quasars as different populations and they have fitted the redshift and peak frequency distributions of the available samples. They found a good agreement between model and observed distributions both for galaxies and quasars but substantially different evolution properties are required for GPS galaxy and quasar populations: the quasar luminosity function must evolve strongly up to $z \sim 1$, while the

data on galaxies may be consistent with no evolution. The local luminosity functions of the two populations have a similarly flat slope, significantly flatter than those of conventional radio sources (Dunlop & Peacock 1990). The derived values for parameters characterizing the evolution with the source age of the emitted power and of the turnover frequencies are much larger than expected in the self-similar model by Begelman (1996, 1999). The authors underline that the physical meaning of these results needs to be further investigated and that many uncertainties come from various selections effects and the lack of redshift information and doubtful identifications.

Since then, new relevant surveys of GPS sources have been published, extending the coverage of the peak frequency-redshift plane. The Dallacasa et al. (2000) and Bolton et al. (2004) samples contain sources with high turnover frequencies (HFPs), which are presumably the youngest radio sources. Snellen et al. (2002) and Edwards & Tingay (2004) selected samples of southern GPS sources, thus improving the sky coverage. Snellen et al. (2004) focused on the relatively rare low-z sources. The first year WMAP survey (Bennett et al. 2003b) has provided a complete sample of over 200 sources with simultaneous flux density measurements at 4 frequencies (22.8, 33.0, 40.7, 60.8, and 93.5 GHz), that can be exploited to search for extreme GPS sources, peaking at mm wavelengths.

Moreover, the variability study of the Dallacasa et al. (2000) sample, carried out by Tinti et al. (2005) (see Chapter 4, Sect. 4.2), has shown that most HFP candidates classified as quasars are most likely blazars caught by during a flare of a highly self-absorbed component dominating the emission, while candidates classified as galaxies are consistent with being "bona fide" HFPs. Polarisation measurements (Dallacasa et al., in preparation) lend further support to this conclusion. Torniainen et al. (2005) from a study of the long term variability of 33 objects previously classified as GPS or HFP sources, mostly identified with quasars and mostly peaking above 5 GHz, concluded that only 5 keep the GPS properties over time. Clearly, a serious blazar contamination of GPS samples may lead astray analyses of their statistical properties. A similar conclusion is reached in the case of radio sources showing a convex spectrum in the simultaneous WMAP data and identified as quasars.

In view of these new data, the previous conclusions on the evolution of the GPS

Name	$S_{4.8}$ Jy	S_{23} Jy	S_{33} Jy	S_{41} Jy	S_{61} Jy	S_{94} Jy	α_{23}^{33}	$\alpha_{4.8}^{23}$	
GB6 J0136+4751	2.036	4.5	4.7	4.2	3.3	2.9	-0.12	-0.51	BL (Terasranta)
GB6 J0237+2848	2.962	3.9	4.0	3.9	1.8	0.0	-0.10	-0.18	BL (Terasranta)
PMN J0253-5441	1.193	2.7	3.1	3.5	2.9	2.2	-0.38	-0.52	BL? (this work)
PMN J0403-3605	1.851	2.7	2.9	2.5	2.6	2.1	-0.20	-0.24	BL (this work)
PMN J0450-8100	1.357	2.0	2.2	1.8	2.5	1.6	-0.30	-0.25	BL (this work)
PMN J0455-4616	1.653	3.0	4.0	3.7	3.4	3.8	-0.80	-0.38	BL (this work)
PMN J0457-2324	1.863	3.3	3.8	3.8	3.5	2.7	-0.39	-0.37	BL (this work)
PMN J0538-4405	4.805	7.9	8.2	8.8	7.9	6.7	-0.10	-0.32	BL (Donato)
PMN J1147-3812	1.825	2.9	3.3	2.9	2.8	0.0	-0.36	-0.30	BL (Donato)
GB6 J1159+2914	1.905	3.5	3.6	3.4	3.0	2.1	-0.10	-0.39	BL (Terasranta)
PMN J1256-0547	11.19	23.5	24.9	25.7	24.5	19.	-0.16	-0.48	BL (Terasranta)
PMN J1337-1257	2.838	6.3	6.7	7.3	6.6	3.7	-0.17	-0.51	BL (this work)
PMN J1427-4206	2.597	2.6	3.0	2.6	0.0	0.0	-0.40	0.0	BL (this work)
GB6 J1608+1029	1.581	3.2	3.3	2.7	3.1	3.1	-0.10	-0.45	BL (Terasranta)
GB6 J1635+3808	3.382	4.6	5.6	6.0	5.9	4.2	-0.54	-0.20	BL (Terasranta)
GB6 J1753+2847	0.562	2.1	2.2	2.7	3.2	2.2	-0.13	-0.85	BL (this work)
PMN J1957-3845	1.944	3.2	3.7	2.9	2.6	2.8	-0.40	-0.32	BL (this work)
PMN J2258-2758	2.127	9.6	9.8	9.8	8.9	6.3	-0.06	-0.97	BL (this work)

Table 5.1: WMAP data of the 18 objects with inverted spectrum ($\alpha \leq 0$) from 22.8 to 33 GHz and from 4.85 to 22.8 GHz.

population need to be reconsidered in depth. In this chapter I present a new analysis, still in the framework of Begelman's scenario (1996,1999). As mentioned above, since there is strong evidence that samples of GPS sources identified as quasars are heavily contaminated by flaring blazars, we confine our analysis to GPS galaxies.

5.2 The WMAP inverted spectrum sources

The WMAP point source catalogue (Bennett et al. 2003b) comprises 208 point sources with a $\geq 5\,\sigma$ detection in any of the 5 WMAP bands, in the range 22.8–93.5 GHz; 203 sources have counterparts in existing 4.85 GHz catalogues, the remaining 5 sources being probably spurious. All the point sources in the catologue are present in the GB6 catalog (Gregory et al. 1996) and in the PMN catalog (Griffith et al. 1994, 1995; Wright et al. 1994, 1996) that cover respectively the northern and the southern celestial hemisphere.

Therefore the information on the flux density at 4.85 GHz is also avaliable.

This is the first simultaneous multifrequency survey at mm wavelengths and is therefore well suited to select extreme HFPs. Although the completeness limit is at $S_{22.8\mathrm{GHz}} \simeq 1.25\,\mathrm{Jy}$ (De Zotti et al. 2005), to avoid that the estimates of spectral indices are too affected by measurement errors we have confined ourselves to sources with $S_{22.8\mathrm{GHz}} \geq 2\,\mathrm{Jy}$, and we have picked out those with inverted spectrum ($\alpha < 0$) from 22.8 to 33 GHz (33 sources) and from 4.85 to 22.8 GHz. There are 18 sources satisfying both these criteria (see Tab. 5.1), a number close to the prediction of the De Zotti et al. (2000) model, for a maximum initial peak frequency of 200 GHz. Most of these sources are well known calibrators and have therefore many observations at many frequencies (see Trushkin 2003). They all show strong variability, consistent with that observed for blazars; 9 of them are classified as blazars by Terasranta et al. (1998) or Donato et al. (2001) (see column 10 of Tab. 5.1). Only few objects in the southern hemisphere have very little information in other bands. We have tried to fit the data of these objects with an hyperbolic function to determine the peak flux densities and frequency but we failed to find a good fit. In Fig. 5.1 the blue points are the WMAP data while the red ones are the data collected by Truskin (2003) at many frequencies. I have reported the performed fit for one of the source (J0253-5441) with uncertain classification. The dashed line is the fit to the WMAP data only while the solid line is the fit to the overall set of data. The data at lower frequencies are not compatible with a global inverted spectrum.

The data on the WMAP sample thus confirm that most quasars showing a peak at tens of GHz are likely blazars caught during a phase when a flaring, strongly self-absorbed synchrotron component dominates the emission spectrum (Tinti et al. 2005).

5.3 The adopted evolutionary model

We adopted the young, evolving sources scenario studied by De Zotti et al. 2000, elaborating on the analytic self-similar evolution model proposed by Begelman (1996, 1999) to account for the observed population properties of peaked radio sources. The evolutionary model is derived in detail in Appendix A. Here I report only the main assumptions:

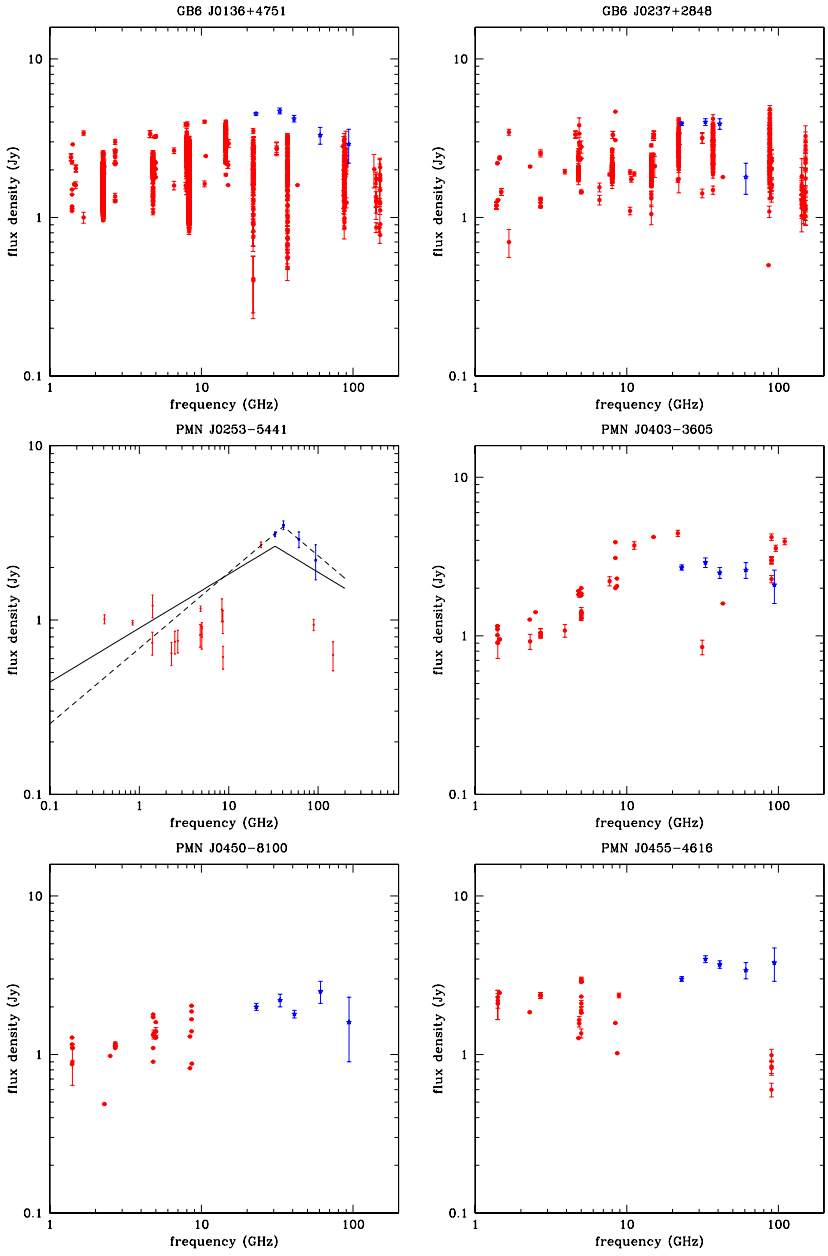

Figure 5.1: The spectra of the 18 WMAP sources selected with $\alpha < 0$ between 4.8, 22.8 and 33 GHz. The blue points are the WMAP data while the red ones are the data collected by Truskin (2003) at many frequencies.

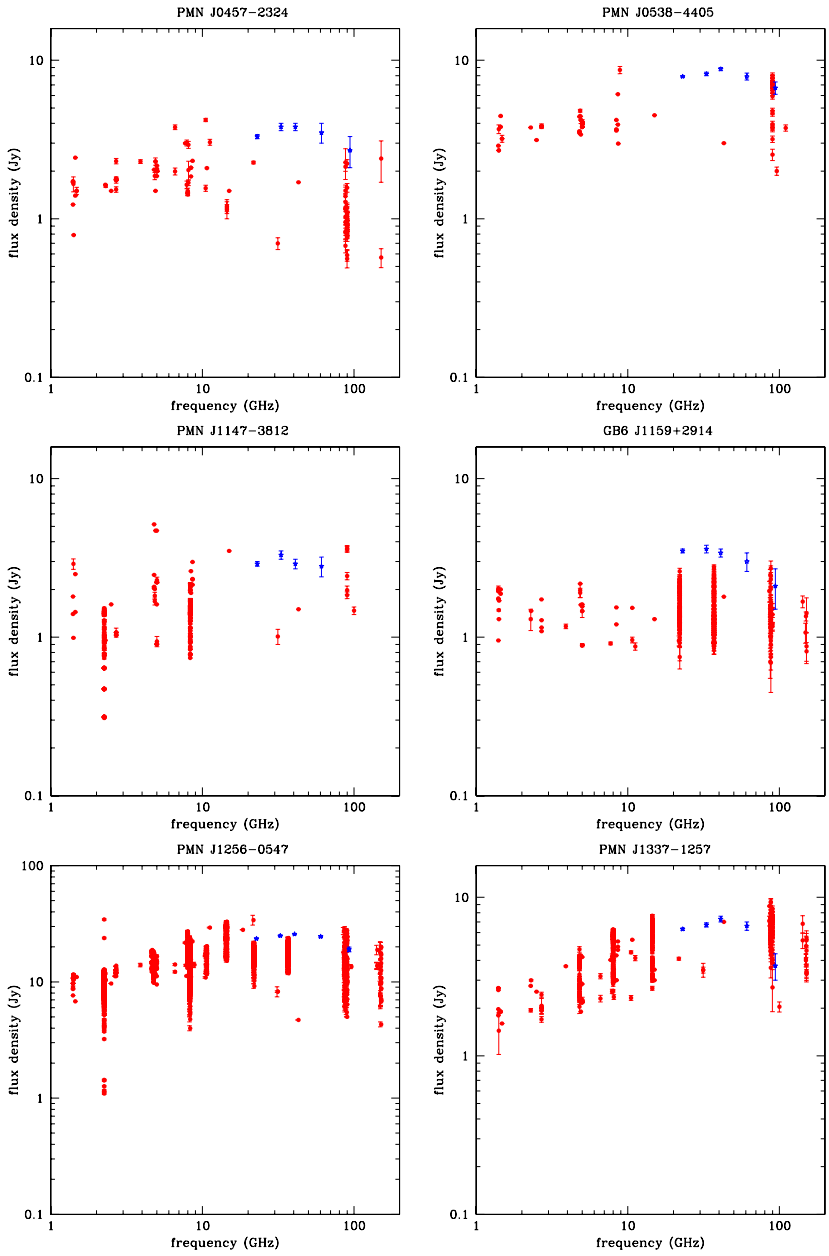

Figure 5.1: (continued)

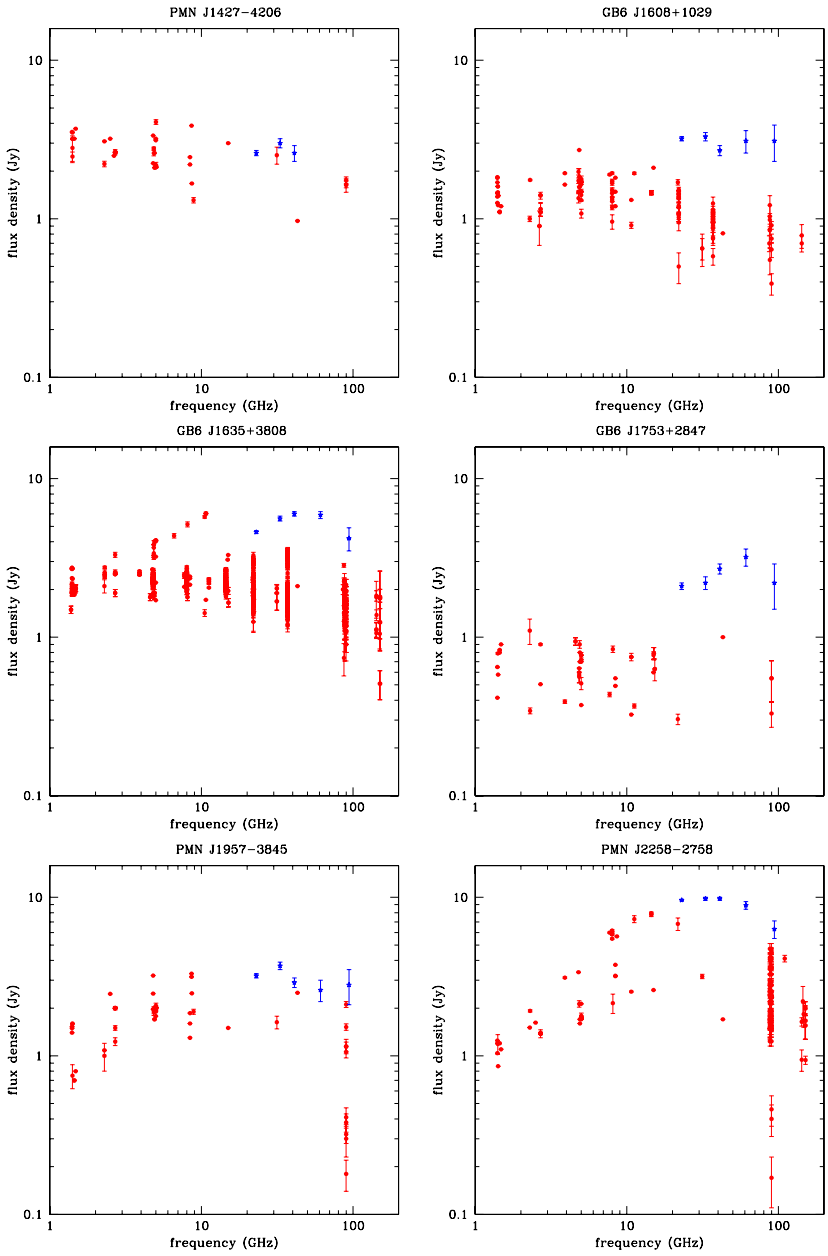

Figure 5.1: (continued)

1. The initial radio luminosity function (in units of $\mathrm{Mpc}^{-3}\,\mathrm{d}\log {L_i}^{-1}$) is described by a power law:
$$n(L_i) \propto \left(\frac{L_i}{L_\star}\right)^{-\beta}, \quad L_{i,\min} \leq L_i \leq L_{i,\max}, \tag{5.1}$$
where L_i is the luminosity before self-absorption.

2. In the GPS phase, the properties of the sources are determined by the interaction of a compact, jet-driven, overpressured, non thermal radio lobe with a dense interstellar medium (Begelman 1996, 1999; Bicknell et al. 1997); the timescale of the interaction is very short in comparison with the cosmological-expansion timescale, so that the luminosity evolution of individual sources occurs at constant z. As the radio lobe expands in the surrounding medium, the emitted radio power varies with the source age, τ, as $L_i \propto \tau^{-\eta}$, and its linear size l varies as $l \propto \tau^{\epsilon}$. If the density of the surrounding medium scales with radius as $\rho_e \propto r^{-n}$, we have (Begelman 1996, 1999) $\eta = (n+4)/[4(5-n)]$ and $\epsilon = 3/(5-n)$. There is a clear anticorrelation between intrinsic turnover frequency, ν_p, and linear size (O'Dea & Baum 1997): $\nu_p \propto l^{-\delta}$, with $\delta \simeq 0.65$. It follows that ν_p scales with time as $\nu_p \propto \tau^{-\lambda}$, with $\lambda = \delta\epsilon$.

3. The spectra of GPS sources are described by:
$$L_\nu = L_p \times \begin{cases} (\nu/\nu_p)^{\alpha_a} & \text{if } \nu < \nu_p \\ (\nu/\nu_p)^{-\alpha} & \text{if } \nu > \nu_p \end{cases} \tag{5.2}$$
with $\alpha_a = 0.8$ and $\alpha = 0.75$, the mean values found by Snellen et al. (1998b).

As the radio lobe expands, the peak luminosity L_p varies as the consequence of the variation of both the emitted radio power and of ν_p. Hence:
$$L_p(\nu_p) = L_{p,i}\tau^p = L_{p,i}\left(\frac{\nu_p}{\nu_{p,i}}\right)^{-p/\lambda} = L_{p,i}\left(\frac{\nu_p}{\nu_{p,i}}\right)^{\eta/\lambda-\alpha} \tag{5.3}$$
with $L_{p,i}(z) \propto L_i(z)$ and $p = -\eta + \alpha\lambda$.

If the birth rate of GPS sources is constant on time scales much shorter than the cosmological-expansion timescale, the peak luminosity function per unit $\mathrm{d}\log L_p$ is:
$$n(L_p) \propto L_p^{1/p}. \tag{5.4}$$

Also, since, in this case, the *comoving* number of sources of age τ within $\mathrm{d}\tau$ is simply proportional to $\mathrm{d}\tau$ and $\mathrm{d}\tau/\mathrm{d}\nu_p \propto (\nu_p/\nu_{p,i})^{-(1+1/\lambda)}$, the epoch dependent luminosity function at a given frequency ν ($\mathrm{Mpc}^{-3}\,\mathrm{d}\log {L_\nu}^{-1}\,\mathrm{GHz}^{-1}$) writes:

$$n(L_\nu,\nu_p,z) = n_0 \left(\frac{L_{p,i}(L_\nu,\nu_p)}{L_\star(z)}\right)^{-\beta} \left(\frac{\nu_p}{\nu_{p,i}}\right)^{-(1+1/\lambda)} \quad , \tag{5.5}$$

where $L_\star(z)$ is the redshift-dependent normalization luminosity. We have assumed luminosity evolution and adopted a very simple parameterization for it:

$$L_\star(z) = L_0 \times \begin{cases} (1+z)^k & \text{if } z < z_c \\ (1+z_c)^k & \text{if } z > z_c \end{cases} \tag{5.6}$$

The redshift z_c at which the luminosity evolution levels off is a model parameter. We have normalized monochromatic luminosities to $L_0 = 10^{32}\,\mathrm{erg\,s^{-1}\,Hz^{-1}}$.

The luminosity function at a frequency ν_2 is related to that at a frequency ν_1 by:

$$n(L_{\nu_2}) = n(L_{\nu_1}) \times \begin{cases} (\nu_2/\nu_1)^{-\alpha_a} & \text{if } \nu_1 < \nu_2 < \nu_p \\ (\nu_1/\nu_p)^{\alpha_a}(\nu_2/\nu_p)^{\alpha} & \text{if } \nu_1 < \nu_p < \nu_2 \\ (\nu_2/\nu_1)^{\alpha} & \text{if } \nu_p < \nu_1 < \nu_2 \end{cases} \tag{5.7}$$

The number counts per steradian of GPS sources brighter than S_ν at the frequency ν, with an observed peak frequency $\max(\nu,\nu_{p,\min}) < \nu_{p,0} < \nu_{p,\max}$ are given by

$$\begin{aligned} N \quad (>S_\nu;\nu_{p,0}>\nu) &= \int_0^{\min\left[z_f,z_m(S_\nu)\right]} \mathrm{d}z\,\frac{\mathrm{d}V}{\mathrm{d}z} \times \\ \times \quad & \int_{\max[\nu_{p,\min}(1+z),\nu(1+z)]}^{\min[\nu_{p,\max}(1+z),\nu_{p,i}]} \mathrm{d}\nu_p \times \\ \times \quad & \int_{\log L_{\min}(S_\nu,z,\nu_p)}^{\log L_{\max}(z)} \mathrm{d}\log L_\nu\, n(L_\nu,\nu_p,z)\,, \end{aligned} \tag{5.8}$$

where z_f is the redshift of formation of the first GPS sources, z_m is the maximum redshift at which sources can have a flux $\geq S_\nu$, $L_{\min}$ is the minimum luminosity of a source of given z and ν_p yielding a flux $\geq S_\nu$, $\mathrm{d}V/\mathrm{d}z$ is the *comoving* volume element within a solid angle ω:

$$\frac{\mathrm{d}V}{\mathrm{d}z} = \frac{c}{H_0}\omega\frac{d_L^2}{(1+z)^2E(z)} \tag{5.9}$$

$d_L(z)$ being the luminosity distance:

$$d_L(z) = \frac{c}{H_0}(1+z)\int_0^z \frac{dz'}{E(z')} \tag{5.10}$$

and

$$E(z) \equiv \left(\Omega_M (1+z)^3 + \Omega_\Lambda\right)^{1/2} . \tag{5.11}$$

The flux density at the frequency ν is related to the rest-frame luminosity L_ν by:

$$S_\nu = \frac{L_\nu K(z)}{4\pi d_L^2} \tag{5.12}$$

$$K(z) = (1+z)\frac{L_{\nu(1+z)}}{L_\nu} . \tag{5.13}$$

$K(z)$ being the K-correction.

Similarly, the number counts of GPS sources with an observed peak frequency $\nu_{p,\min} < \nu_{p,0} < \min(\nu, \nu_{p,\max})$ are given by

$$\begin{aligned} N \quad (> S_\nu; \nu_{p,0} < \nu) &= \int_0^{\min\left[z_f, z_m(S_\nu)\right]} \mathrm{d}z \, \frac{\mathrm{d}V}{\mathrm{d}z} \times \\ \times \quad &\int_{\nu_{p,\min}(1+z)}^{\min[\nu\,(1+z), \nu_{p,\max}(1+z), \nu_{p,i}]} \mathrm{d}\nu_p \times \\ \times \quad &\int_{\log L_{\min}(S_\nu, z, \nu_p)}^{\log L_{\max}(z)} \mathrm{d}\log L_\nu \, n(L_\nu, \nu_p, z) , \end{aligned} \tag{5.14}$$

The distribution of observed peak frequencies per unit $\mathrm{d}\nu_{p,0}$ in a flux limited sample, $\mathcal{N}(\nu_{p,0}; > S_\nu)$, is given by:

$$\begin{aligned} \mathcal{N} \quad (\nu_{p,0}; > S_\nu) &= \int_0^{\min\left[z_f, z_m(S_\nu, \nu_{p,0})\right]} \mathrm{d}z \, \frac{\mathrm{d}V}{\mathrm{d}z} \times \\ \times \quad &\int_{\log L_{\min}(S_\nu, z, \nu_{p,0}(1+z))}^{\log L_{\max}(z, \nu_{p,0}(1+z))} \mathrm{d}\log L_\nu \, n[L_\nu, z, \nu_{p,0}(1+z)]. \end{aligned} \tag{5.15}$$

5.4 GPS samples

There is no clear-cut definition of GPS sources and different criteria have been adopted for identifying them. On the other hand, we need to combine at least the most reliable samples to gather enough data for a meaningful statistical analysis to be possible. We now describe the samples used here and the corrections applied to make them as homogeneous as possible. The main properties of the samples are summarized in Table 5.2, where HFP, Stan, B_SA, B_SB, Snel, CORA, Park, and Edwa denote, respectively, the samples by Dallacasa et al. (2000, HFP sample), by Stanghellini et al. (1998), by Bolton et

Sample	$S_{\rm lim}$ Jy	ν_o GHz	area deg^2	$\nu_p^{\rm min}$ GHz	$\nu_p^{\rm max}$ GHz	$N_{\rm tot}^{\rm gal}$
HFP	0.3	4.9	15840	5.34	11.1	5
Stan	1.0	5.0	24600	0.4	4.9	19
B_SA	0.025	15.0	176	3.43	127.0	10
B_SB	0.060	15.0	70	3.29	10.3	0
Snel	0.018	0.325	522	1.0	5.7	14
CORA	0.1	1.4	2850	0.460	2.3	6
Park	0.5	2.7	12802	0.4	5.0	48
Edwa	0.95	5.0	16414	0.7	7.5	9

Table 5.2: Summary of GPS samples.

al. (2004, 9C samples A and B), by Snellen et al. (1998, as revised by Snellen et al. 2000, faint WENSS sample), by Snellen et al. (2004, CORALZ sample), by Snellen et al. (2002, Parkes sample), and by Edwards & Tingay (2004, ATCA sample). Column 1 of Table 5.2 gives the abbreviated name of the sample, column 2 indicates its flux limit, column 3 gives the selection frequency, column 4 the effective area in which the sources have been selected, column 5 and 6 the minimum and the maximum peak frequency of the observed galaxies respectively and finally column 7 gives the total number of galaxies present in the sample.

5.4.1 The 9C samples

Bolton et al. (2004) selected two complete samples of sources from the first three regions of the 9C survey, coincident with the Very Small Array (VSA) fields at $00^h20^m{+}30°$, $09^h40^m + 32°$ and $15^h40^m + 43°$ (J2000.0): a deeper sample **sample A**, complete to **25 mJy** and containing 124 sources over a total area of 176 square degrees; a shallower sample **sample B**, complete to **60 mJy**, comprising 70 sources in an area of 246 square degrees, including the area covered by sample A. Restricting the sample B to the 70 sq. deg. not overlapping with the sample A we are left with 31 sources.

Simultaneous observations of each source were made at frequencies of 1.4, 4.8, 22 and 43 GHz with the VLA and at 15 GHz with the Ryle Telescope. In addition, 51 sources were observed within a few months at 31 GHz with the Owens Valley Radio Observatory (OVRO) 40m telescope. Sources with spectral index between 1.4 and 4.8 GHz $\alpha_{1.4}^{4.8} < -0.1$ ($S_\nu \propto \nu^{-\alpha}$) were referred to as GPS sources.

Name	Sample		S_p	ν_p
			mJy	GHz
J0003+2740	A	Q?	76 ±1	5.4 ±0.1
J0003+3010	A	G?	60 ±3	10.3 ±0.3
J0010+2854	A	Q?	100 ±5	52 ±6
J0012+3353	A	G?	199 ±12	127 ±36
J0012+3053	A	G?	27 ±1	20 ±4
J0020+3152	A	-	43.8±0.8	4.91 ±0.09
J0024+2911	A	Q?	42 ±2	13.9 ±0.5
J0032+2758	A	G	34.4±0.4	4.6 ±0.2
J0919+3324	B	G?	430 ±16	10.3 ±0.5
J0925+3127	B	G?	135 ±2	3.29 ±0.06
J0931+2750	B	G?	169 ±3	8.3 ±0.3
J0935+2917	A	Q?	47.3±0.9	5.7 ±0.2
J0936+3207	A	G	56 ±5	14 ±1
J0936+2624	B	Q?	179 ±18	3.8 ±0.3
J0940+2603	B	G?	495 ±10	6.1 ±0.8
J0945+3534	B	Q?	413 ±8	4.0 ±0.2
J0952+3512	B	Q?	427 ±8	4.1 ±0.2
J0955+3335	B	Q?	107 ±2	5.9 ±0.2
J1506+4239	A	G	766 ±19	14 ±1
J1517+3936	A	G	43 ±2	21 ±3
J1521+4336	A	Q?	431 ±10	6.2 ±0.2
J1526+3712	A	G?	74 ±2	6.9 ±0.3
J1526+4201	A	G	67 ±1	8.1 ±0.2
J1528+3816	A	G?	80 ±3	26 ±5
J1530+3758	A	G	141 ±3	3.43 ±0.06
J1540+4138	A	G	46 ±8	8.8 ±0.2
J1550+4536	A	G	62 ±1	3.5 ±0.07
J1554+4350	A	-	45.0±0.8	10.9 ±0.3
J1554+4348	A	G?	63 ±1	3.7 ±0.1
J1556+4259	A	Q?	94 ±4	4.3 ±0.2

Table 5.3: The rising spectrum sources from Bolton et al. 2004

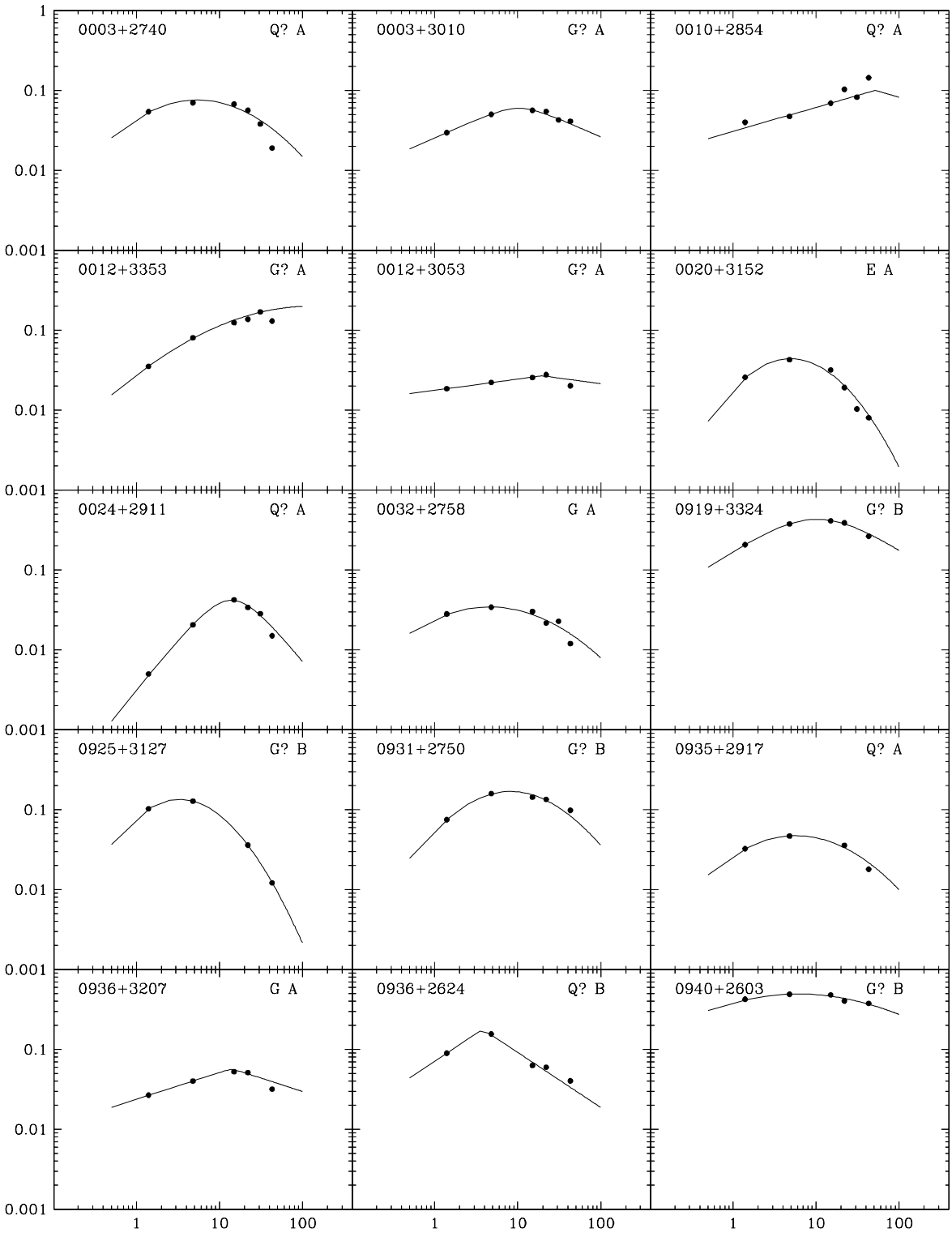

Figure 5.2: Radio spectra of sources [S_ν (Jy) vs ν (GHz)]. Filled circles represent multi-frequency VLA, RT and OVRO data; the solid line shows the corresponding polynomial fits.

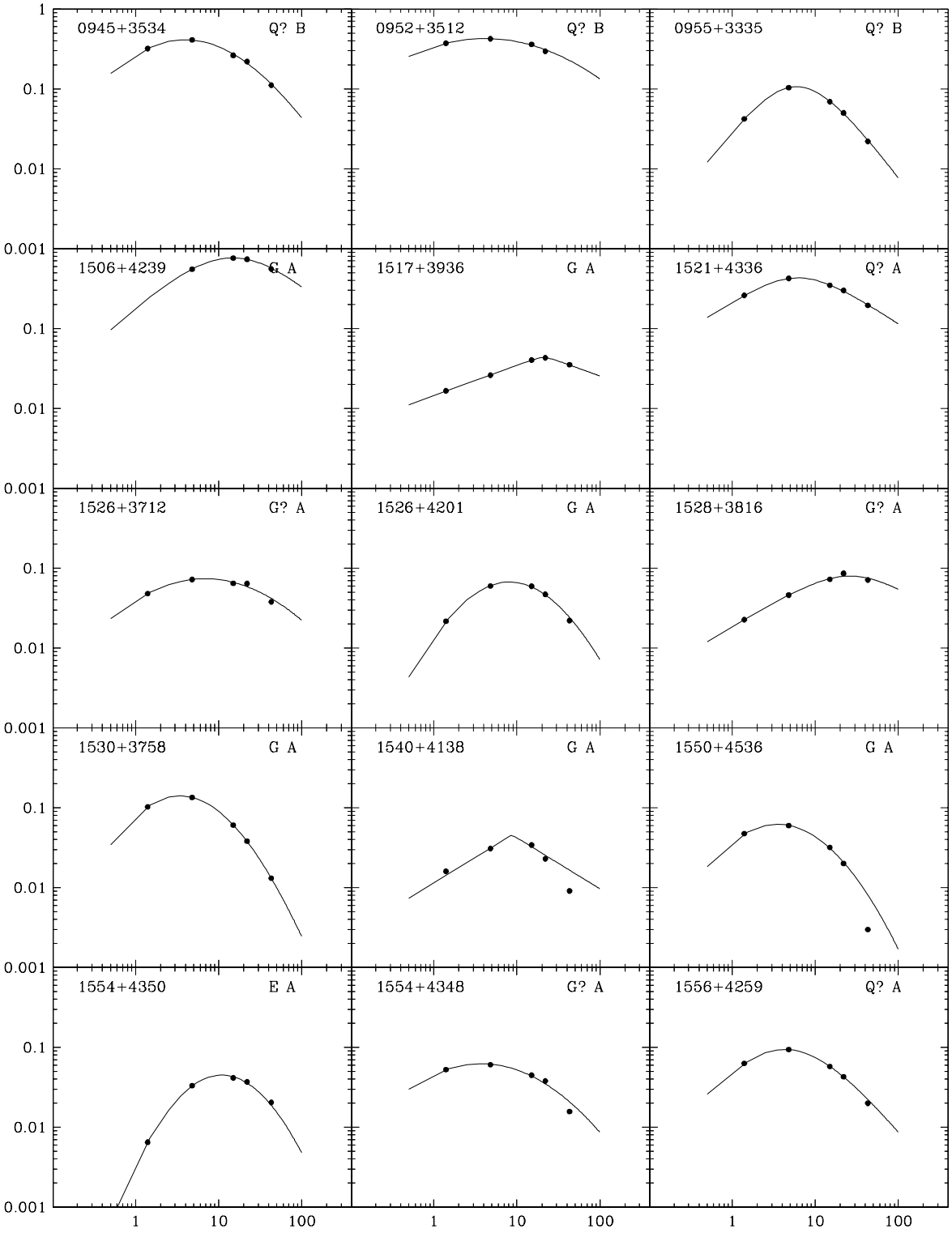

Figure 5.5: (continued)

The adopted criterion implies that sources peaking at $\nu_p \gtrsim 5\,\mathrm{GHz}$ were preferentially (but not exclusively) selected. We have defined two **complete and independent** samples of sources:

- **Sample A**, complete to **25 mJy**, contains 22 sources (14 galaxies, 6 quasars and 2 unidentified sources) in a total area of 176 square degrees.
- **Sample B**, complete to **60 mJy**, contains 8 sources (4 galaxies and 4 quasars) in a total area of 70 square degrees.

In order to estimate the peak flux densities, S_p, and frequencies, ν_p, of the sources, we have fitted the radio spectra with the hyperbolic function used by Tinti et al. (2005) (see Chapter 3, Eq. 3.2). The best fit values of S_p and ν_p, obtained minimizing the chi-square function with the Minuit package (CERN libraries), are reported with their errors in column 4 and 5 of Table 5.3. In the same Table, Column 1 gives the name, column 2 indicates to which sample the source belongs to and column 3 gives the optical identification.

The radio spectra of the sources from Sample A and B are shown in Fig. 5.2 together with the derived fitting curves. The filled circles refer to the VLA, Ryle Telescope (RT) and OVRO multifrequency data and the solid line indicates the corresponding fit.

No redshift measurements are available for these sources. However, as shown by Snellen et al. (1996, 2002), GPS galaxies show a well defined R-band Hubble diagram, with a low dispersion. In terms of Gunn r magnitudes, Snellen et al. (1996) found a best fit relation:

$$r = 22.7 + 7.4\log(z). \tag{5.16}$$

The conversion from the Kron-Cousins R_c magnitudes measured by Bolton et al. (2004) to the Gunn r magnitudes was made taking $r = R_c + 0.3$ (Fukugita et al. 1995). The redshift estimates are given in Table 5.4. We do not count as galaxies the optically point-like objects, classified as "G?" by Bolton et al. (2004) because of their red colours ($O - R \geq 1.6$): if they were bright galaxies at the redshifts estimated from Eq. (5.16) they should be resolved. This leaves 10 GPS galaxies in sample A and zero in sample B (see Table 5.2). All the 20 galaxies from the two samples are reported in Table 5.4: Column 1 gives the source name, column 2 gives R-band magnitude (m_{R_c}), column 3 gives the estimated redshift, column 4

Name	Sample	m_{R_c}	z	ν_p GHz	$\alpha_{1.4}^{4.8}$
J0003+3010	A	20.46	0.55	10.3	0.43
J0012+3353	A	20.15	0.50	127	0.67
J0012+3053	A	19.82	0.45	20	0.14
J0020+3152	A	22.6	1.1	4.91	0.41
J0032+2758	A	20.22	0.5	4.6	0.16
J0936+3207	A	17.29	0.20	14	0.33
J1506+4239	A	19.30	0.38	14	0.48
J1517+3936	A	19.90	0.46	21	0.36
J1526+3712	A	20.80	0.61	6.9	0.33
J1526+4201	A	19.10	0.36	8.1	0.83
J1528+3816	A	20.30	0.52	26	0.58
J1530+3758	A	17.10	0.19	3.43	0.22
J1540+4138	A	16.72	0.17	8.8	0.53
J1550+4536	A	20.20	0.50	3.5	0.19
J1554+4350	A	23.10	1.2	10.9	1.32
J1554+4348	A	19.10	0.36	3.7	0.11
J0919+3324	B	19.00	0.35	10.3	0.48
J0925+3127	B	18.10	0.26	3.29	0.18
J0931+2750	B	20.10	0.49	8.3	0.61
J0940+2603	B	19.21	0.37	6.1	0.12

Table 5.4: The GPS galaxies selected by Bolton et al. 2004

gives the observed peak frequency and column 5 the spectral index calculated between 1.4 and 4.8 GHz.

It is important to note that other criteria for selecting GPS samples include tighter constraints on the low- and/or high-frequency spectral indices. The effect of the different selection criteria is discussed in Sect. 5.5.

5.4.2 The HFP sample

The bright HFP sample by Dallacasa et al. (2000) was selected by cross-correlating the 87GB (Gregory et al. 1996) sources with $S_{4.9\mathrm{GHz}} \geq 300\,\mathrm{mJy}$ with the NVSS catalogue (Condon et al. 1998) at 1.4 GHz and picking out those with inverted spectra ($\alpha < -0.5$). It was then "cleaned" by means of simultaneous multifrequency VLA observations, leaving 55 sources whose single-epoch radio spectrum peaks at frequencies ranging from a few GHz

Name	z	ν_p GHz
0428+3259	0.3	7.3
0655+4100	0.02156	7.8
1407+2827	0.0769	5.34
1511+0518	0.084	11.1
1735+5049	1.5*	6.4

Table 5.5: The HFP galaxy sample. The * denotes an empty field, which was attributed $z = 1.5$.

to about 22 GHz. The sample of HFP candidates comprises 11 galaxies (including a type 1 Seyfert), 36 quasars, and 8 still unidentified sources (Dallacasa et al. 2002), over an area of $15,840\,\mathrm{deg}^2$. The selection criterion here summarized has been discussed in details in Chapter 3.

Although there are, in this sample, some sources with $\nu_p < 4.9\,\mathrm{GHz}$, the selection criterion biases the sample against such values of ν_p in a way that we are unable to quantify. Therefore we have chosen to confine ourselves to sources with $\nu_p > 4.9\,\mathrm{GHz}$. Moreover we have excluded from the sample the objects with 4.9 GHz flux densities smaller than the completeness limit of 300 mJy when they were re-observed by Dallacasa et al. (2000) and Tinti et al. (2005). After having applied these additional constraints, we are left with 5 HFP galaxies, listed in Table 5.5. Column 1 gives the J2000 name, column 2 gives the redshift and column 3 gives the observed peak frequency.

5.4.3 The faint GPS sample from WENSS

The selection of this sample has been described in detail in Snellen et al. (1998a). Snellen et al. (2000) applied stricter criteria allowing a better control of selection effects; they kept only the 14 objects with inverted spectra between 0.325 and 5 GHz, and with 325 MHz flux densities $> 20\,\mathrm{mJy}$, over an area of $522\,\mathrm{deg}^2$ from the regions at $15^h < \alpha < 20^h$ and $58^\circ < \delta < 75^\circ$ and $4^h00^m < \alpha < 8^h30^m$ and $58^\circ < \delta < 75^\circ$. Additional observations at 1.4, 5, 8.4 and 15 GHz were carried out with WSRT and the VLA in order to estimate the peak frequency and the peak flux density. The redshift of identified sources, all classified

Name	z	ν_p GHz
B0400+6042	1.5*	1.0
B0436+6152	1.5*	1.0
B0535+6743	1.5	5.7
B0539+6200	1.4	1.9
B0830+5813	0.093	1.6
B1525+6801	1.1	1.8
B1551+6822	1.3	1.5
B1557+6220	0.9	2.3
B1600+7131	1.5*	1.7
B1622+6630	0.201	4.0
B1655+6446	1.5*	1.0
B1841+6715	0.486	2.1
B1942+7214	1.1	1.4
B1946+7048	0.101	1.8

Table 5.6: The faint GPS galaxies from WENSS. The * denotes empty fields, which were attributed $z = 1.5$. Values of z with 3 significant digits are spectroscopic, the others are photometric estimates.

as galaxies, had to be estimated from their optical magnitudes, using Eq. (5.16). For the 4 unidentified sources, also assumed to be galaxies, a redshift of z=1.5 was assumed. The relevant data for all the 14 objects are given in Table 5.6. Column 1 gives the B1950 name, column 2 gives the redshift and column 3 gives the observed peak frequency.

5.4.4 The bright GPS sample

Stanghellini et al. (1998) selected candidate radio bright GPS sources from the Kühr et al. (1981) catalogue ($S_{5\mathrm{GHz}} \geq 1\,\mathrm{Jy}$), with declination $> -25°$ and galactic latitude $|b| > 10°$, over an area of about $24,600\,\mathrm{deg}^2$. The sample was then cleaned by means of multifrequency VLA and WSRT observations, supplemented with literature data. They picked out GPS candidates with a turnover frequency between 0.4 and 6 GHz, and an optically thin spectral index $\alpha_{\mathrm{thin}} > 0.5$ beyond the peak. The final complete sample consists of 33 GPS sources, 19 of which are identified with galaxies. Four galaxies do not have spectroscopic redshift; estimates by Snellen et al. (2000) from their optical magnitudes [Eq. (5.16)] are denoted by a * in Table 5.7, where the relevant data for the 19 galaxies are

Name	z	ν_p GHz
0019-000	0.305	0.8
0108+388	0.669	3.9
0316+162	1.2*	0.8
0428+205	0.219	1.0
0500+019	0.583	2.0
0710+439	0.518	1.9
0941-080	0.228	0.5
1031+567	0.459	1.3
1117+146	0.362	0.5
1323+321	0.369	0.5
1345+125	0.122	0.6
1358+624	0.431	0.5
1404+286	0.077	4.9
1600+335	1.1*	2.6
1607+268	0.473	1.0
2008-068	0.7*	1.3
2128+048	0.99	0.8
2210+016	1.0*	0.4
2352+495	0.237	0.7

Table 5.7: The bright GPS galaxies from Stanghellini et al. (1998). The * denotes photometric redshift estimates.

listed. Column 1 gives the B1950 name, column 2 gives the redshift and column 3 gives the observed peak frequency.

5.4.5 The ATCA GPS sample

Edwards & Tingay (2004) have used data from an Australia Telescope Compact Array (ATCA) program of multi-frequency, multi-epoch monitoring of the portion of the VSOP survey sample (Hirabayashi et al. 2000) with declinations $< 10°$. The original sample is defined by: $S_{5\mathrm{GHz}} > 0.95\,\mathrm{Jy}$, $\alpha < 0.45$, $|b| > 10°$. Taking into account the further constraint $\delta < 10°$, we estimate that the area covered is $\sim 5\,\mathrm{sr}$. The selected sources have $\alpha_{\mathrm{thin}} > 0.5$ and spectral curvature $\alpha_{\mathrm{thin}} - \alpha_{\mathrm{thick}} > 0.6$.

We have excluded from the sample the gravitationally lensed source $\mathrm{J0414+0534}$ because our models do not include the effect of lensing, and $\mathrm{J1522-2730}$, classified as

Name	z	ν_p GHz
J0241-0815	0.004	7.5
J1543-0757	0.172	0.7
J1658-0739	1.5*	4.8
J1726-6427	1.5*	1.1
J1723-6500	0.014	2.7
J1744-5144	1.5*	1.0
J1939-6342	0.183	1.4
J2257-3627	0.006	2.7
J2336-5236	1.5*	1.1

Table 5.8: The ATCA sample of GPS galaxies from Edwards & Tingay (2004). The * denotes empty fields, which were attributed $z = 1.5$.

a BL Lac object, whose variability properties suggests that it is less likely to be a truly GPS source (Edwards & Tingay 2004). This leaves 7 GPS galaxies (5 having spectroscopic redshifts), 16 quasars (15 with spectroscopic redshift), and 2 empty fields (see Table 5.8).

5.4.6 The CORALZ sample

The sample of Compact Radio sources at Low Redshift (CORALZ) was selected by Snellen et al. (2004) solely on the basis of the radio angular size ($\theta < 2''$), independent of radio spectra, picking out sources associated with relatively bright galaxies and over the redshift range $0.005 < z < 0.16$. It is estimated to be $\simeq 95\%$ complete for $S_{1.4\mathrm{GHz}} > 100\,\mathrm{mJy}$ in a region of 2850 square degrees, with declination, $30^\circ < \delta < 57.5^\circ$, and galactic latitude, $b > 30^\circ$, to make it overlap with the optical APM Palomar Sky Survey (APM/POSS-I) catalogue (McMahon & Irwin 1992), and the WENSS 325-MHz radio survey (Rengelink et al. 1997). The sample comprises 6 GPS galaxies with $\nu_p > 0.4\,\mathrm{GHz}$, all with spectroscopic redshifts (Table 5.9).

5.4.7 The Parkes half-Jy sample

Snellen et al. (2002) selected from the Parkes multifrequency survey data in a region of about 3.9 sr a southern/equatorial ($-40^\circ < \delta < 15^\circ$, $|b| > 20^\circ$) sample of GPS sources with $S_{2.7\mathrm{GHz}} > 0.5\,\mathrm{Jy}$, excluding objects identified as quasars. The sample (see

Name	z	ν_p GHz
J073328+560541	0.104	0.460
J073934+495438	0.054	0.950
J083139+460800	0.127	2.200
J090615+463618	0.085	0.680
J131739+411545	0.066	2.300
J171854+544148	0.147	0.480

Table 5.9: The CORALZ sample of local GPS galaxies (Snellen et al. 2004).

Table 5.10) consists of 49 objects with spectra peaking at $\nu_p > 0.4\,\mathrm{GHz}$, 38 of which are identified with galaxies, 10 are too faint to be identified and 1 is too close to a bright star to allow identification, and is excluded from the statistical analysis. The authors argue that, based on the magnitude distribution of other GPS samples, the 10 faint sources are unlikely to be quasars, and we assume them to be galaxies. Spectroscopic redshifts are available for 18 objects. Estimates, or lower limits, for the others have been obtained through Eq. (5.16). No restrictions on either the low- or the high-frequency spectral index are mentioned.

5.5 Impact of different selection criteria

The observational properties that generally define the different samples are:

- the flux density at the frequency of selection;
- the turnover frequency range;
- the spectral index in the optically thin and thick part of the spectrum;

To effectively explore the luminosity and peak frequency evolution of GPS sources, we need samples that provide a wide coverage of the ν_p–S_p plane. The coverage provided by the present samples is shown in Fig. 5.6. HFP sources (Dallacasa et al. 2000) have turnover frequencies higher than 4.9 GHz, at or above the upper limits of the samples of Stanghellini et al. (1998) and Snellen et al. (1998, 2002, 2004). Because of their high selection frequency, 15 GHz, the Bolton et al. (2004) samples explore the high peak frequency region.

Name	m_R	z	ν_p GHz
J0022+0014	18.10	0.305	0.6
J0108-1201	22.39	1.0*	1.0
J0206-3024	21.00	0.65*	0.5
J0210+0419	24.1	1.5*	1.3
J0210-2213	23.52	1.4*	1.5
J0242-2132	17.10	0.314	1.0
J0323+0534	19.20	0.37*	0.4
J0401-2921	21.0	0.65*	1.0
J0407-3924	20.40	0.54*	0.4
J0407-2757	21.14	0.68*	1.5
J0433-0229	19.10	0.36*	0.4
J0441-3340	21.0	0.65*	1.2
J0457-0848	20.30	0.52*	0.4
J0503+0203	21.0	0.583	2.5
J0943-0819	17.50	0.228	0.4
J0913+1454	20.0	0.47*	1.1
J1044-2712	21.0	0.65*	0.8
J1057+0012	21.0	0.65*	1.6
J1109+1043	20.50	0.55*	0.5
J1110-1858	19.60	0.497	1.0
J1120+1420	20.10	0.362	0.4
J1122-2742	21.0	0.65*	0.8
J1135-0021	16.50	0.16*	0.4
J1203+0414	18.80	0.34*	0.4
J1345-3015	21.0	0.65*	2.5
J1347+1217	15.20	0.122	0.4
J1350-2204	20.93	0.63*	0.4

Table 5.10: The Parkes half-Jansky sample of GPS galaxies (Snellen et al. 2002). The * denotes photometric redshift estimates.

Name	m_R	z	ν_p GHz
J1352+0232	20.00	0.47*	0.4
J1352+1107	21.0	0.65*	3.6
J1447-3409	21.00	0.65*	0.5
J1506-0919	19.70	0.43*	0.6
J1521+0430	22.10	1.296	1.0
J1543-0757	17.40	0.172	0.4
J1546+0026	20.10	0.556	0.6
J1548-1213	21.88	0.883	0.4
J1556-0622	22.20	0.94*	0.4
J1604-2223	18.75	0.141	0.6
J1640+1220	21.36	1.150	0.4
J1648+0242	21.0	0.65*	3.4
J1734+0926	20.80	0.61*	1.0
J2011-0644	21.18	0.547	1.4
J2058+0540	23.40	1.381	0.4
J2123-0112	23.30	1.158	0.4
J2130+0502	22.21	0.990	1.0
J2151+0552	20.20	0.740	5.0
J2212+0152	22.0	0.88*	0.4
J2325-0344	23.50	1.4*	1.4
J2339-0604	22.91	1.2*	0.4

Table 5.10: (continued)

The samples by Bolton et al. (2004) have flux limit similar to the faint GPS sample selected by Snellen et al. (1998), although at a very different frequency, while the HFP and the Stanghellini et al. (1998), and the Parkes samples contain bright sources.

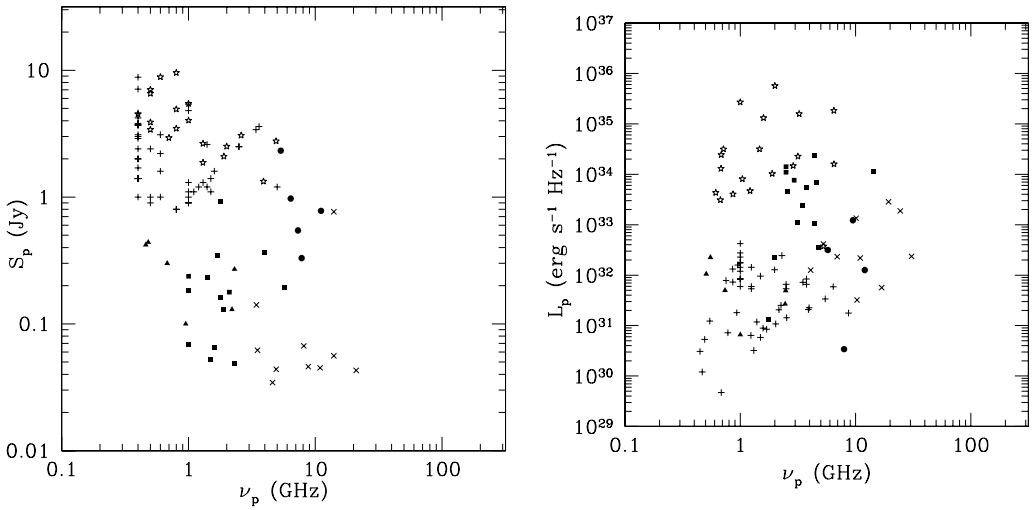

Figure 5.6: Peak flux density versus observed peak frequency (left) and peak luminosity versus rest frame turnover frequency (right) for GPS galaxies in the various samples. HFP: filled circles; Bolton sample A: $\times$; WENSS: filled squares; CORALZ: filled triangles; Stanghellini: $\star$; Parkes: $+$.

The redshift distributions of the galaxies in the various samples are shown in Fig. 5.7. Many redshifts are estimated from optical magnitudes. The peak at $z = 1.5$ is mostly due to optically unidentified GPS sources, assumed, following Snellen et al. (2000), to have that redshift.

As noted above, selection criteria include constraints on the spectral indices in the optically thick and/or in the optically thin spectral region. Stanghellini et al. (1998) required $\alpha_{\rm thin} \geq 0.5$, Dallacasa et al. (2000) demanded $\alpha_{\rm thick} \leq -0.5$; Edwards & Tingay (2004) applied both constraints. For other samples, the adopted spectral criteria are less explicit. Snellen et al. (1998, 2000) require an inverted spectrum at low frequencies and that the Full Width at Half Maximum of the spectrum is less than 2 decades in frequency. This constrains can be interpreted as a condition on the spectral index:

$$\frac{S_{\nu_p}}{S_{\nu_p/10}} = \frac{\nu_p^{\alpha}}{(\nu_p/10)^{\alpha}} > log(2) \quad \Rightarrow \quad \alpha > 0.3$$

where the frequencies are expressed in GHz. The latter condition implies that, typically, $\alpha_{\rm thin}$ and $-\alpha_{\rm thick}$ are ≥ 0.3, a somewhat less restrictive constraint than adopted for the previously mentioned samples. An even looser criterion was adopted by Bolton et al. (2004):

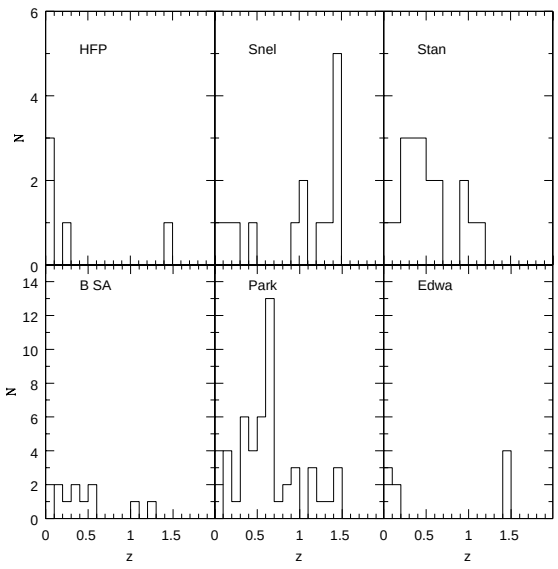

Figure 5.7: Distributions of measured and estimated redshifts for the HFP, Stanghellini et al. (1998), Snellen et al. (1998), Bolton et al. (2004, sample A), Parkes, and ATCA GPS galaxy samples. Note that the peaks at $z = 1.5$ are due to unidentified sources, assumed to be galaxies at that redshift.

$\alpha_{1.4}^{4.8} < -0.1$. Not many details are given on spectral criteria for the Parkes sample (Snellen et al. 2002), while the CORALZ sample (Snellen et al. 2004) was selected on the basis of radio morphology, not of the spectra.

In Fig. 5.8 we compare the shapes of the radio spectra of the sources in the different samples, normalized to the peak frequencies and to the peak flux densities. It is clear, and visible in Table 5.11, that the median $\alpha_{\rm thick}$ of Bolton et al. (2004) sources is considerably flatter than for the other samples. To homogenize this sample to the others, we have dropped sources with $\alpha_{\rm thick} > -0.5$.

5.6 Results

We have fitted separately the redshift and the observed peak frequency, ν_p, distributions of GPS galaxies in the samples described above. The best fit values of the parameters have been obtained minimizing the chi-square function with the Minuit package (CERN libraries). We need to determine:

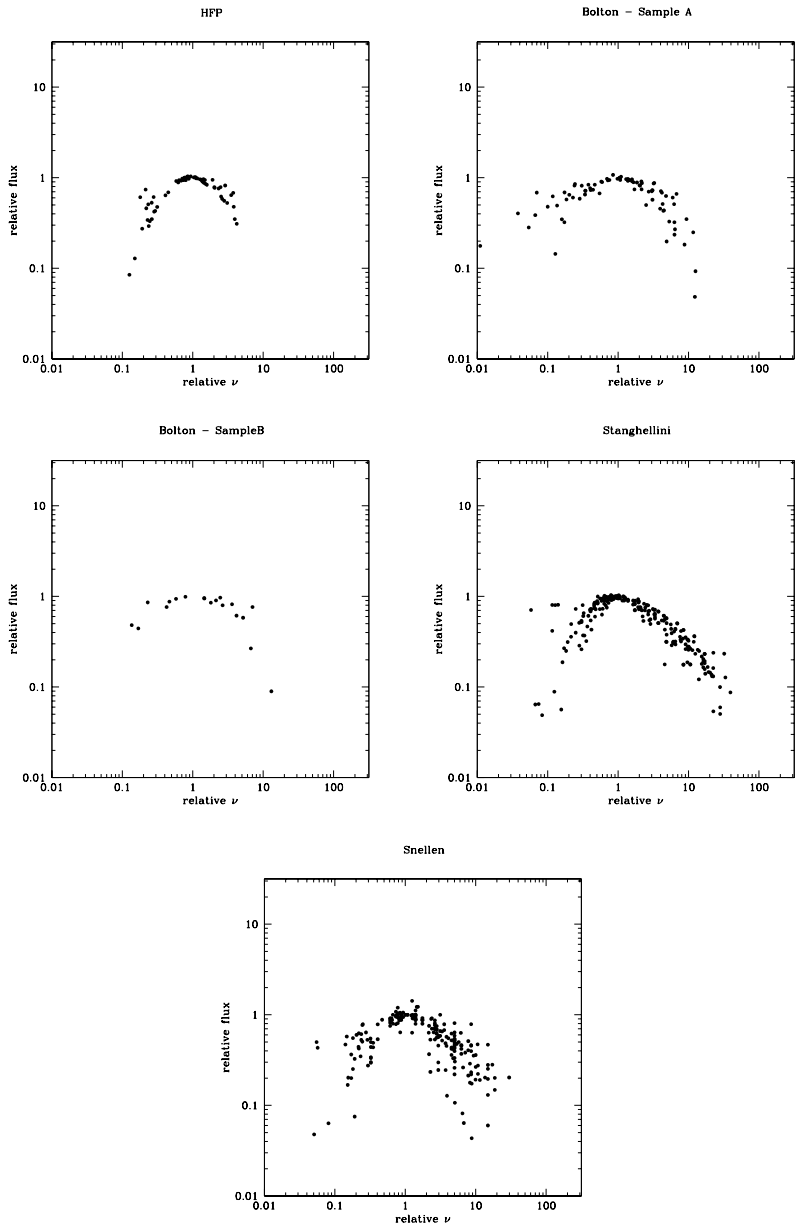

Figure 5.8: Spectra of GPS sources in the various samples, normalized in both frequency and flux density

Sample	α_{thick}	α_{thin}
HFP	-0.86	0.61
Stan	-0.76	0.67
B_SA	-0.38	0.76
B_SB	-0.43	0.82
Snel	-0.67	0.64

Table 5.11: Median values of the optically thick and thin spectral indices for the various samples.

- the parameters characterizing the luminosity function, i.e. the normalization n_0 and the slope β; the minimum and maximum luminosities, $\mathrm{L_{min}}$ and $\mathrm{L_{max}}$ respectively, both referred to the frequency of 300 MHz, below the conventional minimum peak frequency of GPS sources, have been set at the minimum and maximum observed values: $L_{\mathrm{max}}(300\mathrm{MHz}) = 5 \cdot 10^{35}\,\mathrm{erg\,s^{-1}\,Hz^{-1}}$, $L_{\mathrm{min}}(300\mathrm{MHz}) = 10^{29}\,\mathrm{erg\,s^{-1}\,Hz^{-1}}$;
- the slope, η, of the power-law dependence of the emitted radio power on source age;
- the slope, λ, of the power-law dependence of the peak frequency on source age;
- the initial value of the peak frequency, $\nu_{p,i}$;
- the redshift of formation of the first peaked spectrum sources, z_f;
- the parameter k characterizing the cosmological evolution of the luminosity function.

We have checked that the data do not require cosmological evolution of the luminosity function of GPS galaxies, confirming the finding of De Zotti et al. (2000), and we have therefore set $k = 0$. We thus have $L_\star(z) = \mathrm{const} = L_0 = 10^{32}\,\mathrm{erg\,s^{-1}\,Hz^{-1}}$ [Eq. (5.6)]. The fit is also insensitive to the value of z_f, provided that it is larger than the maximum estimated redshift of GPS galaxies in the considered samples. We have therefore fixed $z_f = 1.5$.

Figures 5.9 and 5.10 compare the model with the observed redshift and peak frequency distributions. The overall agreement is reasonably good, indicating that the underlying scenario is consistent with the current data.

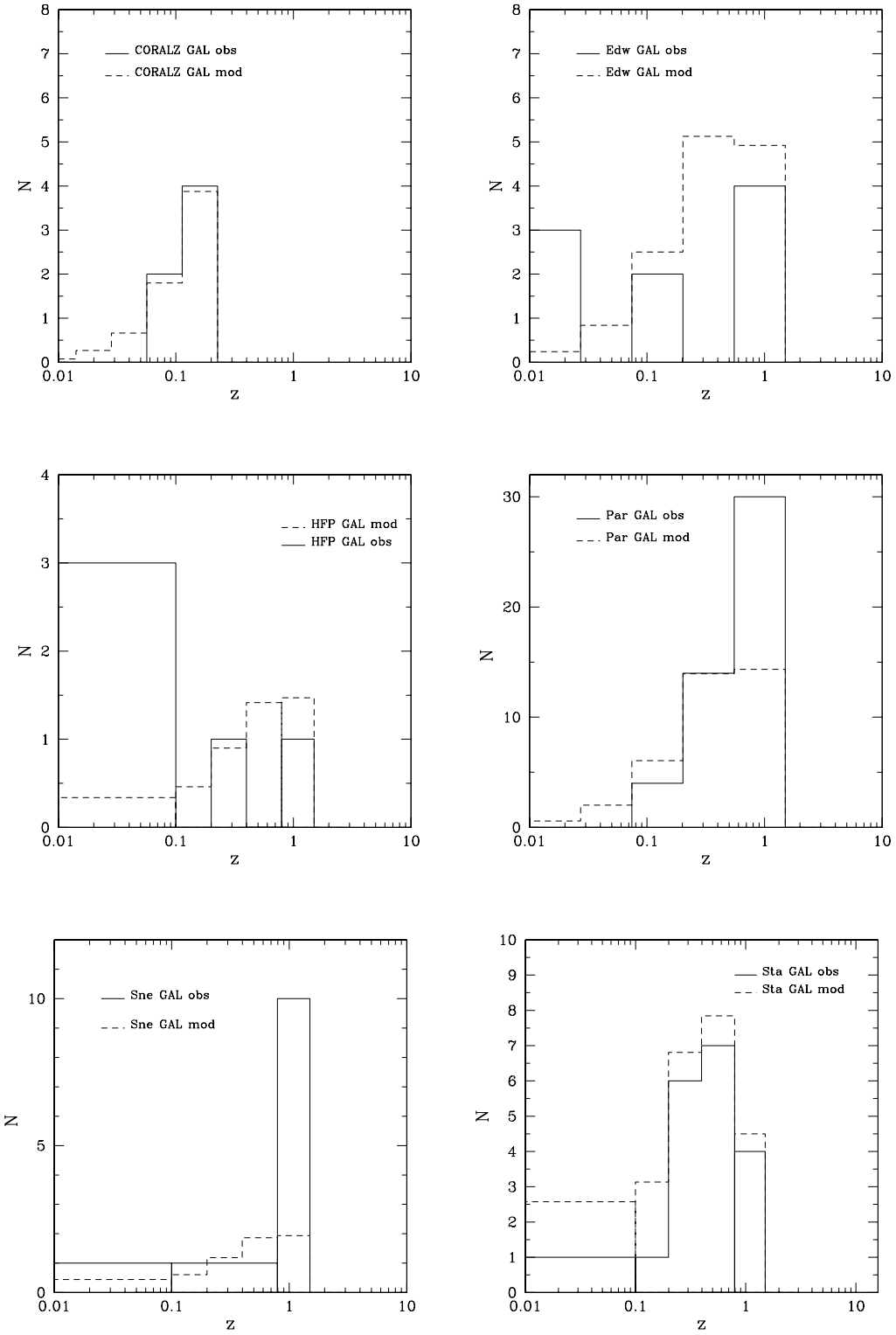

Figure 5.9: Comparison of the redshift distributions yielded by the best fit model (dashed) with the observed ones (solid).

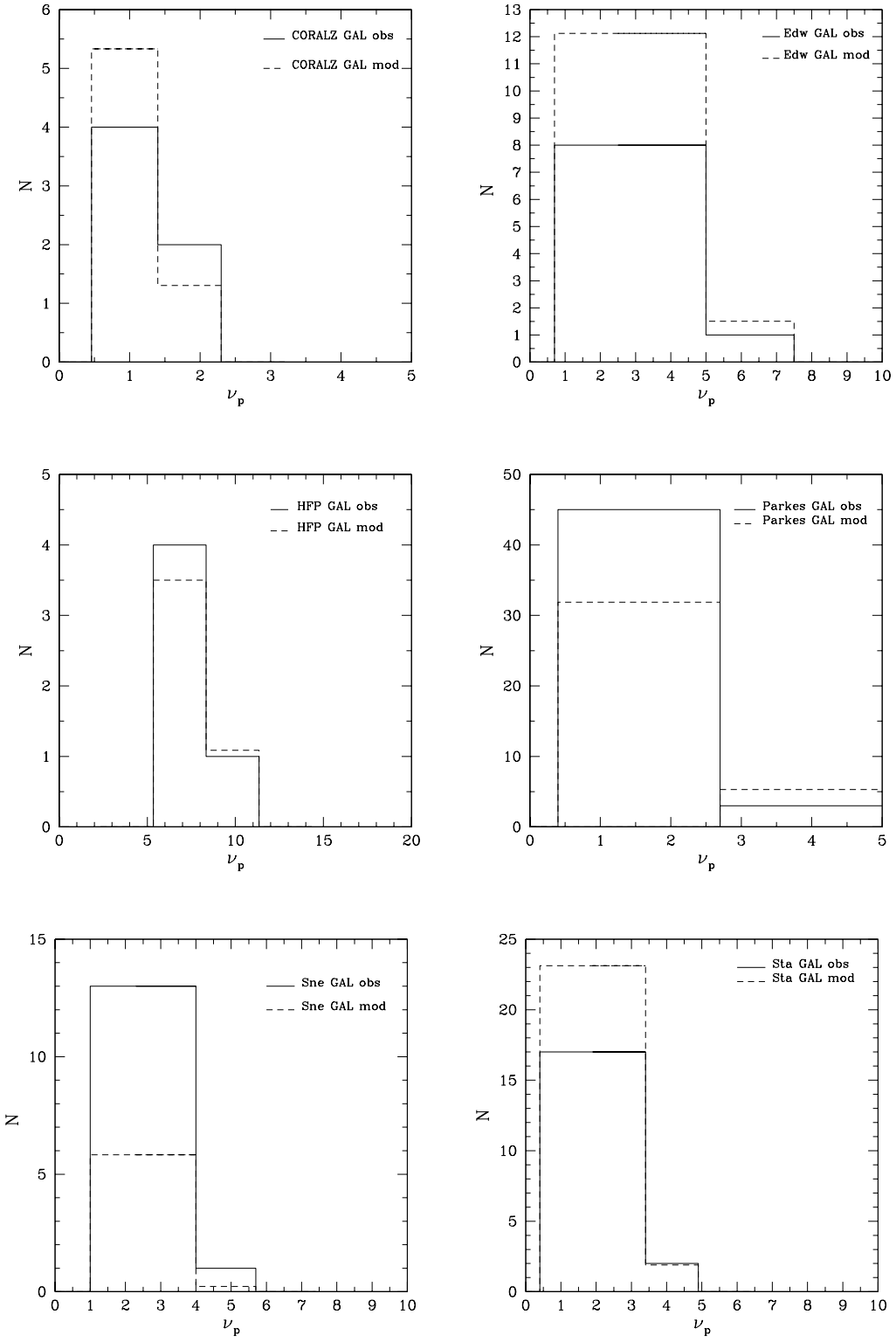

Figure 5.10: Comparison of the peak frequency distributions yielded by the best fit model (dashed) with the observed ones (solid).

$\log(n_0)\,[\mathrm{Mpc}^{-3}\,(d\log L_\nu)^{-1}\,\mathrm{GHz}^{-1}]$	-14.13
β	0.83
$\log(\nu_{p,i})$ (GHz)	2.98
η	1.20
λ	0.0125

Table 5.12: Best fit values of the model parameters for GPS galaxies.

The best fit values of the parameters are given in Table 5.12. The formal errors on them derived from the χ^2 statistics are rather small, but we regard them as unrealistic in view of the many uncertainties due to the difficulties in the sample selection; also the redshift distributions are largely built using photometric redshift estimates rather than spectroscopic measurements. Thus we prefer not to report uncertainties that are likely to be deceitful. The real uncertainties are probably large as indicated by a comparison of the present best-fit values of the parameters with those found by De Zotti et al. (2000) analyzing some of the samples considered here. In particular, the values of η and λ are widely different [the difference of n_0 follows from that of λ, see Eq. (5.5)]. Still both analyses find positive values of η and negative values of $p = -\eta + \alpha\lambda$, implying that both the emitted radio power and the peak luminosity *decrease* with increasing source age, at variance with the evolution model by Snellen et al. (2000) and Alexander (2000). The slope of the luminosity function is more stable: we find $\beta = 0.83$ while De Zotti et al. (2000) found $\beta = 0.75$. Both values are not far from the slope of the low luminosity portion of the luminosity function of steep spectrum radio sources, $\beta_{ss} \simeq 0.69$ (Dunlop & Peacock 1990; Magliocchetti et al. 2002).

5.7 Discussion and conclusions

Although new samples have substantially improved the coverage of the luminosity–redshift–peak frequency space of GPS galaxies, the assessment of their evolutionary properties is still difficult. First of all, there is no fully agreed set of criteria to ascertain whether a source is truly a GPS. The frequently adopted GPS identification conditions rely on the spectral shape. However, as mentioned in Sects. 5.4 and 5.5, different spectral requirements have been adopted by different groups and recovering a homogeneous set of data is not easy

and may be even impossible. Other properties that GPS sources should have, include a compact structure (size $\lesssim 1\,\mathrm{kpc}$), low polarisation, low variability, and sub-luminal component motions. Regrettably, measurements of these quantities are available only for a limited number of GPS candidates. The samples we are using may therefore be contaminated by sources of different nature.

Also, a significant fraction of objects are still unidentified, and spectroscopy of identified objects is highly incomplete, so that many redshifts are estimated from optical magnitudes. Although GPS galaxies seem to have a rather well defined redshift–magnitude relationship, its dispersion is significant and may increase with redshift.

With these premises we cannot expect to be able to come out with a clear assessment of the evolutionary properties of GPS galaxies. Still, some interesting conclusions can be drawn. First, the simple luminosity evolution scenario for individual sources outlined in Sect. 5.3 appears to be fully consistent with the data. We note however that, although the formalism stems from the self-similar evolution models by Fanti et al. (1995) and Begelman (1996, 1999), according to which both the parameters η and λ are determined by the slope n of the density profile of the ambient medium, the data can be satisfactorily fitted only if the two parameters are treated as independent. This is not surprising, since self-similarity can be easily broken under realistic conditions, and indeed deviations from self-similarity were found in the two-dimensional hydrodynamical simulations of Carvalho & O'Dea (2002).

The fit is obtained for a positive value of η and a negative value of p, implying a decrease of the emitted power and of the peak luminosity with source age or with decreasing peak frequency, at variance with the Snellen et al. (2000) model. On the other hand, our analysis confirms the rather flat slope of the luminosity function, found by Snellen et al. (2000) who also report indications of a high luminosity break, not required by the data sets we have used. Snellen et al. (2000) argue that, in the framework of a scenario whereby GPS sources increase their luminosity until they reach a size $\sim 1\,\mathrm{kpc}$ and dim thereafter, during the CSS and extended radio source phases, the luminosity function of GPS galaxies can evolve into that of extended radio sources. Our results suggest that the GPS galaxies are the precursors of extended radio sources with luminosities below the break of the luminosity function ($L_{\mathrm{break}} \sim 10^{33}\,\mathrm{erg\,s^{-1}\,Hz^{-1}}$ at 2.7 GHz, cf. Dunlop &

Peacock 1990, De Zotti et al. 2005). Our best fit model implies that the source luminosity is, roughly, inversely proportional to the source age. If GPS sources have typical ages of $\simeq 10^3$ yr and extended radio sources of $\simeq 10^7$ yr, we expect the latter to be $\sim 10^4$ times less powerful than the former; as shown by Fig. 5.6, the maximum value of the peak luminosity we found is $\sim 10^{36}\,\mathrm{erg\,s^{-1}\,Hz^{-1}}$ (but this may be a lower limit, since we have arbitrarily set the maximum redshift at $z_f = 1.5$), i.e. about 3 orders of magnitude larger than $L_{\rm break}$. The GPS sources in the samples considered here are thus expected to evolve into large-scale radio galaxies with $L < L_{\rm break}$.

It must be stressed, however, that the uncertainties are very large, so that firm conclusions must await for larger samples and more complete redshift information. In particular, we have checked that still acceptable fits can be obtained setting the exponent η of the relationship between the emitted radio power and the source age to the value implied by Begelman's model for $n = 2$, i.e. $\eta = 0.5$ (the total χ^2 increases by $\delta\chi^2 \simeq 2$). In this case, the source luminosities would typically decrease by a factor of ~ 100 from the GPS to the extended radio source phase, and GPS sources could be the progenitors of extended radio sources with luminosities both above and below $L_{\rm break}$. It is plausible that sources have a distribution of values of η whereby the lower values become increasingly rare, to account for the steepening of the luminosity function above $L_{\rm break}$. Alternatively, the fraction of prematurely fading sources may increase with luminosity. If $\eta = 0.5$, the best fit value of λ is 1.02, and the peak luminosity, $L_p(\nu_p)$ *increases*, albeit slowly, with *decreasing* peak frequency [$L_p(\nu_p) \propto \nu_p^{-0.25}$, cf. eq. (A.20)]. The other values of the parameters keep values very close to those in Table 5.12.

Another key observable quantity potentially providing crucial constraints on evolutionary models is the linear size. The self-similar evolution models predict its dependence on source age, given the density profile of the ambient medium, and on the other fundamental observable, the radio power. However, as noted above, we could not fit the data with strictly self-similar models, so that we no longer have a well defined relationship between radio power and linear size. Such a relationship, however, can be recovered through the *observed* relationship between turnover frequency and linear size, $\nu_p \propto l^{-\delta}$, with $\delta \simeq 0.65$; we have $L \propto l^{-\eta\delta/\lambda}$. The anticorrelation between the latter quantities implies that, since

the radio power *decreases* with decreasing peak frequency, it decreases with increasing linear size. Once again, however, the uncertainties are very large. The formal best fit values of the parameters would imply an unrealistically steep decrease of the radio power, L, with increasing linear size, l, but, if $\eta = 0.5$, $L \propto l^{-0.32}$ and $L_p(\nu_p) \propto l^{p\delta/\lambda} \propto l^{0.17}$.

In turn, fixing the exponent λ of the relationship between peak frequency and source age to the value implied by Begelman's model for $n = 2$, i.e. $\lambda = \delta = 0.65$, we get again an increase of the minimum χ^2 by $\delta\chi^2 \simeq 2$, the best fit value of η is 0.76, while the other parameters are essentially unchanged. In this case we have $L_p(\nu_p) \propto \nu_p^{0.42}$, $L \propto l^{-0.76}$, and $L_p(\nu_p) \propto l^{-0.27}$.

These examples illustrate the importance of the determination of linear sizes for large complete samples of GPS sources. Given their extreme compactness and their redshift distribution, images with milli-arcsec resolution are generally required. It is thus not surprising the the currently available information is scanty and inhomogeneous. New VLBA data are however being acquired and analyzed, for example on the HFP sample (Orienti et al. 2005). Future evolutionary models should comply also with the distributions of linear sizes and with relationships of sizes with radio power.

Complementary information on the proposed evolutionary sequence linking GPS sources to large scale radio sources is provided by CSS sources, which could correspond to the intermediate phase when sources have expanded out of the narrow line region but are still within the host galaxy. More complete evolutionary studies should take into account also these sources.

Chapter 6

Conclusions

The work presented in this thesis is focused on the extreme GPS sources, dubbed High Frequency Peakers (HFP), that may correspond to the earliest evolutionary phases of radio sources. We have investigated the properties of these sources in the framework of the currently accepted *youth scenario* that relates the linear size of these sources to their age.

Our study comprises two main parts:

1. observational work and analysis of a complete sample of candidate HFPs, aiming at identifying truly young sources;

2. investigation of evolutionary properties of the GPS source population.

6.1 Observational study of a sample of extreme GPS sources

We have carried out an extensive observational program on the complete sample of bright candidate GPS sources peaking above $\simeq 5\,\mathrm{GHz}$ (HFPs), selected by Dallacasa et al. (2000): VLA multifrequency observations at a second epoch separated by 3 to 4 years from the original observations, VLA polarimetric measurements, and high-resolution VLBA imaging. These data have been used to assess the nature of the sources, and, in particular, to discriminated between truly newborn sources and beamed, flat-spectrum quasars caught during a flaring phase of a strongly self-absorbed component that dominates the radio spectrum (see also Snellen et al. 1999, Stanghellini et al. 2003).

Repeated high sensitivity simultaneous multifrequency observations allowed us to investigate the variability properties of candidate HFPs. Our analysis has shown that while the HFPs associated with galaxies do not show significant variability, most of those identified with quasars do. In general, the variability properties (amplitude, timescales, correlation between peak luminosity and peak frequency of the flaring component) of the variable quasar sub-sample resemble those of blazars. We thus conclude that most HFP candidates identified with quasars may well be flaring blazars. A similar conclusion is reached in the case of radio sources showing a convex spectrum in the simultaneous WMAP data and identified as quasars: again a closer look reveals that most or all of them are blazars.

Polarimetric VLA multifrequency observations have revealed that HFP quasars have a wide range of fractional polarisation, with values of up to 6%, while all the galaxies are not polarised. Three out of the seven sources without optical identification also have a significant polarisation level. Polarised emission is expected if HFP quasars are large-scale radio sources with the jet aligned to the line of sight, so that the radiation comes from a region external to the high local ionization close to the AGN, where strong Faraday depolarisation occurs. Therefore polarisation measurements lend further support to the hypothesis that most HFP quasars are likely blazars caught by during a flare.

To study the milli-arcsecond morphology of the HFPs we have acquired high resolution VLBA observations. The analysis of the data is still in progress. Of the 53 sources analyzed, 33 appear resolved by the VLBA. There is a clear segregation in radio morphology between quasars and galaxies. The majority of galaxies ($\sim$80%) show a "Double/Triple" morphology and have been classified as CSO candidates (56% if we consider also the empty fields), while quasars are generally either Core-Jet ($\sim$31%) or Unresolved ($\sim$ 40%). This is consistent with the idea that the HFP spectrum in galaxies and quasars originates from intrinsically different emitting regions: mini-lobes and/or hot spots in galaxies, compact regions related to the core in quasars.

On the basis of the data we have collected, we have discussed six different criteria to discriminate between young sources and flaring blazars and we found that in most cases they yield consistent indications on the source nature. In particular, we found a substantial agreement among the classifications yielded by the variability and by the polarisation criteria

for 87% of the sources. In 70% of the cases, the observed morphology corresponds to that expected on the basis of the polarimetric and variability classification.

For the statistical analysis of the sample we have referred to the variability criterion quantified by the variable V [Eq. (4.1)], since, at present, this is the quantity on which we have the most complete information. The distribution of V for the less variable sources is close to the χ^2 distribution with two degrees of freedom, as may be expected since variations of spectra of young sources are controlled by two parameters, S_p and ν_p. If so, sources with $V > 9$ have a probability < 0.01 of being extracted from such a distribution and are therefore likely blazars. But, while sources with $V > 9$ are likely blazars, there is no guarantee that those with $V < 9$ are truly young radio sources. We have also analyzed a stricter criterion, $V < 3$ that considers as blazar candidates all sources with variability significant at more than 3σ. However, this limit does not grant the rejection of blazars in a quiescent phase and may reject some truly young sources. It is thus necessary to complement variability studies with polarisation measurements and high-resolution imaging.

From the analysis of the HFP sample we can conclude that all the galaxies are consistent with being truly young, possibly recurrent, sources, while most quasars are consistent with being blazars. We have verified that also sources showing a convex spectrum in the simultaneous WMAP data, all identified as quasars, have variability properties consistent with a blazar classification.

6.2 An evolutionary model for young radio sources

The self-similar evolution model proposed by Begelman (1996, 1999) implies that the evolution of the radio power as the source expands, depends on the radial profile of the external density. To test this scenario and to constrain the birth rates and the evolutionary properties of radio sources, detailed comparisons of the model predictions with survey data are necessary. An exploratory study in this direction was presented by De Zotti et al. (2000), who showed that this kind of models may account for the observed counts, redshift and peak frequency distributions of the samples then available, but for values of the parameters not consistent with the predictions of Begelman's model.

Since then, new important surveys of GPS sources have been published, extending the coverage of the peak frequency-redshift plane. We have carried out a new analysis, still in the framework of Begelman's (1996, 1999), confining ourselves to GPS galaxies on account of the evidences that samples of GPS sources identified as quasars are heavily contaminated by flaring blazars. Care was taken to properly allow for the different selection criteria used to define the samples. We find that the observed redshift and peak frequency distributions can be satisfactorily accounted for in terms of a simple luminosity evolution of individual sources, along the lines discussed by Fanti et al. (1995) and Begelman (1996, 1999), although the derived parameter values have large uncertainties due to ambiguities in the selection of GPS sources and to the incompleteness of redshift measurements. However the simplest self-similar model, whereby the evolution is controlled only by the radial profile of the density of the ambient medium is not good enough and one additional parameter needs to be introduced. The fit requires a decrease of the emitted power and of the peak luminosity with source age or with decreasing peak frequency, at variance with the models by Snellen et al. (2000) and Alexander (2000). On the other hand, our analysis confirms the rather flat slope of the luminosity function, found by Snellen et al. (2000) who also report indications of a high luminosity break, not required by the data sets we have used. Our results suggest that the GPS galaxies are the precursors of extended radio sources with luminosities below the break of the luminosity function, although the uncertainties are so large that such conclusion must be considered as very preliminary. No cosmological evolution of the GPS galaxy population is required by presently available data.

Appendix A

Evolutionary models for young radio sources

We adopted the evolutionary scenario studied by De Zotti et al. (2000), elaborating on the analytic self-similar evolution model proposed by Begelman (1996, 1999) to account for the observed properties of the population of peaked radio sources.

A key element in this framework is the relationship between size and age since this involves both the power of the jet driving the expansion of the radio lobes and the properties of the ambient medium. In his initial model for Compact Symmetric Objects, Begelman (1996) assumes that the evolution of a lobe occurs in such a way that the mean hot-spot pressure, p_h, is a constant factor times the cocoon pressure, p_c:

$$p_h = \xi \cdot p_c; \qquad \xi \gg 1. \tag{A.1}$$

The mean pressure of the cocoon can be written as $p_c = \rho_e v_c^2$, and similarly the mean hot spot pressure is $p_h = \rho_e v_h^2$, where ρ_e is the density of the external medium, v_h the advance speed of the head and v_c the speed at which the cocoon expands. From Eq. (A.1) we have that $v_h = \xi^{1/2} v_c$. This implies that the cocoon will evolve with a fixed ratio of width (ω_c) and length (l_c):

$$\frac{\omega_c}{l_c} = \xi^{-1/2}. \tag{A.2}$$

The thrust of each jet is given by L_j/c for a relativistic jet, where L_j is the jet power. If

the thrust is spread over an area A_h, the mean hot-spot pressure can be written as:

$$p_h = \frac{L_j}{cA_h}. \tag{A.3}$$

The pressure inside the cocoon scales with the cumulative energy output over the lifetime of the jets and is inversely proportional to the cocoon's volume $V_c \propto (\omega_c^2 l_c)$:

$$p_c \sim \frac{L_j t}{2\pi\omega_c^2 l_c}.$$

From Eq. (A.1) and Eq. (A.2) we can therefore derive the expression for the area, A_h:

$$A_h = \frac{2\pi\omega_c^2 l_c}{\xi tc} = \frac{2\pi l_c^3}{\xi^2 tc}. \tag{A.4}$$

The source growths at a speed:

$$v_h = \frac{\mathrm{dl_c}}{\mathrm{dt}} = \left(\frac{L_j}{\rho_e c A_h}\right)^{1/2} = \left(\frac{L_j}{\rho_e}\right)^{1/2} \xi \frac{1}{2\pi} \frac{t^{1/2}}{l_c^{3/2}}. \tag{A.5}$$

The source age, t, can be obtained by integrating Eq. (A.5):

$$\int l_c^{3/2} \mathrm{dl_c} = \int \frac{1}{2\pi} \xi \left(\frac{L_j}{\rho_e}\right)^{1/2} t^{1/2} \mathrm{dt}$$

Finally we get:

$$t = \left(\frac{6\pi}{5}\right)^{2/3} \xi^{-2/3} \left(L_j/\rho_e\right)^{-1/3} l_c^{5/3} \tag{A.6}$$

We can now derive from Eqs. (A.5) and (A.3) the advance speed of the head and the cocoon pressure:

$$v_h = \frac{1}{2\pi} \left(\frac{6\pi}{5}\right)^{1/3} \xi^{2/3} \left(\frac{L_j}{\rho_e}\right)^{1/3} l_c^{-2/3} \tag{A.7}$$

$$p_c = \left(\frac{1}{2\pi}\right)^2 \left(\frac{6\pi}{5}\right)^2 \xi^{1/3} L_j^{2/3} \rho_e^{1/3} l_c^{-4/3}. \tag{A.8}$$

In order to derive the parameters characterizing the sources, the advance speed of the head, the age of the source and the cocoon pressure, a density profile of the ambient medium have to be specified. Begelman (1996) assumes a density profile that decreases with the distance from the core, r, as a power law.

$$\rho_e = \rho_0 \times r^{-n}. \tag{A.9}$$

In more recent models Snellen et al. (2000) and Alexander (2000) assume a King density profile where the density remains constant within the core radius (r_c), thus avoiding the divergence at $r = 0$, and then decreases at $r > r_c$:

$$\rho_e = \begin{cases} \rho_0 & r < r_c \\ \rho_0 r^{-n} & r > r_c. \end{cases} \tag{A.10}$$

The self-similar solutions for the two regions can be combined requiring that they match at $r = r_c$, assuming that the change of the density profile of the ambient medium does not disrupt the jet.

Under the assumption of self-similar evolution, if L_j is constant, the equations that give the advance speed of the head (v_h), the age of the source (t) and the cocoon pressure (p_c), can be written in terms of the length l_c:

$$v_h \propto l_c^{(n-2)/3} \tag{A.11}$$

$$t \propto l_c^{(5-n)/3} \tag{A.12}$$

$$p_c \propto l_c^{-(n+4)/3}. \tag{A.13}$$

In order to make predictions about the luminosity evolution of a radio source, Begelman (1996), Snellen et al. (2000) and Alexander (2000) suppose that the efficiency of the synchrotron emission is close to the maximum possible value (i.e. equipartition). Then the radio luminosity scales as:

$$L_s \propto p_c^{(p+5)/4} V_{\rm em} \tag{A.14}$$

where $V_{\rm em}$ is the effective emitting volume and p is the spectral index of the power-law energy distribution of electrons. Begelman (1996) argues that the synchrotron emission is likely dominated by the high pressure region close to the head of the jet; therefore he adopts $V_{\rm em} \sim A_h^{3/2}$. From Eq. (A.4) and (A.12) we have that

$$V_{\rm em} \propto (l_c^3 t^{-1})^{3/2} \propto l_c^{(4+n)/2}.$$

On the other hand, Snellen et al. (2000) and Alexander (2000) assume that the volume of the radio source is simply:

$$V_{\rm em} \propto l_c^3.$$

The different dependence of the volume from l_c leads to different expressions of the luminosity. Using Eq. (A.14) we have

$$L_s \propto \begin{cases} l_c^{-(p-1)(n+4)/12} & \text{Begelman (1996)} \\ l_c^{[(16-4p)-n(p+5)]/12} & \text{Snellen et al. (2000), Alexander (2000)} \end{cases} \tag{A.15}$$

or in terms of the source age

$$L_s \propto \begin{cases} t^{-[(p-1)(n+4)]/[4(n-5))]} & \text{Begelman (1996)} \\ t^{[(16-4p)-n(p+5)]/[4(5-n)]} & \text{Snellen et al. (2000), Alexander (2000)} \end{cases} \tag{A.16}$$

The spectral index of the power-law energy distribution of relativistic electrons, p, is related to the spectral index of the optically thin part of the radio spectrum of the source α by $\alpha = (p-1)/2$. All the cited authors assume $p = 2$ (i.e. $\alpha = 0.5$), therefore Eq. (A.15) becomes:

$$L_s \propto \begin{cases} l_c^{-(n+4)/12} & \text{Begelman (1996)} \\ l_c^{(8-7n)/12} & \text{Snellen et al. (2000), Alexander (2000).} \end{cases} \tag{A.17}$$

In Begelman's model the luminosity decreases with the source size for $n \geq 0$. On the other hand, both Snellen et al. (2000) and Alexander (2000) find that the radio luminosity increases as $l_c^{2/3}$ if n=0 (i.e. within the core radius) and then decreases as $l_c^{-0.5}$ for n=2 in the large scale phase at $r > r_c$. Evolutionary tracks where the luminosity increases within the core radius and then decreases in a falling atmosphere in the power-diameter plane are also presented by Carvalho & O'Dea (2003) based on the results of a series of numerical hydrodynamical simulations.

An important feature of the spectrum of GPS sources is the turnover frequency. Observational studies have shown that the spectra of peaked radio sources are well described by:

$$L_\nu = L_p \times \begin{cases} (\nu/\nu_p)^{\alpha_a} & \text{if } \nu < \nu_p \\ (\nu/\nu_p)^{-\alpha} & \text{if } \nu > \nu_p \end{cases} \tag{A.18}$$

with $\alpha_a = 0.8$ and $\alpha = 0.75$, the mean values found by Snellen et al. (1998b).

The best determined observed relationship for GPS/CSS sources relates the radio turnover frequency to the projected linear size $\nu_p \propto (LS)^{-\delta}$, with $\delta \simeq 0.65$ (O'Dea & Baum

1997). It follows that ν_p decreases with time as

$$\nu_p = \nu_{p,i} t^{-\lambda} \tag{A.19}$$

where $\nu_{p,i}$ is the initial, maximum value of the turnover frequency, $\lambda = \delta \cdot \epsilon$ and $\epsilon = 3/(5-n)$.

As the radio lobes expand, the peak luminosity L_p varies as a consequence of two factors: the decrease of the emitted radio power (Eq. A.16) and the decrease of ν_p (Eq. A.19). Hence:

$$L_p = L_i \left(\frac{\nu_p}{\nu_{p,i}} \right)^{-\alpha}$$

where

$$L_i = L_{p,i} t^{-\eta} = L_{p,i} \left(\frac{\nu_p}{\nu_{p,i}} \right)^{\eta/\lambda}$$

where $L_{p,i}$ is the initial, maximum value of the luminosity at the frequency $\nu_{p,i}$. We get:

$$L_p(\nu_p) = L_{p,i} \left(\frac{\nu_p}{\nu_{p,i}} \right)^{\eta/\lambda - \alpha} . \tag{A.20}$$

The simplest statistics useful for studies of the population properties of sources are the number counts. In general, the mean differential number counts *per steradian* dN/dS at a given flux S can be written as:

$$\frac{\mathrm{dN}}{\mathrm{dS}} = \int_{z_i}^{z_f} \mathrm{dz} \frac{\mathrm{dV}}{\mathrm{dz}} \frac{\mathrm{dL(S;z)}}{\mathrm{dS}} \mathrm{n[L(S,z),z]} \tag{A.21}$$

where $n[L(S,z),z]$ is the epoch-dependent luminosity function and dV/dz is the volume element *per unit solid angle*.

We have made the simplest assumption for the radio **luminosity function** (in units of $\mathrm{Mpc^{-3} dlogL_i^{-1}}$) of GPS sources, i.e. a power-law:

$$n(L,z) \approx n_0 (L/L_\star)^{-\beta} \tag{A.22}$$

We have normalized monochromatic luminosities to $L_0 = 10^{32}\,\mathrm{erg\,s^{-1}\,Hz^{-1}}$.

We assume that the birth rate of GPS sources is constant on time scales much shorter than the cosmological-expansion timescale. The number of sources of age t within $\mathrm{d}t$ is simply proportional to $\mathrm{d}t$ and from Eq.A.19 we find that $t = (\nu_p/\nu_{p,i})^{-1/\lambda}$ and $\mathrm{d}t/\mathrm{d}\nu_p$ is

$$\frac{\mathrm{d}t}{\mathrm{d}\nu_p} = -\frac{1}{\lambda \nu_{p,i}} (\nu_p/\nu_{p,i})^{-(1+1/\lambda)},$$

From the previous relation the epoch dependent luminosity function at a given frequency ν, $n(L_\nu,\nu_p,z)\mathrm{dlogL}_\nu\mathrm{d}\nu_\mathrm{p}$=$n(L_\nu,\nu_p,z)\mathrm{dlogL}_\nu\frac{\mathrm{dt}}{\mathrm{d}\nu_\mathrm{p}}\mathrm{d}\nu_\mathrm{p}$ ($\mathrm{Mpc}^{-3}\,\mathrm{d}\log {L_\nu}^{-1}\,\mathrm{GHz}^{-1}$) can be written as:

$$n(L_\nu,\nu_p,z) = n_0 \left(\frac{L_{p,i}(L_\nu,\nu_p)}{L_\star(z)}\right)^{-\beta} \left(\frac{\nu_p}{\nu_{p,i}}\right)^{-(1+1/\lambda)}.$$

Using Eq. (A.20) $L_{p,i}$ is given by

$$L_{p,i} = L_\nu \left(\frac{\nu_p}{\nu_{p,i}}\right)^{-\eta/\lambda+\alpha} \begin{cases} (\nu/\nu_p)^{-\alpha_a} & \text{if } \nu < \nu_p \\ (\nu/\nu_p)^{\alpha} & \text{if } \nu > \nu_p \end{cases} \tag{A.23}$$

and the final expression for the luminosity function is:

$$n(L_\nu,\nu_p,z) = n_0 \left(\frac{L_\nu}{L_\star(z)}\right)^{-\beta} [f(\nu_p)]^{-\beta} \left(\frac{\nu_p}{\nu_{p,i}}\right)^{-(1+1/\lambda)} \tag{A.24}$$

where

$$f(\nu_p) = \left(\frac{\nu_p}{\nu_{p,i}}\right)^{-\eta/\lambda+\alpha} \begin{cases} (\nu/\nu_p)^{-\alpha_a} & \text{if } \nu < \nu_p \\ (\nu/\nu_p)^{\alpha} & \text{if } \nu > \nu_p \end{cases} \tag{A.25}$$

The expression (A.24) of the luminosity function has been used in Chapter 5 to derive the redshift and peak frequency distributions of GPS sources.

We have also checked whether cosmological evolution of the GPS source population is required by the data. We have assumed pure luminosity evolution and adopted a very simple parameterization for it:

$$L_\star(z) = L_0 \times \begin{cases} (1+z)^k & \text{if } z < z_c \\ (1+z_c)^k & \text{if } z > z_c \end{cases} \tag{A.26}$$

The redshift z_c at which luminosity evolution levels off and the index k are model parameters. No significant improvement of the fits to the data were obtained adding these two additional parameters.

Bibliography

[1] Alexander, P. 2000, MNRAS, 319, 8

[2] Aller, M. F., Aller, H. D., & Hughes, P. A. 1992, ApJ, 399, 16

[3] Antonelli, L. A., & Fiore, F. 1997, Memorie della Societa Astronomica Italiana, 68, 299

[4] Akujor, C. E., & Garrington, S. T. 1995, A&AS, 112, 235

[5] Baum, S. A., O'Dea, C. P., de Bruyn, A. G., & Murphy, D. W. 1990, A&A, 232, 19

[6] Begelman, M.C., 1996, in *Cygnus A: Study of a Radio Galaxy*, ed. Carilli C. & Harris D.

[7] Begelman, M.C. 1999, in The Most Distant Radio Galaxies, proc. of the KNAW colloquium held in Amsterdam, 15-17th October 1997, eds. H.J.A. Röttgering, P.N. Best, M.D. Lehnert, KNAW, Amsterdam, p. 173

[8] Bennett, C.L., Halpern, M., Hinshaw, G., et al. 2003a, ApJS, 148, 1

[9] Bennett, C.L., Hill, R.S., Hinshaw, G., et al. 2003b, ApJS, 148, 97

[10] Bicknell, G. V., Dopita, M. A., & O'Dea, C. P. O. 1997, ApJ, 485, 112

[11] Bolton, R.C., Cotter, G., Pooley, G.G., et al. 2004, MNRAS, 354, 485

[12] Browne, I. W. A., Wilkinson, P. N., Patnaik, A. R., & Wrobel, J. M. 1998, MNRAS, 293, 257

[13] Carvalho, J. C., & O'Dea, C. P. 2003, Publications of the Astronomical Society of Australia, 20, 98

[14] Cawthorne, T. V., Wardle, J. F. C., Roberts, D. H., & Gabuzda, D. C. 1993a, ApJ, 416, 519

[15] Ciaramella, A., et al. 2004, A&A, 419, 485

[16] Condon, J. J., Cotton, W. D., Greisen, E. W., Yin, Q. F., Perley, R. A., Taylor, G. B., & Broderick, J. J. 1998, AJ, 115, 1693

[17] Cotton, W. D., et al. 2003, Publications of the Astronomical Society of Australia, 20, 12

[18] Dallacasa, D. 2003, Publications of the Astronomical Society of Australia, 20, 79

[19] Dallacasa, D., Falomo, R., & Stanghellini, C. 2002a, A&A, 382, 53

[20] Dallacasa, D., Fanti, C., Giacintucci, S., Stanghellini, C., Fanti, R., Gregorini, L., & Vigotti, M. 2002b, A&A, 389, 126

[21] Dallacasa, D., Tinti, S., Fanti, C., Fanti, R., Gregorini, L., Stanghellini, C., & Vigotti, M. 2002c, A&A, 389, 115

[22] Dallacasa, D., Falomo, R., & Stanghellini, C. 2002, A&A, 382, 53

[23] Dallacasa, D., Stanghellini, C., Centonza, M., & Fanti, R. 2000, A&A, 363, 887

[24] De Young, D. S. 1993, ApJ, 402, 95

[25] de Vries, W. H., Barthel, P. D., & O'Dea, C. P. 1997a, A&A, 321, 105

[26] de Vries, W. H., et al. 1997, ApJS, 110, 191

[27] de Vries, W. H., O'Dea, C. P., Baum, S. A., & Barthel, P. D. 1999, ApJ, 526, 27

[28] de Vries, W. 2003, Publications of the Astronomical Society of Australia, 20, 6

[29] De Zotti, G., Granato, G.L., Silva, L., Maino, D., & Danese, L. 2000, A&A, 354, 467

[30] de Zotti, G., Ricci, R., Mesa, D., Silva, L., Mazzotta, P., Toffolatti, L., & González-Nuevo, J. 2005, A&A, 431, 893

[31] Donato, D., Ghisellini, G., Tagliaferri, G., & Fossati, G. 2001, A&A, 375, 739

[32] Dunlop, J.S., & Peacock, J.A. 1990, MNRAS, 247, 19

[33] Edwards, P.G.,& Tingay, S.J. 2004, A&A, 424, 91

[34] Elvis, M., Fiore, F., Wilkes, B., McDowell, J., & Bechtold, J. 1994, ApJ, 422, 60

[35] Fanti, R., Fanti, C., Schilizzi, R. T., Spencer, R. E., Nan Rendong, Parma, P., van Breugel, W. J. M., & Venturi, T. 1990, A&A, 231, 333

[36] Fanti, C., Fanti, R., Dallacasa, D., Schilizzi, R. T., Spencer, R. E., & Stanghellini, C. 1995, A&A, 302, 317

[37] Fanti, C., et al. 2000, A&A, 358, 499

[38] Fanti, C., Pozzi, F., Dallacasa, D., Fanti, R., Gregorini, L., Stanghellini, C., & Vigotti, M. 2001, A&A, 369, 380

[39] Fanti, C., & Fanti, R. 2002,in Issues in Unification of Active Galactic Nuclei, ASP Conference Series 258, ed R. Maiolino, A. Marconi & N. Nagar (San Francisco: ASP), 261

[40] Fukugita, M., Shimasaku, K., & Ichikawa, T. 1995, PASP, 107, 945

[41] Gopal-Krishna. 1995, Publ. Nat. Acad. Sci., 92, 11399

[42] Grainge K., Edge A., 1998, In: Trn Thanh Vn J., Giraud-Hraud Y., Bouchet F., et al., Fundamental Parameters in Cosmology. Proc. XXXIII Rencontres de Moriond, Ed. Frontires, p. 151

[43] Gregory, P. C., Scott, W. K., Douglas, K., & Condon, J. J. 1996, ApJS, 103, 427

[44] Griffith, M. R., Wright, A. E., Burke, B. F., & Ekers, R. D. 1994, ApJS, 90, 179

[45] Griffith, M. R., Wright, A. E., Burke, B. F., & Ekers, R. D. 1995, ApJS, 97, 347

[46] Heckman, T. M., Miley, G. K., Balick, B., van Breugel, W. J. M., & Butcher, H. R. 1982, ApJ, 262, 529

[47] Hirabayashi, H., Fomalont, E.B., Horiuchi, S., et al. 2000, PASJ, 52, 997

[48] Hughes, P. A., Aller, H. D., & Aller, M. F. 1992, ApJ, 396, 469

[49] Impey, C. D., & Neugebauer, G. 1988, AJ, 95, 307

[50] Jackson, C. A., Wall, J. V., Shaver, P. A., Kellermann, K. I., Hook, I. M., & Hawkins, M. R. S. 2002, A&A, 386, 97

[51] Jaffe W.J., Perola G.C., 1974, A&A 26, 423

[52] Jauncey, D. L., et al. 2003, Publications of the Astronomical Society of Australia, 20, 151

[53] Jenkins, C. J., Pooley, G. G., & Riley, J. M. 1977, MmRAS, 84, 61

[54] Kardashev, N. S. 1962, Soviet Astronomy, 6, 317

[55] Kellermann, K. I. 1964, ApJ, 140, 969

[56] Kellermann, K. I. 1966b, ApJ, 146, 621

[57] Kellermann, K.I., Vermeulen R.C., et al., 1998, ApJS, 1125, 1318

[58] King, E. A. 1994, Ph.D. Thesis

[59] King, E. A., & The SHEVE Team 1993, Sub-arcsecond Radio Astronomy, 152

[60] Kuehr, H., Witzel, A., Pauliny-Toth, I. I. K., & Nauber, U. 1981, A&AS, 45, 367

[61] Magliocchetti, M., Maddox, S.J., Jackson, C.A., et al. 2002, MNRAS, 333, 100

[62] Mantovani, F., Junor, W., Fanti, R., Padrielli, L., Browne, I. W. A., & Muxlow, T. W. B. 1992, MNRAS, 257, 353

[63] Mantovani, F., Junor, W., Fanti, R., Padrielli, L., & Saikia, D. J. 1994, A&A, 292, 59

[64] McMahon R. G., Irwin M. J., 1992, in MacGillivray H. T., Thomson E. B., eds, Astroph. Space Sci. Libr., Vol. 174, Digitised Optical Sky Surveys. Kluwer, Dordrecht, p. 417

[65] Murgia, M., Fanti, C., Fanti, R., Gregorini, L., Klein, U., Mack, K.-H., & Vigotti, M. 1999, A&A, 345, 769

[66] Murgia, M. 2003, Publications of the Astronomical Society of Australia, 20, 19

[67] Mutoh, M., Inoue, M., Kameno, S., Asada, K., Kenta, F., & Uchida, Y. 2002, PASJ, 54, 131

[68] Nartallo, R., Gear, W. K., Murray, A. G., Robson, E. I., & Hough, J. H. 1998, MNRAS, 297, 667

[69] O'Dea, C. P., Baum, S. A., Stanghellini, C., Morris, G. B., Patnaik, A. R., & Gopal-Krishna 1990b, A&AS, 84, 549

[70] O'Dea, C. P., Baum, S. A., & Stanghellini, C. 1991, ApJ, 380, 66

[71] O'Dea, C. P., Baum, S. A., & Gallimore, J. F. 1994a, ApJ, 436, 669

[72] O'Dea, C. P., Stanghellini, C., Baum, S. A., & Charlot, S. 1996, ApJ, 470, 806

[73] O'Dea, C. P., & Baum, S. A. 1997, AJ, 113, 148

[74] O'Dea, C. P. 1998, PASP, 110, 493

[75] O'Dea, C. P., De Vries, W. H., Worrall, D. M., Baum, S. A., & Koekemoer, A. 2000, AJ, 119, 478

[76] O'Dea, C. P., et al. 2002, AJ, 123, 2333

[77] Peacock J.A., Wall J.V., 1981, MNRAS, 194, 19

[78] Peacock, J. A., & Wall, J. V. 1982, MNRAS, 198, 843

[79] Phillips, R. B., & Mutel, R. L. 1982, A&A, 106, 21

[80] Owsianik, I., & Conway, J. E. 1998, A&A, 337, 69

[81] Owsianik, I., Conway, J. E., & Polatidis, A. G. 1998, A&A, 336, L37

[82] Pacholczyk, A. G. 1970, Radio Astrophysics (San Francisco: Freeman & Co.)

[83] Patnaik, A. R., Browne, I. W. A., Wilkinson, P. N., & Wrobel, J. M. 1992, MNRAS, 254, 655

[84] Peck, A. B., Taylor, G. B., Fassnacht, C. D., Readhead, A. C. S., & Vermeulen, R. C. 2000, ApJ, 534, 104

[85] Peck, A. B., & Taylor, G. B. 2000, ApJ, 534, 90

[86] Perley, R. A. 1982, AJ, 87, 859

[87] Readhead, A. C. S., Taylor, G. B., Xu, W., Pearson, T. J., Wilkinson, P. N., & Polatidis, A. G. 1996, ApJ, 460, 612

[88] Rengelink, R. B., Tang, Y., de Bruyn, A. G., Miley, G. K., Bremer, M. N., Roettgering, H. J. A., & Bremer, M. A. R. 1997, A&AS, 124, 259

[89] Reynolds, C. S., & Begelman, M. C. 1997, ApJL, 487, L135

[90] Rudnick, L., & Jones, T. W. 1982, ApJ, 255, 39

[91] Saikia, D. J., Singal, A. K., & Cornwell, T. J. 1987, MNRAS, 224, 379

[92] Saikia, D. J., Jeyakumar, S., Wiita, P. J., Sanghera, H. S., & Spencer, R. E. 1995, MNRAS, 276, 1215

[93] Sanghera, H. S., Saikia, D. J., Ldke, E., Spencer, R. E., Foulsham, P. A., Akujor, C. E., & Tzioumis, A. K. 1995, A&A, 295, 629

[94] Siemiginowska, A., Aldcroft, T. L., Bechtold, J., Brunetti, G., Elvis, M., & Stanghellini, C. 2003, Publications of the Astronomical Society of Australia, 20, 113

[95] Snellen, I. A. G., Bremer, M. N., Schilizzi, R. T., Miley, G. K., & van Ojik, R. 1996, MNRAS, 279, 1294

[96] Snellen, I. A. G. 1997, Ph.D. Thesis, University of Leiden

[97] Snellen, I. A. G., Schilizzi, R. T., de Bruyn, A. G., & Miley, G. K. 1998a, A&A, 333, 70

[98] Snellen, I. A. G., Schilizzi, R. T., de Bruyn, A. G., Miley, G. K., Rengelink, R. B., Roettgering, H. J., & Bremer, M. N. 1998c, A&AS, 131, 435

[99] Snellen, I. A. G., Schilizzi, R. T., Bremer, M. N., Miley, G. K., de Bruyn, A. G., Rottgering, H. J. A. 1999, MNRAS, 307, 149

[100] Snellen, I. A. G., Schilizzi, R. T., Miley, G. K., de Bruyn, A. G., Bremer, M. N., Rottgering, H. J. A. 2000, MNRAS, 319, 445

[101] Snellen, I.A.G., Lehnert, M.D., Bremer, M.N., & Schilizzi, R.T. 2002, MNRAS, 337, 981

[102] Snellen, I.A.G., Mack, K.-H., Schilizzi, R.T., & Tschager, W. 2004, MNRAS, 348, 227

[103] Snellen, I. A. G., Mack, K.-H., Schilizzi, R. T., & Tschager, W. 2004, MNRAS, 348, 227

[104] Spencer, R. E., McDowell, J. C., Charlesworth, M., Fanti, C., Parma, P., & Peacock, J. A. 1989, MNRAS, 240, 657

[105] Stanghellini, C., Baum, S. A., O'Dea, C. P., & Morris, G. B. 1990a, A&A, 233, 379

[106] Stanghellini, C., & et al. 1990b, Compact Steep-Spectrum and GHZ-peaked Spectrum Radio Sources, 55

[107] Stanghellini C., Dallacasa D., O'Dea C.P., Baum S.A., Fanti R., Fanti C., 1996, in proc of 2nd workshop on GPS&CSS Radio Sources, eds. I. Snellen, R.T. Schilizzi, H.J.A. Rttgering and M.N. Bremer, p.4

[108] Stanghellini, C., O'Dea, C. P., Dallacasa, D., Baum, S. A., Fanti, R., & Fanti, C. 1998, A&AS, 131, 303

[109] Stanghellini, C. 1999, Memorie della Societa Astronomica Italiana, 70, 117

[110] Stanghellini, C. 2003, Publications of the Astronomical Society of Australia, 20, 118

[111] Stanghellini C., O'Dea C.P., Dallacasa D., Cassaro P., Baum S.A., Fanti R., Fanti C. 2005, accepted for publication on A&A

[112] Stevens, J. A., Robson, E. I., Gear, W. K., Cawthorne, T. V., Aller, M. F., Aller, H. D., Teraesranta, H., & Wright, M. C. H. 1998, ApJ, 502, 182

[113] Taylor, G. B., Readhead, A. C. S., & Pearson, T. J. 1996, ApJ, 463, 95

[114] Taylor, G. B., Marr, J. M., Pearson, T. J., & Readhead, A. C. S. 2000, ApJ, 541, 112

[115] Teräsranta, H., Tornikoski, M., Mujunen, A., et al. 1998, A&AS, 91, 121

[116] Tinti, S., Dallacasa, D., de Zotti, G., Celotti, A., & Stanghellini, C. 2005, A&A, 432, 31

[117] Torniainen, I., Tornikoski, M., Teräsranta, H., Aller, M.F., & Aller H.D. 2005, A&A, 435, 839

[118] Trushkin, S.A. 2003, Bull. Spec. Astrophys. Obs. N. Caucasus, 55, 90, astro-ph/0307205

[119] Tzioumis, A. K., et al. 1989, AJ, 98, 36

[120] van Breugel, W. J. M., Fanti, C., Fanti, R., Stanghellini, C., Schilizzi, R. T., & Spencer, R. E. 1992, A&A, 256, 56

[121] van Breugel, W., Heckman, T., Miley, G., 1984a, ApJ, 276, 79

[122] van Breugel, W., Miley, G., Heckman, T., 1984b, AJ, 89, 5

[123] van Breugel, W. J. M., Fanti, C., Fanti, R., Stanghellini, C., Schilizzi, R. T., & Spencer, R. E. 1992, A&A, 256, 56

[124] Wilkinson, P. N., Polatidis, A. G., Readhead, A. C. S., Xu, W., & Pearson, T. J. 1994, ApJ, 432, L87

[125] Wilkinson, P. N., Browne, I. W. A., Patnaik, A. R., Wrobel, J. M., & Sorathia, B. 1998, MNRAS, 300, 790

[126] Wright, A. E., Griffith, M. R., Burke, B. F., & Ekers, R. D. 1994, ApJS, 91, 111

[127] Wright, A. E., Griffith, M. R., Hunt, A. J., Troup, E., Burke, B. F., & Ekers, R. D. 1996, ApJS, 103, 145